Continuous flow-mode synthesis of (chiral) amines with transaminase: a strategic biocatalytic approach to essential building blocks

Hippolyte Meersseman Arango,[a] Ludivine van den Biggelaar,[a] Patrice Soumillion,[b] Patricia Luis,[c] Tom Leyssens,[a] Francesca Paradisi,[d] Damien P. Debecker[a,*]

[a] Institute of Condensed Matter and Nanosciences (IMCN), Université catholique de Louvain (UCLouvain), Place Louis Pasteur, 1, 1348 Louvain-La-Neuve, Belgium

[b] Louvain Institute of Biomolecular Science and Technology (LIBST), Université catholique de Louvain, Place Croix du Sud, 4-5, 1348 Louvain-la-Neuve, Belgium

[c] Materials & Process Engineering (iMMC-IMAP), Université Catholique de Louvain, Place Sainte Barbe 2, 1348 Louvain-la-Neuve, Belgium

[d] Department of Chemistry and Biochemistry, University of Bern, Freiestrasse 3, Bern, Switzerland

* damien.debecker@uclouvain.be

Abstract

Chiral amines are essential building blocks to manufacture a plethora of valuable compounds, including active pharmaceutical ingredients (API). It is estimated that about half of the current API contain chiral amines in their structure. However, the current production of chiral amines often involves multi-step synthesis requiring expensive homogeneous catalysts and high energy consumption for subsequent purification. Biocatalytic routes have gained considerable attention in the last decades, as effective and potentially more sustainable alternatives. Indeed, amine transaminases (ATAs) can catalyse transamination reactions and produce chiral amines with excellent enantioselectivity and in mild conditions. Industrial applications of biocatalytic transamination, however, remain scarce as the enzymes often operate in restricted operational conditions and display limited stability. Batch reactors utilizing the free enzyme in solution also face issues regarding catalyst separation, recovery, and reuse. Moreover, the synthesis of most compounds of interest is thermodynamically unfavoured. Taking a side step, catalysis scientists design heterogenized biocatalysts that are more versatile, more stable, and amenable to continuous flow processes. A number of improvement strategies have been deployed: modifications of the transaminase itself (*via* genetic engineering), optimization of immobilization strategies, design of structured supports, development of integrated equilibrium shifting strategies, concatenation with purification, etc. Here, we summarize and exemplify these advances leading to more efficient biocatalytic systems based on transaminases operating in continuous flow mode.

Keywords

Transaminase, biocatalysis, flow chemistry, enzyme immobilization, enantioselective catalysis

1. Introduction

Chemo-catalytic synthesis processes used for the production of active pharmaceutical ingredients (APIs) have been identified as problematic from an environmental point of view [1–3]. The molecular complexity of APIs requires multistep synthesis that consumes large amounts of reagents and solvents. Moreover, while highly (enantio)pure products are generally needed for the targeted applications, chemo-catalytic reactions are rarely 100% (enantio)selective. Because of this, laborious, costly, and waste-generating downstream purifications steps have to be applied [4]. The pharmaceutical industry is known to generate significant waste per unit mass of product produced (e-factor often above 250). It is estimated that the pharmaceutical industry is responsible for the formation of about 10 billion kg of waste per year for active pharmaceutical ingredients (APIs) production, which implies a disposal cost of more than $20 billion per year [5].

The specific case of the synthesis of chiral amines is telling. Chiral amines are essential building blocks used to manufacture a plethora of APIs. It is estimated that about half of the current APIs contain chiral amines in their structure [6,7]. Pharmaceutical industries have been relying on chemocatalytic processes to produce chiral amines for decades [8], usually *via* indirect reductive amination (of an imine precursor)[9] using chiral organometallic homogeneous catalysts [10]. The latter operate at relatively high temperature, require pressurized hydrogen, are difficult to recover, and are often based on toxic and depleted heavy metals [10,11]. The incentives and opportunities to the make such processes greener are evident.

In this context, the development of alternative synthesis methods of chiral amines following more closely the principles of green chemistry and the good practice of sustainability in catalysis science [12,13], is of particular importance. Green chemistry is more than preventing waste and minimizing energy consumption; it is also about operating in a more sustainable way, increasing efficiency and reducing hazards for operators, for consumers, and for the environment. In addition to focusing on the reduction of waste quantity and cost, managing inputs (*e.g.* solvents, reagents, catalysts) is an important driver. Life cycle analyses of API production processes indeed demonstrated that the synthesis of material inputs account for at least 80% of the overall life cycle impact [14].

The last two decades saw the emergence of biocatalysis as a potential greener approach for pharmaceutical processes. Biocatalysis represents a vibrant field of research since enzymes tend to be highly enantioselective, non-toxic and usually work in mild conditions (*e.g.* aqueous

media, low temperature) [15]. Interestingly, amine transaminases (ATAs) enable the direct synthesis of chiral amines from pro-chiral ketones using cheap and readily available amino donors (*e.g.* isopropylamine, amino-acids) through transamination. As highlighted by the ACS Green Chemistry Institute Pharmaceutical Roundtable, such transamination may present major advantages in terms of overall efficiency and atom economy with respect to conventional indirect reductive amination of imines (which involve multistep production and isolation of imine precursors) [3]. As a result, ATAs are catching the eye and getting increasingly studied [16]. For instance, the greener production of Sitagliptin (Figure 1) taking advantage of a genetically engineered transaminase has been implemented at the pilot scale by Merck [17,18]. Also, the production of Pseudoephedrine by transaminases was recently demonstrated [19].

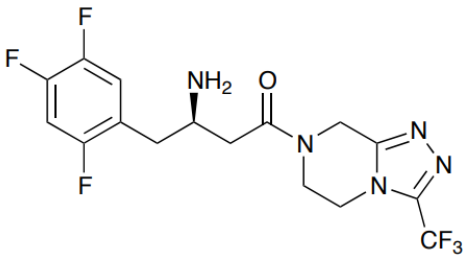

Figure 1. R-Sitagliptin is an anti-diabetic drug. An engineered transaminase is able to catalyse the synthesis of this compound at large scale from the corresponding ketone.

Nevertheless, despite notable examples of kg and pilot-scale batch processes employing ATAs (see section 4.1), industrial applications remain currently scarce as they suffer from several limitations, mainly linked with substrate and product inhibition and with the unfavourable thermodynamic equilibrium for the targeted reactions [20]. Additionally, the enzymes are often employed in the "free" form, i.e. as homogenous biocatalysts, that are hardly reusable, remain restricted to batch reactors, and feature limited stability. To overcome these limitations, strategies aiming at enhancing chiral amine production by transaminases have been intensively investigated. Of particular interest: (i) the development of equilibrium shifting strategies, as well as (ii) the design of more versatile and reusable heterogenized biocatalysts amenable to continuous flow-mode processes.

In this review, we first summarize the state of the art on the production of chiral amines and we highlight the key – emerging – role of biocatalysis. The focus is then put on transaminase enzymes themselves, for which we describe the main properties and the catalytic mechanism. After highlighting the main issues that currently preclude a general deployment of chiral amine synthesis using transaminases at the industrial level, we discuss and exemplify a number of

strategies that have been proposed to round these corners. This includes methods to expand the substrate scope and robustness, to shift the thermodynamic equilibrium, to enhance recoverability and reusability (mainly by immobilization). Importantly, the transition from homogeneous batch processes – where the enzyme is free in the liquid phase – to heterogeneous flow processes – where the enzyme is immobilized on a suitable carrier – is identified as a key to develop greener processes. Continuous flow processes will allow envisaging more robust, green, and productive syntheses [21]. Thus, the state of the art on the immobilization of transaminases and their implementation in flow transamination processes is presented.

2. Chiral amines

2.1 Importance of chiral amines

Chiral compounds represented 56 % of active pharmaceutical ingredients (API) available on the drug market in 2005 [22]. In 2020, more than 95 % of the commercialized API are chiral [23]. This is not surprising, given that all living organisms are built on chiral biomolecules, and drug targets such as proteins, that are built from L-amino acids, will interact differently with R- and S-enantiomers of a given compound. In biology, proteins are built exclusively from L-amino acids (plus glycine which does not bear any chiral centre) [24]. For chiral drugs, the enantiomer that exhibits the desired physiologic properties is called the eutomer, while the other enantiomer is called the distomer [25]. The latter may exhibit weak positive properties (sometimes different from the eutomer properties), or can be totally inactive. For example, the R-enantiomer of methamphetamine is a powerful decongestant, while S-methamphetamine is a recreational drug [26]. In the worst cases, however, the distomer is highly toxic. S-Penicillamine (Figure 2) is a chiral amine drug prescribed for the treatment of polyarthritis, while R-Penicillamine is highly toxic [27]. Nevertheless, 88 % of current chiral drugs are sold as racemic mixture [22]. In such case, it is obviously crucial to know the properties of each enantiomer. Since 1992, the U.S. Federal Food and Drug Administration (FDA) demands that the drug manufacturers either clinically test both enantiomers when selling a racemic mixture, or commercialize only the pure eutomer [28,29]. Getting enantiomerically pure drugs is still a complicated task; it requires to either produce only the eutomer (need for enantioselective chemical methods) or to produce a racemic mixture and resolve or deracemize it [30] (which is often expensive and generates waste).

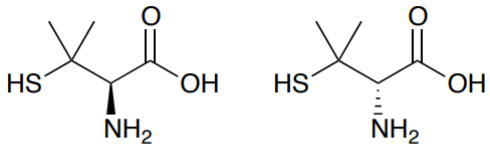

(S)-Penicillamine *Polyarthritis treatment* **(R)-Penicillamine** *Toxic*

Figure 2. Penicillamine enantiomers. The enantiomers of Penicillamine have different properties: the S-eutomer is a drug used in polyarthritis treatment; the R-distomer is toxic.

Chiral amines can be defined as compounds bearing a nitrogen atom adjacent, or α, to a stereogenic carbon [4]. 45% of the current drugs contain a chiral amine in their structure[6,7]. Therefore, most of the largest pharmaceutical industries are actively looking into chiral amine synthesis: Pseudoephedrine (Sinutab®, Johnson & Johnson), Sertraline (Zoloft®, Pfizer), Oseltamivir (Tamiflu®, Roche), Rivastigmine (Exelon®, Novartis), Clopidogrel (Plavix®, Sanofi), Sitagliptine (Januvia®, Merck), Lisdexamfetamine (Vyvanse®, Shire), Linagliptine (Tradjenta®, Boehringer-Ingelheim Pharmaceuticals), etc. are all chiral amine drugs. Those highly consumed medicines act as decongestants, anti-depressants, antiviral drugs, treatments for neurological disorders, diabetes, etc. For instance, Clopidogrel – antiplatelet agent – is prescribed to more than 100 million people worldwide [31], Sertraline – a treatment against neurological disorder – was prescribed to more than 37 million people in the USA in 2011 [32]. As for all chiral drugs, the development of enantioselective synthesis methods (i.e. to obtain directly enantiomerically pure chiral amines) is of crucial importance[33].

2.2. Chiral amine synthesis

There are two conventional ways to produce chiral amines using a chemical approach: asymmetric synthesis and chiral resolution [4]. These are presented here briefly as benchmark case (section 2.2.1.), before putting the focus of the review on biocatalytic routes (section 2.2.2.) which arguably represent a promising alternative.

2.2.1. Chemical routes

In the first approach (asymmetric synthesis), only one enantiomer is produced, leading to a maximal theoretical yield of 100 %, starting from a non-chiral substrate, or optically pure chiral substrate. There are three main kinds of asymmetric synthesis [22]. First, an enantioselective

catalyst – typically a chiral homogeneous organometallic catalysts [34] – can be used for the production of a chiral compound with a high enantiomeric excess. As subsequent purification of the desired enantiomer is usually needed, as well as removal of the catalyst from the final product, further purification steps are imposed [35,36]. In a second type of asymmetric synthesis, a chiral auxiliary is temporarily added to a compound to guide the reaction towards the production of the desired enantiomer, after which the auxiliary is removed. In a third approach, the enantioselective compound is built starting from a chiral precursor (for example, an amino-acid) [37].

Asymmetric synthesis is ubiquitous in the pharmaceutical sector. Hereafter, we briefly present three examples for chiral amines. S-Clopidogrel (Figure 3) is the second world most sold medicine [31]. Its current production involves the reduction of a carbonyl centre into a chiral alcohol. This step is catalysed by a ruthenium-based organometallic catalyst, [Ru(*p*-cymene)Cl_2]$_2$, using a chiral ligand to bring enantioselectivity to the process. The reaction is run at 0 °C, requiring extra energy for cooling. The final product exhibits an enantiomeric excess of 92 % [38,39].

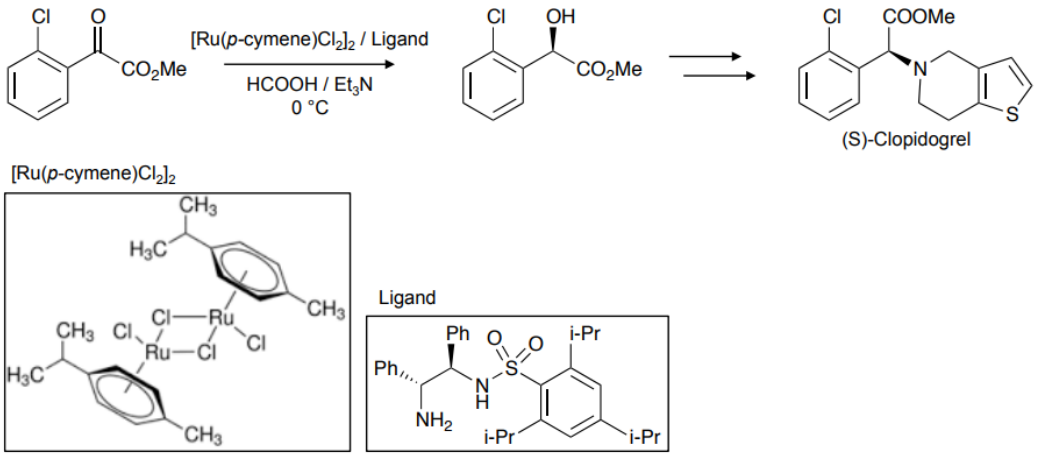

Figure 3. S-Clopidogrel synthesis, adapted from Li *et al.* [38].

R-Sitagliptin (Figure 4), produced by Merck, is used in the treatment of type II diabetes. Its chemocatalytic synthesis, implemented for decades, involves the use of a Ru- or Rh-based organometallic enantioselective catalyst with a chiral ligand featuring phosphine groups (such as [Rh(COD)Cl]$_2$-^{t}Bu-JOSIPHOS) [40]. After the imination of a ketone group, the imine group is reduced under high-pressure hydrogen (17 bars) with the enantioselective catalyst. The final

enantiomeric excess reaches 95 % [41]. Further purification of the R-enantiomer, as well as a final step to obtain the sitagliptin phosphate salt (the active form), are required. Recently, a greener biocatalytic pathway (vide infra) has been implemented by Merck.

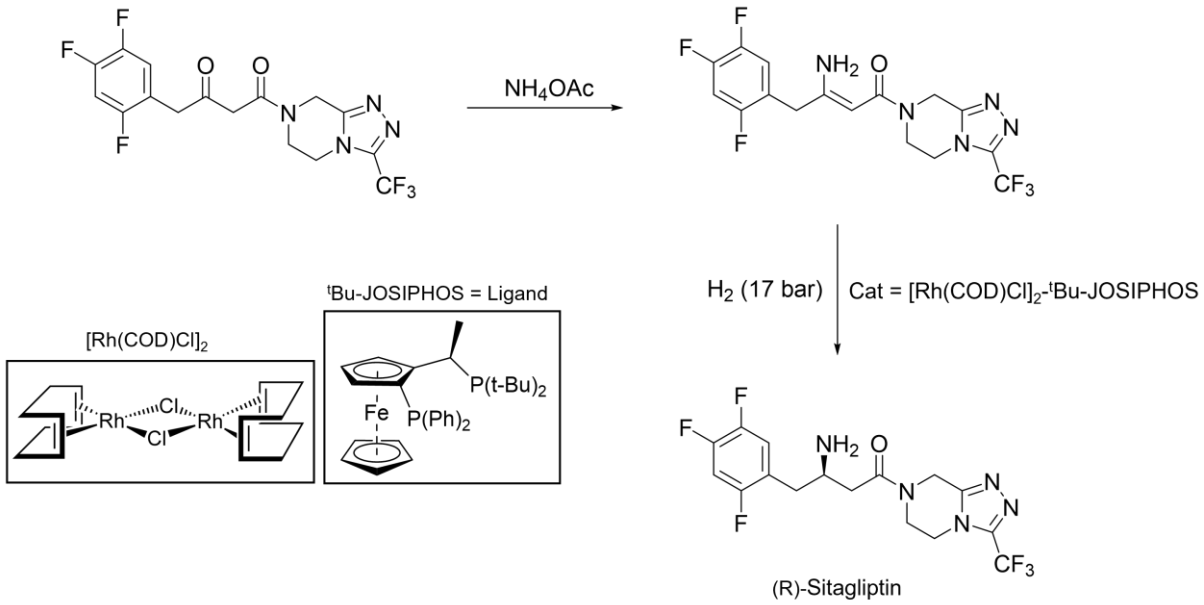

Figure 4. R-Sitagliptin synthesis, adapted from Hansen *et al.* [40].

S-Rivastigmine (Figure 5) is a chiral amine used in the treatment of Alzheimer disease. The synthesis pathway typically involved the enantioselective transformation of a ketone into a chiral alcohol. This step is catalysed by an iridium-based enantioselective catalyst, under gaseous hydrogen (10 atm). A relatively toxic solvent (tetrahydrofuran) is used [42]. Recently, a biocatalytic pathway has been implemented (see vide infra).

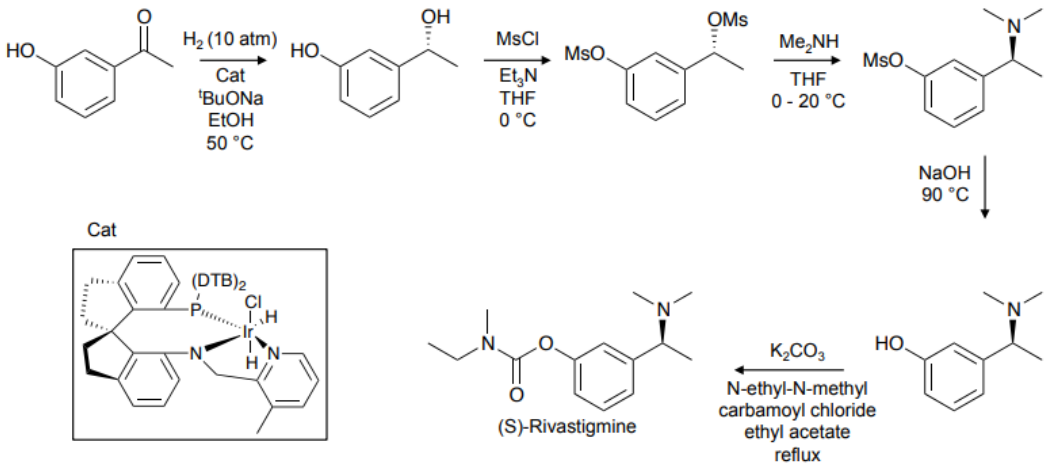

Figure 5. S-Rivastigmine synthesis, adapted from Che *et al.* [42].

In the second approach (chiral resolution), a racemic mixture is first produced. Then, the enantiomers are separated and the distomer is eliminated (removed, consumed, or recycled in the most favourable cases). Thus, the maximal theoretical yield of the chiral resolution is only 50 %. Such a method is applied in industry when no suitable enantioselective catalyst can be found to perform an asymmetric synthesis [43]. Preparative chiral High Performance Liquid Chromatography (HPLC) – based on the use of chiral stationary phase – can in some cases be used to separate enantiomers [44]. However, most methods for enantiomer separation are based on the formation of diastereoisomers (enantiomers that are combined with optically pure chiral compounds) [22]. Diastereoisomers can then be separated according to their physico-chemical properties. For example, when a mixture of diastereoisomers is cooled, one compound crystallizes first and can therefore be removed from the medium while the other compound remains in solution. A liquid mixture of diastereoisomers can also be separated by preparative HPLC on a non-chiral phase. These methods, however, often score poorly in terms of sustainability metrics (large amounts of solvents, low atom economy, etc.).

To illustrate the chiral resolution approach for the synthesis of a chiral amine, Figure 6 shows the synthesis of (S,S)-Sertraline. A S-imine precursor is produced first, starting from the ketone and using methylamine as a reagent in hot toluene. Then, the non-enantioselective reduction of the imine is carried out under pressurized hydrogen with a palladium reduction catalyst. The intermediate product is a diastereoisomeric mixture of (S,R) and (S,S) compounds. The last step consists in the separation of the diastereoisomers, using R-mandelic acid: (S,S)-Sertraline forms an insoluble salt with R-mandelic acid, which crystallizes and is easy to

recover. The other salt (S,R)-Sertraline-mandelate remains soluble [45]. The maximal yield is only 50 % [46,47].

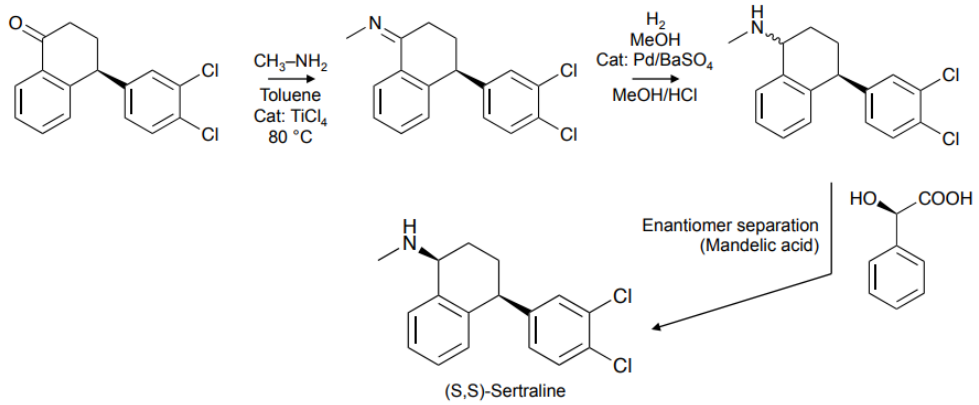

Figure 6. (S,S)-Sertraline synthesis, adapted from Khamar and Modi [47].

A sub-case of chiral resolution is kinetic resolution: starting from a racemic mixture, an enantioselective catalyst aims at the consumption of the distomer, while the eutomer stays unreacted. This method of resolution, that needs an efficient enantioselective catalyst, is of particular interest when the direct asymmetric synthesis of the eutomer is not thermodynamically favoured. Thus, for such reactions, starting from a racemic mixture, the distomer is removed from the reaction medium as it is converted into the product, keeping the eutomer unreacted.

As already mentioned, the above-shown chemocatalytic methods, often score poorly in terms of sustainability. To better align the routes to chiral amines with the principles of green chemistry, it is essential to develop alternative synthesis strategies.

Enzymatic routes to chiral amines

Enzymes are Nature's catalysts, designed along the timespan of evolution to catalyse the chemical transformations in living organisms. They usually exhibit high activity: most of them show turnover rates between 10 and 10000 catalytic cycles per second. Most enzymes are also highly enantioselective (i.e. 100% enantioselective for their natural reactions), and they usually work in mild conditions: aqueous media, mild pH, and low temperature. Cherry on the cake: they are biodegradable and non-toxic (traces of enzymes in the final product would not represent an important issue in many cases) [15].

Various characterized enzymes are currently available in large libraries, ready for industrial use [48]. Moreover, thanks to the great advances in genetic technologies of the last decades, and especially with the advent of directed evolution technologies, recently recognized by a Nobel Price [49], it is now possible to engineer enzymes towards mutated variants endowed with desired properties, *e.g.* higher resistance to organic solvent, higher temperature or pressure resistance, tuned (enantio-)selectivity, broader substrate specificity or even as catalysts of non-natural chemistries [17,50]. Thus, enzymes seem to be the ideal catalysts to process chemical reactions of industrial interest in a greener way. Enzymes can be used to replace some steps in a given chemical process, and can easily be combined with non-enzymatic steps [51,52].

Several enzymes are able to catalyse reactions leading to the production of chiral amines [53]. A selection of these is presented in Figure 7. Lipases have been used by BASF to resolve chiral amines, by catalysing enantioselective amidation, leading to optically pure chiral amines and amides, with excellent enantioselectivity (Figure 7a) [54]. L-selective amidases have been implemented by DSM to produce non-proteinogenic amino acids (*i.e.* that are not naturally found in living organisms): a racemic mixture of 2-aminoamides was converted into optically pure L-amino acids and D-amino amides (Figure 7b) [54]. Similarly, hydrolases catalyse the enantioselective hydrolysis of amides into chiral amines starting form a racemic mixture of amides (Figure 7c) [4]. Ammonia-lyases (AL) are a class of enantioselective enzymes that are able to add ammonia on a carbon-carbon double bound, leading to chiral amines. Among them, aspartic acid ammonia-lyase (AAAL) has been used by Holland Sweetener Company: the addition of ammonia on fumaric acid led to L-aspartic acid, precursor of the famous sweetener Aspartame (Figure 7d) [54]. Tyrosine Ammonia-lyase (TAL) catalyses the enantioselective addition of ammonia on coumaric acid, providing L-tyrosine amino acid (Figure 7e) [55].

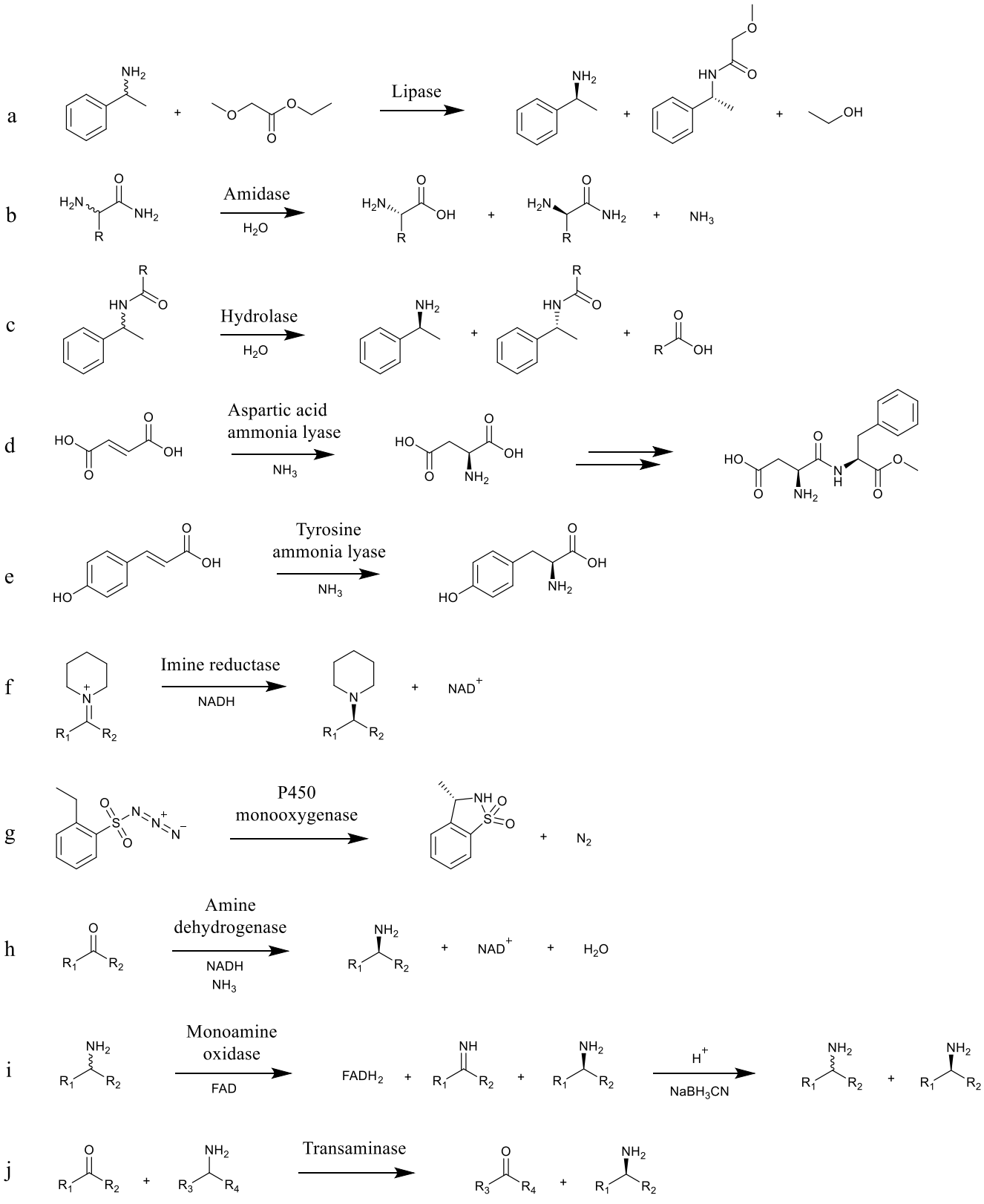

Figure 1. Selection of enzymes catalysing chiral amines production. (a) lipase, (b) amidase, (c) hydrolase, (d) aspartic acid ammonia-lyase and (e) tyrosine ammonia-lyase, (f) imine reductases, (g) P450 monooxygenase, (h) amine dehydrogenase, (i) monoamine oxidase; and (j) transaminase. NADH stands for Nicotinamide Adenine Dinucleotide reduced form, and is a reductant. FAD stands for Flavine Adenine Dinucleotide oxidized form.

Chiral amines can also be produced by the reduction of an imine using imine reductases (Figure 7f). Importantly, such enzymes enable the asymmetric synthesis of chiral secondary amines (*via* reductive amination of ketones). For years, this technology was limited to a narrow scope of substrates that are accepted by the enzyme (mostly cyclic secondary imines) [4,53,56], and required important molar equivalents of amino substrate. However, recent discoveries reported IREDs activity towards acyclic imines, even at low amine:ketone ratios (c.a. 1:1) [57]. Such reports led to the creation of a sub-class of IREDs called the reductive aminases (RedAms). Since its discovery [58], this technology has developed very rapidly in both the academic and industrial sectors (*e.g.* Pfizer), leading to multi-kilograms scale chiral amine syntheses [59].

P450 monooxygenase (Figure 7g) is an enzyme that catalyses chiral intra-molecular C-H amidation, leading to cyclic chiral amines [60]. Amine dehydrogenases and amino-acid dehydrogenases (Figure 7h) catalyse the reductive amination of carbonyl centres into chiral amines. Such enzymes catalyse the addition of ammonia on a carbonyl centre, using NADH as a cofactor [56,61].

Monoamine oxidases (MAO) catalyse the enantioselective oxidation of the distomer amine into a non-chiral imine, using FAD as cofactor (flavine adenine dinucleotide; Figure 7i), leaving the eutomer untouched. The imine is then reduced back to the racemic amine with a non-chiral chemical reagent and can be re-oxidised by MAO. Multiple chemo-enzymatic cycles of oxidation and reduction affords full deracemization of the starting amine [62]. Variants with broader specificities have been engineered to accommodate a wide variety of amine substrates.

Finally, transaminases (TA), also called amino-transferases, are enzymes that catalyse the reversible enantioselective transfer of an amino group from an amino donor (*e.g.* an amine) to an amino-acceptor (*e.g.* a ketone; Figure 7j) [4]. Transaminases currently represent a vibrant field of research for the greener and more concise synthesis of chiral primary amines as they allow shortening their synthesis methods (*e.g.* by avoiding protecting steps) and hence, reducing chemical waste compared to their chemical counterparts [63–65]. Moreover, they show relatively broad substrate scope [63,66], and their cofactor, pyridoxal 5'-phosphate (PLP) is not consumed during the reaction. These aspects make them particularly appealing from an industrial point of view.

3. Transaminases

3.1 Classification

For the transamination catalytic act, transaminases need a cofactor, namely pyridoxal 5'-phosphate (PLP, Figure 8) [67]. This molecule is biosynthesized from vitamin B6. Around 240 different reactions are catalysed by PLP-dependent enzymes that are divided into seven classes (based on the enzyme structure): (I) aspartate transaminase, (II) tryptophan synthase, (III) alanine racemase, (IV) D-alanine transaminase, (V) glycogen phosphorylase, (VI) D-lysine-5,6-aminomutase and (VII) lysine-2,3-aminomutase. PLP-dependent enzymes catalyse racemization, transamination, decarboxylation, elimination, retro-aldol cleavage or Claisen condensation reactions. Many of these enzymes are involved into the metabolism of amino-compounds (amino acids, amino-sugars, polyamines, etc.) [18,67].

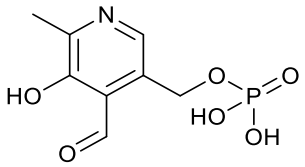

Figure 8. Pyridoxal 5'-phosphate (PLP), the cofactor of PLP-dependent enzymes.

Transaminases are PLP-dependent enzymes of types I and IV (depending on the folding). In living organisms, TAs are involved in the synthesis and the degradation of amino acids, and in the synthesis of some secondary metabolites [20,68,69].

There are two sub-classes of transaminases. α-TA catalyse the transfer of an amino function between alpha-amino acids and alpha-keto acids (the acceptor-carbonyl functions is directly bound to a carboxylic function). ω-TA catalyse the amino transfer on a non-alpha carbon (in addition to the acceptor-carbonyl function, the acceptor molecule may contain a carboxylic function, but is not located on the α-carbon). Among ω-TA, amine-transaminases (ATA), are enzymes that accept amino-acceptors even if they do not bear a carboxylic function next to the carbonyl-acceptor function. Thus, ATA enzymes can convert ketones and aldehydes [18,70,71].

The R-selective ATA transaminase from the soil microorganism *Arthrobacter sp*. KNK 168 has been intensively studied and characterized in the last decade [72,73]. A homologue of this enzyme (99.7% identity) has been commercialized by Codexis, as ATA-117, and the 3D structure has been recently published [74]. It has been the starting point for the production of an engineered enzyme, ATA-117-11Rd, that was developed for the biocatalytic production of R-Sitagliptin [17], and Suvorevant [75,76]. We use this enzyme as the starting point for a more detailed

description of the structure, active site, specificity and reaction mechanism; then we discuss the limitations of ATA and the corresponding mitigation strategies.

3.2 Structure, specificity, and mechanism

ATA transaminases are homo-dimeric enzymes. Two half-active sites are located on each monomer. The two monomers must be assembled for the active sites to be catalytically active [77] (Figure 9, left).

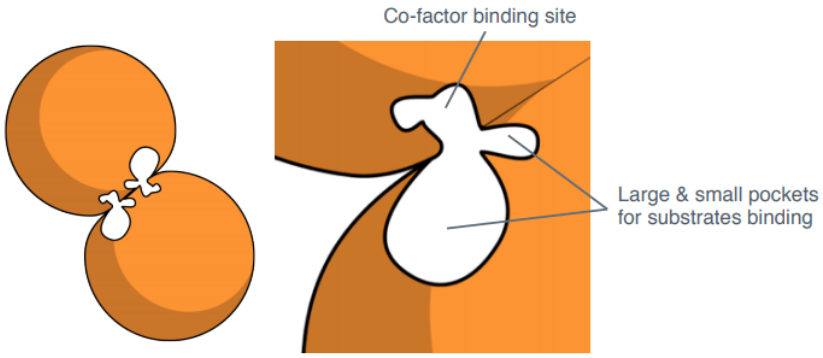

Figure 9. Schematic representation of ATA enzymes. (Left) Scheme of ATA homo-dimers. Subunits must be assembled to form two sites that are catalytically active. The two active sites are located at the interface between subunits. (Right) Schematic representation of an active site.

The active site is made of three pockets: one is dedicated to the PLP binding (Figure 9, right), the two others are assigned to the substrate binding. The PLP-binding pocket exhibits an essential lysine residue for the reversible covalent fixation of the cofactor in its imine derivative (see mechanism, Figure 10). The small substrate pocket only accepts small organic functions (*e.g.* methyl groups). The large pocket is more versatile and accepts larger organic groups (alkyls chains, carboxylic acids, ethers functions, aromatics, etc.) [50]. Thus, ATA-117 is able to catalyse the formation/consumption of amines that contain a methyl group on one side, and larger organic functions on the other side of the amine.

Transaminases act through a “ping-pong bi-bi” mechanism [18,78,79] (Figure 10), catalysing two successive bi-molecular reactions (hence “bi-bi”), the second one following the exact reversed sequence of the forward one. The enzyme reaches an intermediate state after the first half-reaction, and “bounces back” into its initial state after the end of the second half-reaction (hence “ping-pong”).

The first step (Figure 10a) consists in the formation of internal aldimine: the cofactor is covalently, but reversibly, bound to the lysine residue located in the PLP-binding pocket. Then,

the amino donor (here, represented as an amino acid, *e.g.* D-alanine) enters into the active site and is placed in its binding pocket (Figure 10b). The active site only accommodate one enantiomer of a given chiral amine, hence the enantiospecificity of the transaminase [20]. Then, by imine-amine exchange, the amine function (from the amino donor) substitutes the lysine residue (bounded to PLP), and binds the cofactor as an imine intermediate (the lysine anchoring point is then released). In the next step (Figure 10c), a basic residue located in the active site tears off the proton located on the alpha-carbon and the pyridinium ring of the cofactor pulls the delocalized electrons. Electrons are then pushed back and the cofactor is protonated on the other side of the substrate nitrogen by acid catalysis. Hence, electron displacement and acid/base catalysis result in the isomerization of the imine intermediate into a so-called external imine formed between the nitrogen and the alpha-carbon of the amino donor. As a last step of the first half-reaction (Figure 10d) the external imine is hydrolyzed, releasing a carbonyl compound as a by-product (here, an α-keto acid). The cofactor stays in the active site in an aminated form, namely pyridoxamine 5'-phosphate (PMP). Thus, the first half-reaction consists in the deamination of the amino donor (transformed into a keto derivative) and the amination of the PLP (into PMP). Then, the second half-reaction occurs in the exact reverse sequence of events (Figure 10 from e to h), but using a keto-substrate as amino-acceptor and releasing a chiral amine [80–82]. As the transamination reaction is an equilibrated chemical reaction, this mechanism can be read in both ways.

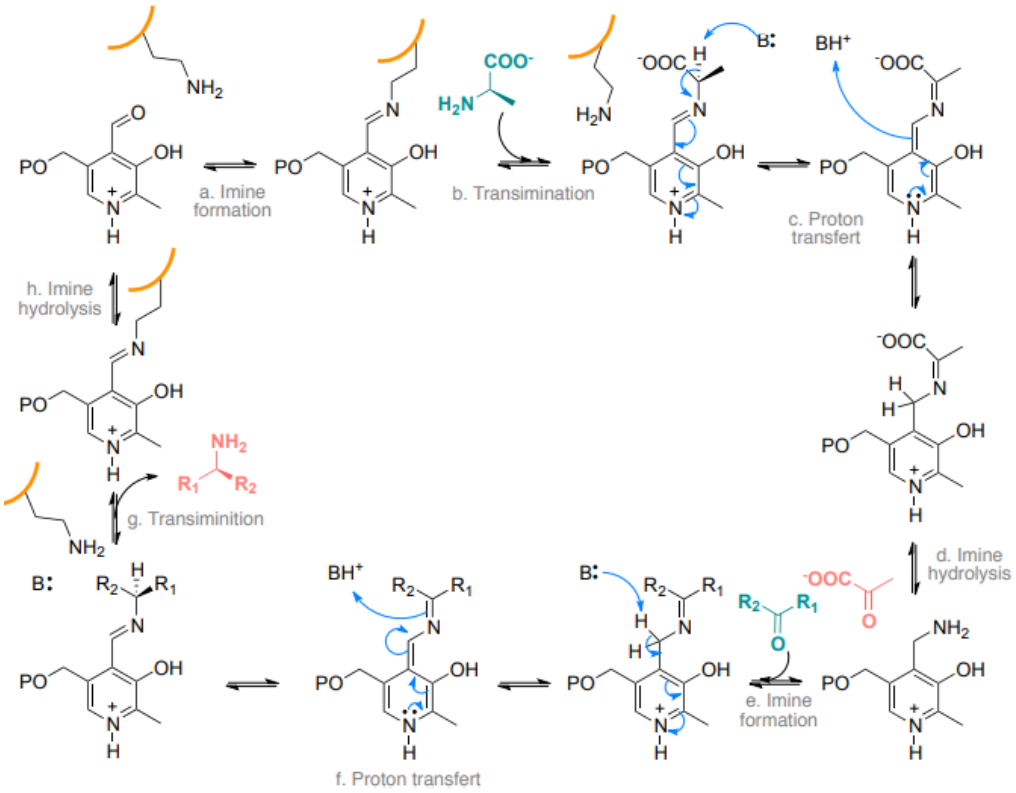

Figure 10 – Transamination mechanism. Substrates and products of the reaction are depicted in green and red respectively. Two half-reactions execute the ping-pong bi-bi mechanism: from (a) to (d), the amine substrate reacts with the PLP cofactor to form the ketone by-product and a PLP amine-derivative (PMP, Pyridoxamine phosphate); from (e) to (h), the ketone substrate reacts with the PMP to form the PLP and release the amine product. PO stands for phosphate, and B for base. Adapted from [80–82].

4. Transaminase-catalysed synthesis of amines: industrial relevance, challenges, and opportunities

Chiral amines can be produced via three different types of enzymatic reactions using ω-transaminases [71,83] (Figure 11): (i) kinetic resolution, (ii) asymmetric synthesis, and (iii) deracemization.

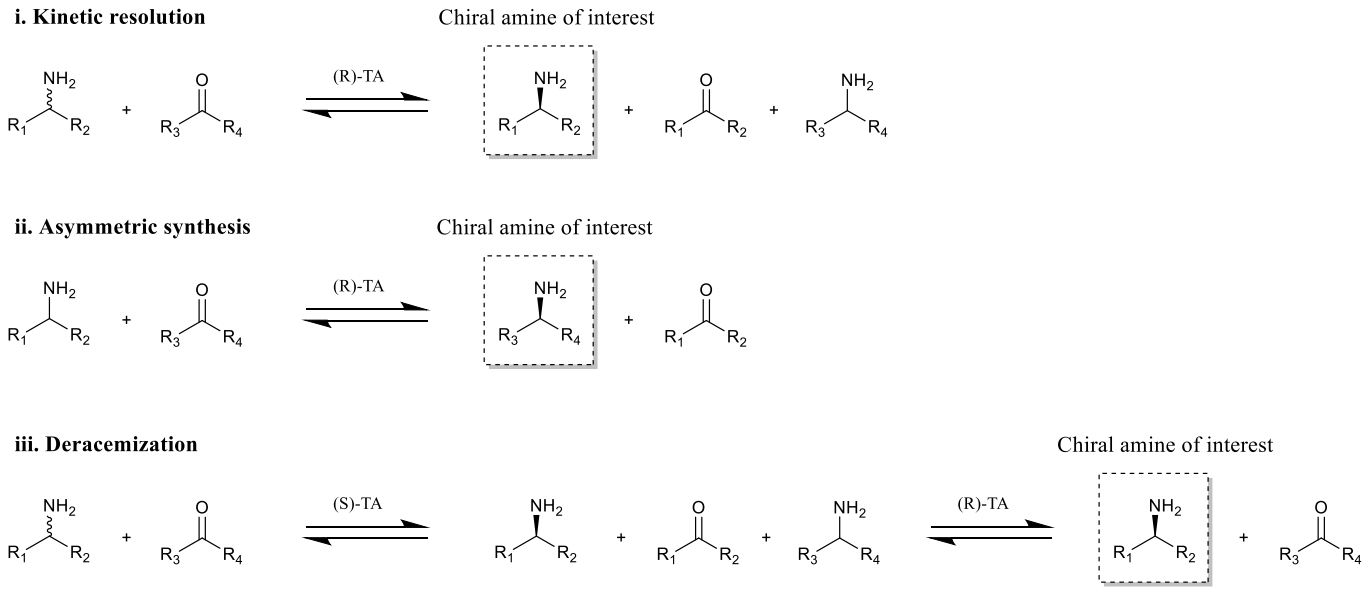

Figure 11. Reactions catalysed by transaminases for the production of chiral amines.

The kinetic resolution starts with a racemic mixture of enantiomers, and the enantioselective enzyme converts only one enantiomer into the corresponding keto-compound. At the end of the kinetic resolution, one enantiomer of the racemic mixture has been converted into ketone, the other one stays unconverted. An aminated by-product is also present in the final mixture. Thus, the maximal yield for the production of chiral amines using kinetic resolution is only 50 %. Also, when using amines (not amino acids) as amino donor, the co-product is a ketone (not a keto acid as in the biological systems) that can inhibit the transaminase if it accumulates in the medium [20,71,84]. The main advantage of the kinetic resolution is that it only requires one enantioselective enzyme [80].

In the asymmetric synthesis, a pro-chiral ketone is converted into a chiral amine using an amino donor and producing a ketone by-product. If the enzyme is perfectly enantioselective and the chemical equilibrium position is favourable, the maximal yield is 100 % as all the pro-chiral ketone is stoichiometrically transformed into chiral compound. Moreover, this method only requires one enzyme. However, the asymmetric synthesis *via* transamination suffers from two severe limitations: first, most transaminases are inhibited by ketones (*e.g.* acetone when the amino donor is isopropylamine, IPA). Second, the asymmetric synthesis of chiral amines (that are not amino acid) is not favoured thermodynamically [71,80]. In Nature, transaminations between α-keto acids and α-amino acids are fairly equilibrated reactions (Figure 12, top), because α-keto acids and α-amino acids substrates and products have similar free energies [20].

However, thermodynamically, amines (*i.e.* not amino acids) are less stable than amino acids, while ketones (as compared to α-keto acids) are more stable than α-keto-acids (Figure 12, bottom). Thus, the chemical equilibrium is driven in the unwanted direction [20]. Employing amines as amino-donor (*e.g.* IPA) instead of amino-acids allows benefiting from a less unfavourable thermodynamic equilibrium.

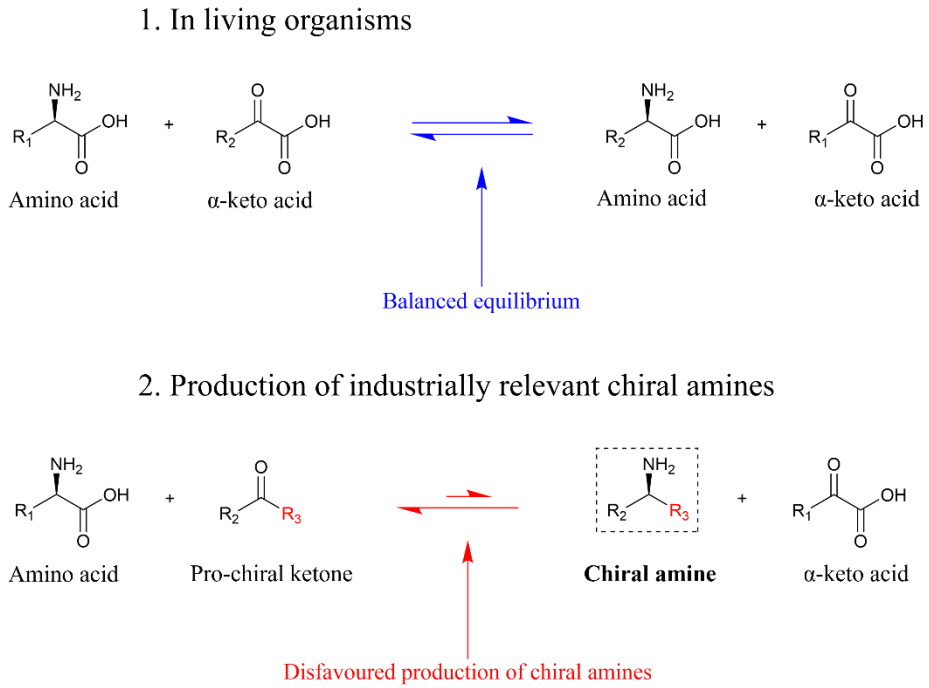

Figure 12. Transamination for the production of chiral amines. Transaminations that involve only α-amino acid and α-keto acids (as mostly the case in living organisms) are governed by a well-balanced equilibrium. As the chemical and pharmaceutical industries need to produce chiral amines that are not amino acids (*i.e.* R is not a carboxylic acid), the transamination requires the use of ketones that are not α-keto acids. However, ketones are not easily aminated. Thus, the equilibrium reaction to produce chiral amines is not favoured.

Deracemization involves a kinetic resolution, starting with a racemic mixture, followed by an asymmetric synthesis. First, an enantioselective transaminase (*e.g.* S-selective TA) converts the distomer from the racemic mixture into the corresponding ketone, leaving the eutomer untouched. Then, a second transaminase of reversed enantioselectivity (*e.g.* R-selective TA) back-converts the ketone into the eutomer. Thus, by this method, the maximal theoretical yield is 100 % [85], and no inhibiting ketone is accumulated, as only α-keto acid is accumulated at the end of deracemization (if starting from α-keto acid as amino acceptor). However, this method requires two enzymes (and suffers from unfavourable thermodynamics in the asymmetric synthesis reaction) [86].

4.1 Industrial relevance

Some transamination reactions are already developed at kilo- and pilot-scales for drug manufacture in batch reactors [87], *e.g.* Sitagliptin (anti-diabetic drug), Suvorexant (sleep regulation) and Ivabradine (heart-rate regulation) production. R-Sitagliptin is produced by Merck at high concentration (250 g/L), in 50 % DMSO at 50 °C, using the engineered transaminase ATA-117-11Rd (Figure 13a). In 2009, Merck scaled up the new process to pilot scale, and plans to commercialize this technology are now moving forward [88]. Thus, the transamination reaction should be implemented instead of the chemocatalytic synthesis involving a rhodium catalyst and high-pressure hydrogen [17,18]. The product obtained by the biocatalytic approach had higher optical purity which made further crystallization steps unnecessary; the total waste production was cut by approximately 20% and the productivity of the global process was increased by ca. 53% [89].

The same enzyme is used by Merck to produce Suvorexant (MK-4305) at kg scale: the biocatalytic transamination reaction uses IPA as the amino donor and significantly shortens the synthetic pathway by leading to a key-intermediate (Figure 13b). The entire synthesis requires only four linear steps for completion and proceeds in 43% overall yield [90,91].

ATA-117 is also employed to produce a key building block in the synthesis of another candidate for the treatment of insomnia: Filorexant (MK-6096) [75]. Performed in a 100 L total volume and starting from 4.5 kg keto-diester substrate, the transamination reaction uses D-alanine as amino donor and a coupled Lactate dehydrogenase/Glucose dehydrogenase (LDH/GDH) regeneration system. It resulted in 74% yield and 99% enantiomeric excess. This transamination reaction was integrated in the nine-steps chemoenzymatic synthesis of MK-6096 (at kg-scale). A 13% overall yield was first achieved. Improvements of the biocatalytic system (*i.e.* CDX-010 transaminase employing IPA and a different keto-diester precursor, enabling the use of a single-enzyme system) allowed further increasing the synthesis efficiency [92,93] (Figure 13c). The MK-6096 target is now synthesized through a four-step process based on crystallization-induced dynamic resolution (CIDR) of the chiral intermediate, reaching 40% overall yield.

Another remarkable example is the use of ATA from *Vibrio fluvialis* (*Vf*-ATA) in a pre-industrial process developed by AstraZeneca for the production of a key intermediate in the synthesis of a kinase (*i.e.* JAK2) inhibitor, AZD1480 (used for the treatment of idiopathic

myelofibrosis) [94,95] (Figure 13d). S-MBA was used as amino donor and an in-situ co-product removal (IScPR)-based strategy was employed to push the equilibrated reaction towards the formation of the targeted intermediate [96]. Briefly, the acetophenone co-product was extracted from the aqueous phase by the use of a biphasic system (20 % (v/v) toluene). Subsequent scale-up of the biotransformation allowed reaching 68% yield and 99% enantiomeric excess when employing the Codexis enzyme, TA-P1-A06. The intermediate has been then used in the chemoenzymatic synthesis of AZD1480 on a 100 L scale, which resulted in > 30% overall yield.

In 2017, Burns et al. (Pfizer Inc.) reported a chemo-enzymatic route for the synthesis of key chiral intermediates of a γ-secretase inhibitor, employing a transaminase and an alcohol dehydrogenase [97] (Figure 13e). The researchers performed a screening of a relatively large enzyme library for the conversion of a substituted tetralone to the corresponding S-amine intermediate. ATA-47 from LCeta, was selected to run the reaction at large scale. The scaled-up transamination enabled the production of nearly 40 kg of enantiopure amino-compound, in a 94% isolated step yield.

In 2021, an efficient large-scale production of a chiral precursor of Sacubitril (a key component of the heart failure drug Entresto), was reported by researchers at Codexis Inc [98] (Figure 13f). Starting from a *Vf*-ATA variant (ATA-217) displaying unsatisfactory biocatalytic performance, 11 rounds of directed evolution were performed to obtain a more active mutant. Additionally, an IScPR strategy based on acetone evaporation was employed to drive the thermodynamic equilibrium (by running the reaction at as high as 58 °C). In lab-scale assays, the final variant (CDX-043) reached 90% conversion at high IPA (1 M) and ketone substrate concentration (75 g/L) within 24h at 58 °C. CDX-043 was subsequently selected for the multi-kg scale sacubitril production. To this end, a large-scale fermentation was implemented to produce c.a. 200 kg of CDX-043 (lyophilized clarified cell lysate), which was in turn used to produce a total amount of c.a. 20 kg of the sacubitril precursor.

A novel synthesis pathway featuring a transamination reaction leading to MK-7246 drug (used for the treatment of respiratory disease) was recently implemented at pilot-plant scale production (> 100 kg). This route proceeds in eight steps, requires no chromatographic purification and features a dramatically improved overall yield and productivity with respect to the previous reported chemo-catalytic syntheses. CDX-017 transaminase, with IPA as amino donor, were employed for the transamination reaction [76] (Figure 13g).

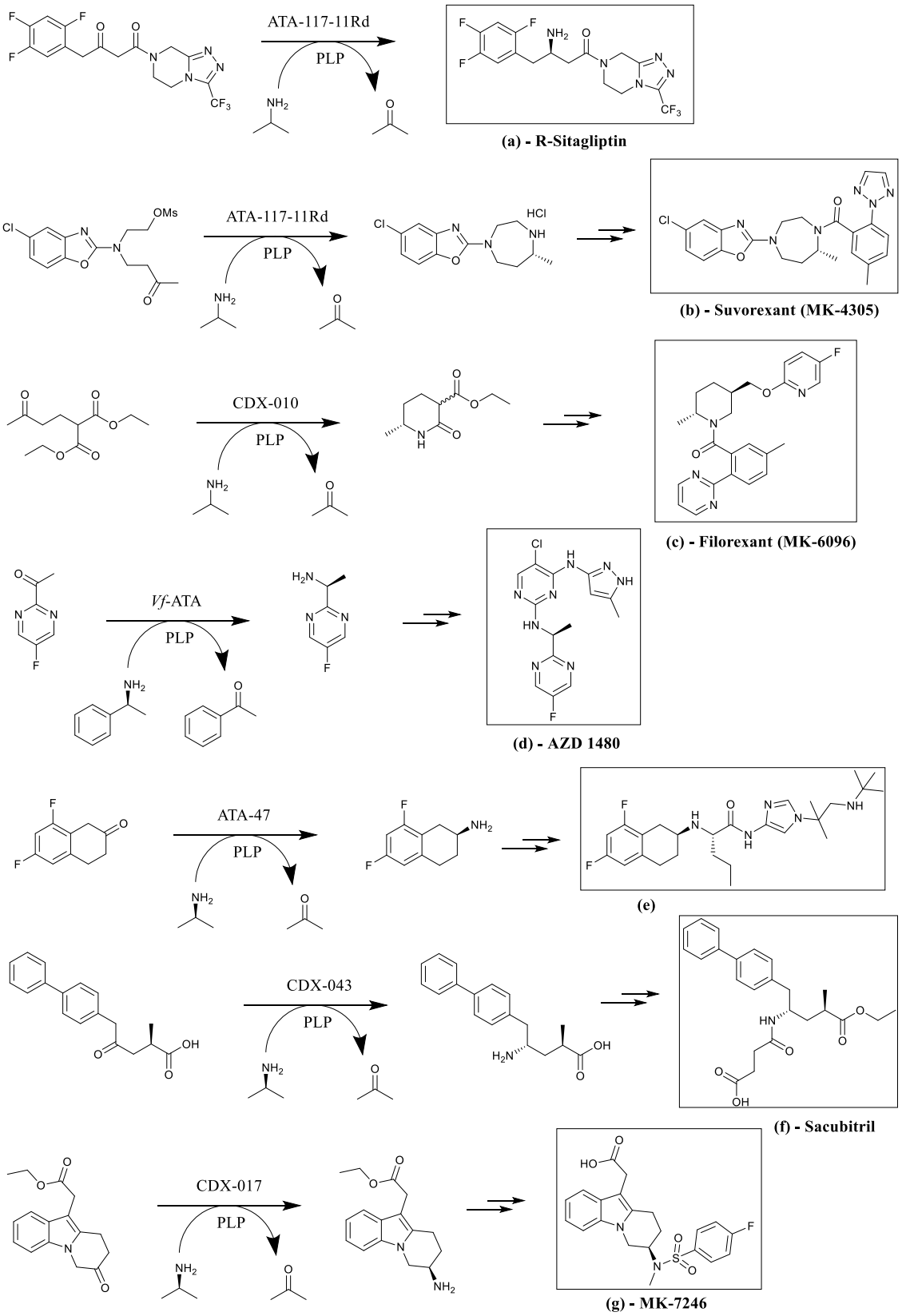

Figure 13. Selected applications including transaminations implemented at large-scale (industrial and multi-kg scale) in batch. OMs stands for methanesulfonate (mesylate) group. Framed compounds represent the target chiral amine of interest.

Other interesting examples were reported using commercially available ATAs, although on a smaller scale (> 100 mg to g scale) [66,99]. Typically, a *Vf*-ATA variant (*Vf*-TA r414) displaying a 60-fold increase in activity toward the oxooctanoate substrate with respect to its wild-type counterpart, allowed the straightforward synthesis of Imagabalin (277 mg, 95% diastereomeric excess) [100]. Similarly, S-Ivabradine was successfully synthesized at a preparative scale, by means of a four-step sequence including transamination reaction (i.e. using transaminase from Codexis with IPA as amino donor). A 50% overall yield and excellent enantioselectivity were obtained [18,101]. Besides, an ATA from *Chromobacterium violaceum* (*Cv*-ATA) was employed to efficiently perform the asymmetric synthesis of a key intermediate for the production of the anti-allergic drug Ramatroban. The practical applicability of this transamination reaction was demonstrated on a 500-mg scale. Excellent yield (96%) of the R-amine (in enantiopure form) was obtained [102]. In 2021, von Langermann *et al.* [103] implemented a crystallization-assisted semi-continuous transamination for the gram-scale preparation of S-(3-methoxyphenyl)ethylamine, a valuable intermediate of Rivastigmine. Briefly, the authors leveraged on an *in-situ* product crystallization (assisted by the evaporation of the by-product, acetone, under mild vacuum) to shift the transamination reaction towards completion. The resulting crystal was easily recovered via filtration, and the enantiopure amine product was obtained at high concentration (> 1 M). The transaminase from *Silicibacter pomeroyi* (*Sp*ATA) was employed for this study. Kohrt and co-workers demonstrated the synthesis of a valuable chiral spirocyclic intermediate (1-Oxa-8-azaspiro[4.5]decan-3-amine) at the gram scale (580g), employing Codexis ATA-200. Such biocatalytic reaction reached 82% yield and allowed boosting the enantiomeric excess from 70% to 97.8% with respect to the chemocatalytic route (*i.e.* a hazardous azide-mediated S_N2 reaction followed by a Staudinger reduction) [104]. Last but not least, we must mention the production of S-methoxy-isopropylamine by an optimized transaminase from *Bacillus megaterium*, using IPA as the amino donor [105]. The product is a key-intermediate for the production of Metolachlor, a widely used herbicide [34].

4.2 Challenges and mitigation strategies

Despite the successful examples cited in the previous section, the use of transaminases for the production of chiral amines suffers from two major limitations: (i) when using amines as amino donor, the transaminases are strongly inhibited by the ketone by-product; and (ii) the thermodynamics does not favour the production of chiral amines that are not amino acids. Those

limitations hamper the enzymatic production of chiral amines at industrial scale. Therefore, strategies have been developed to obtain chiral amines at high yield, and high concentration. They can be split in three categories (Figure 14): (i) strategies aiming at enhancing the enzyme performance or robustness, (ii) strategies aiming at shifting the equilibrium by physico-chemical effects (mono-enzymatic methods) or by combining several enzymes in addition to TA (multi-enzymatic methods) [20,106], and (iii) strategies aiming at enhancing the enzyme recoverability by immobilization in/on solid supports. In practice, many studies have combined several strategies [6], and the classification is not so straightforward.

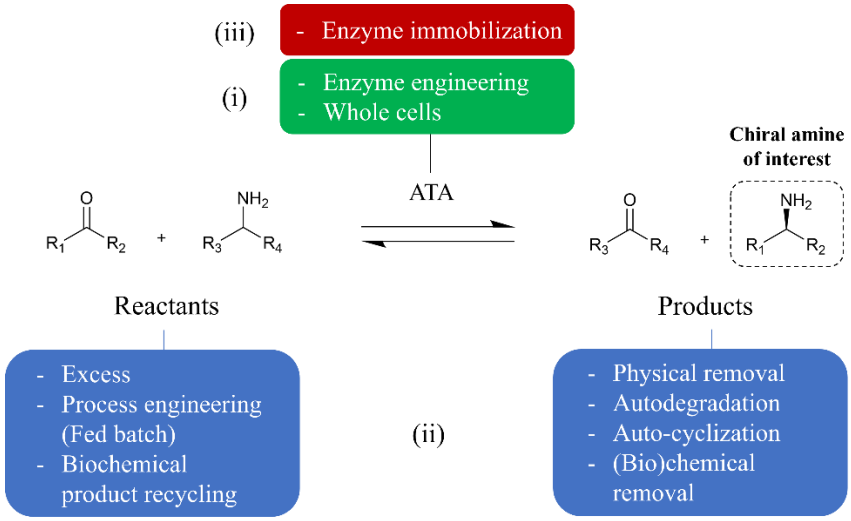

Figure 14. Enhancement strategies. Strategies addressing the issues of ketone inhibition and unfavourable thermodynamics.

4.2.1 Enhancing enzyme scope and robustness

At the enzyme scale, there are three approaches to prevent enzyme inhibition by ketone compounds: applying enzyme engineering techniques on available enzymes, using whole cells, and exploiting extremophiles-derived enzymes.

The enzyme engineering strategy allows the production of enzyme mutants that exhibit new properties as compared to the wild type enzyme. For example, engineered transaminase could be more tolerant to high substrate and/or product concentrations. The resulting enzyme would not be inhibited anymore (or at a lower level) [20]. This strategy allows getting enzymes that are more suitable for industrial applications: stable under non-physiological conditions (high

concentrations, organic solvent), increased working and storage duration [20,107]. In practice, there are two ways to produce mutated enzymes [71]. First, directed evolution approaches based on iterative cycles of random mutagenesis and variant screening can be envisioned [108]. In this strategy, the enzyme structure is not necessarily known and mutations are introduced in the gene encoding the enzyme of interest in a random or partially random manner. A library of microorganisms expressing the enzyme variants is then created. Then, the library is screened to identify the colonies that express the enzyme exhibiting the interesting properties. The interesting colonies are then selected. For example, Kim *et al.* [109] created and identified a mutated version of *Vibrio fluvialis* transaminase that shows better tolerance to aliphatic ketones (as compared to the wild-type transaminase). The second method for mutated enzymes production is based on site-specific mutagenesis. This requires knowing the enzyme structure. By a rational design approach (identifying the link between amino acid sequence and enzyme 3D structure), it is possible to predict the properties of a desired mutant where a specific amino acid would be replaced by another (predictions and modelization *in silico*) [71]. However, our capacity to rationally predict mutations that will modify the properties of an enzyme in a desired way is still very limited and many strategies are combining rational and random approaches. For example, Savile *et al.* [17] used a substrate walking approach to predict the effects of mutations of the active site on the substrate pocket affinity. The wild type enzyme (ATA-117) does not accept large substrate in its pocket. After 11 rounds of mutations (a combination of site-directed and random mutations), a mutated enzyme (ATA-117-11Rd, exhibiting 27 mutations) was able to accept larger substrate in its active site pocket. Then, the mutated enzyme was able to catalyse the synthesis of Sitagliptin, an anti-diabetic drug (see Figure 1), with excellent yield (92%) and enantioselectivity (> 99%). Moreover, the mutated enzyme exhibited better tolerance to the organic solvent (DMSO) and amino donor (IPA). Besides engineering known enzymes, the availability of genome sequences has been increasing exponentially, giving straightforward access to large diversities of genes encoding natural enzymes including ATAs that can be screened for specific activities and used as starting points in directed evolution campaigns [6]. These novel biocatalysts represent a massive addition to the application of ATAs for the industrial synthesis of enantiopure amines [110]. Nevretheless, high cost, time consumption and uncertainty are intrinsically associated with the engineering of enzymes featuring desired properties [20].

In addition to enzyme engineering, the sourcing of biocatalysts from extremophilic organisms also taps into key strategies to address the insufficient stability of ATAs [111–113].

Extremophiles are microorganisms that are adapted to survive in ecological niches such as extreme temperatures (– 5 and 130°C) and pH (0–12), high salt concentrations (3-35%) and high pressure (up to 1000 bar) [114]. The adaptation process of extremophiles has affected the features of their enzymes providing them remarkable properties with respect to their mesophilic counterparts. Although these natural organisms are often difficult to cultivate in large quantities in the laboratory, their genes can be cloned and the corresponding enzymes overexpressed in large amounts, for example in *Escherichia coli* [115]. Accordingly, extremophile enzymes often result in more robust biocatalysts, that offer versatile tools for a variety of industrial applications. For example, halophilic enzymes remain active under extremely high salt concentration and have been reported to be stable under ‘‘dry condition’’ (low water concentration) [116,117]. As salt greatly reduces water activity of the medium, halophilic enzymes might become the choice for biocatalytic processes performed in low water activity environments like aqueous/organic and non-aqueous media [118,119]. Similarly, thermophilic strains provide a rich library of proteins with increased stability not only to high temperatures, but also to organic solvents and proteolytic enzymes [115,120,121].

In 2015, the Paradisi group cloned and expressed the first ATA from a halophilic bacterium, *Halomonas elongata* (HeWT) [122]. HeWT showed good tolerance to a series of co-solvents up to 20% (v/v), and optimum activity at pH 10. It was highly S-selective and showed broad substrate scope, making it a promising candidate for industrial applications [123]. New ATAs have been recently identified from thermophilic microorganisms [124,125], including *Geobacillus thermodenitrificans* and from *Thermomicrobium roseum* [126,127]. These biocatalysts display optimal temperatures at 65 and 80 °C, respectively, and their activity increases after thermal pre-treatment at 60–65 °C.

Arguably, the development of novel ATAs based on extremophiles enzymes that are be further improved through enzyme engineering is currently emerging as major playground researchers who can start exploring pristine chemical spaces [128,129].

Another strategy consists in the use of whole cells. In this case, the interesting transaminase is overexpressed in living cells, which are then used as such as living catalysts. In this way, the enzymes are protected against extreme environment conditions by the natural cytoplasmic membrane. For example, Kroutil *et al.* [130] used *Escherichia coli* cells (containing an over-expressed transaminase) to produce aliphatic chiral amines by kinetic resolution. The main disadvantages in the use of whole cells are (i) substrates and products must be able to penetrate

and come out of the cells; (ii) the need to feed the living cells, and the potential interferences with other metabolic pathways [131].

4.2.2 Enhancing reaction yield by shifting the equilibrium

The equilibrated transamination reaction that is catalysed by the transaminase is often unfavourable, and should be pushed towards the product side either by using an excess of substrate, or removing a product. This can be achieved by chemical, biocatalytic, or engineering strategies.

An excess of IPA (50-fold excess) has been successfully used by Truppo *et al.* [132] in the amination of acetophenone, using ATA-117. The product, R-methylbenzylamine (R-MBA) was obtained at high yield (95 % conversion) and high enantiomeric excess (> 99%). However, most wild-type ATAs do not accept IPA under standard conditions, and need thus to be engineered to display such desirable property [11,122].

Inhibition caused by the substrate (in high concentration) can be avoided by process engineering: a fed-batch strategy allows feeding progressively the reaction medium with the substrate, so that its concentration remains below the inhibition limit. Lye *et al.* [133] used such fed-batch strategy for the progressive addition of IPA in a bioreactor (containing a transketolase and a transaminase). They synthesized a chiral amino-alcohol product ((2S,3S)-2-aminopentane-1,3-diol) with satisfying yield (70 %), avoiding the inhibition caused by high IPA concentration (due to alkaline properties of IPA).

Another strategy used to shift the equilibrium towards the asymmetric synthesis consists in the removal of products and by-products [20]. Shin *et al.* [134] used IPA as amino donor for the production of L-homoalanine (from 2-oxobutyric acid, previously synthesized from L-threonine), leading to the co-production of acetone that was easily eliminated from the reaction medium by evaporation. Products and co-products can also be extracted from the reaction medium by liquid-liquid or liquid-solid extractions [135–138]. Noteworthily, as previously mentioned, researchers from von Langermann group implemented an *in-situ* product crystallization (ISPC) assisted by co-product (acetone) evaporation to perform the synthesis of S-methylbenzylamine derivatives, such as S-(3-methoxyphenyl)ethylamine (S-MEA) [103,139]. Such an elegant strategy relied on the use of crystallization agent (i.e. bulky carboxylic acid such as 3-diphenylpropionic acid) able to form poorly soluble crystalline salts with S-MEA, hereby driving the transamination equilibrium.

Products can also be removed from the system by an auto-conversion pathway. Green *et al.* [140] propose the use of ortho-xylylenediamine as amino donor for the transamination (using ATA-113). The by-product (1H-isoindole) spontaneously undergoes tautomerization, leading to the formation of 2H-isoindole that polymerizes and precipitates into a blue compound. This spontaneous product tautomerization and subsequent precipitation drives the chemical equilibrium towards the production of S-1-(4-fluorophenyl)propan-2-amine (from (4-fluorophenyl)acetone). However, it should be noted that the amino donor employed in this study is more expensive than alanine or isopropylamine.

Product removal has also been conducted through co-product cyclization. For example, by using lysine as amino donor, Hsu *et al.* [141] produced L-homophenylalanine (from 2-oxo-4-phenylbutanoic acid) in high yield (97 %) and with high enantiomeric excess (> 99.9 %), as the by-product (2-keto-6-aminocaproate) spontaneously cyclizes and then, drives the equilibrium. Also, this cyclization allows avoiding the inhibition by the by-products.

In multi-enzymatic approaches, another enzyme is used in conjunction with the transaminase, either to consume the by-product, or to recycle the by-product into fresh substrate. By using enzymes purified from similar cell media, multi-enzymatic methods (also called enzymatic "cascades") are easily practicable in one-pot system [50] (Figure 15). While several types of cascade have been defined in the field of biocatalysis (linear, parallel, orthogonal, and cyclic) [50], the one that is the most relevant in the field of chiral amine synthesis using transaminase is the orthogonal cascade. In the latter, a first reaction allows the production of a product of interest and a by-product (or intermediate) that is transformed in a second reaction. This kind of cascade allows the equilibrium displacement (by withdrawing the by-product) towards the formation of the product of interest. When alanine is used as amino donor, the transamination leads to the production of pyruvic acid (or pyruvate salt) as the by-product. Several strategies have been implemented to catalyse the consumption of pyruvate to shift the equilibrium.

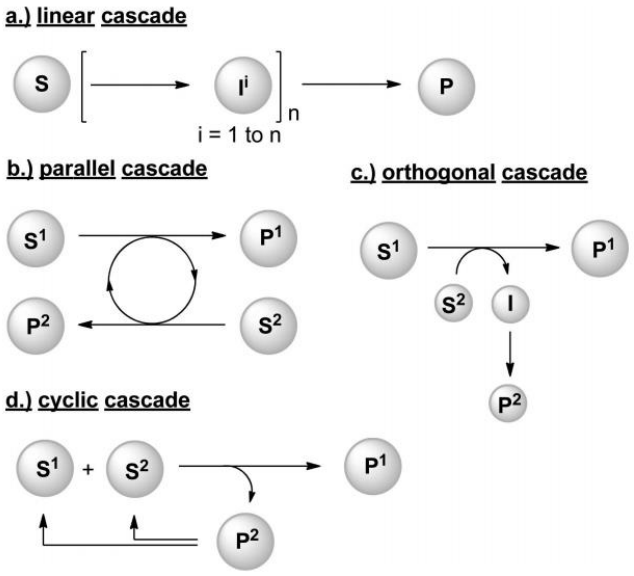

Figure 15. Overview of different types of enzymatic cascades. S, I and P respectively stand for starting material, intermediate, and product. P^1 is the desired product. Reproduced from ref. 50 with permission from American Chemical Society, copyright 2014.

For example, lactate dehydrogenase (LDH) allows converting pyruvate into lactic acid, using NADH as the cofactor (Figure 16) [83,132,142,143]. This strategy has been successfully used by Meadows *et al.* [135] for the production of S-1-(5-fluoropyrimidin-2-yl)ethylamine. Moreover, the amine of interest was extracted in an *in situ* product removal (ISPR) approach by supported liquid membrane (SLM), leading to a final 98 % yield, and high amine purity.

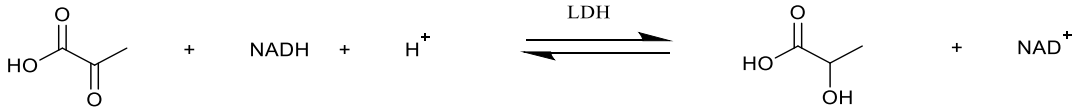

Figure 16. Reaction catalysed by lactate dehydrogenase. Lactate dehydrogenase (LDH) allows to transform pyruvic acid into lactic acid, using NADH.

Other enzymes allow converting pyruvic acid. For example, pyruvate decarboxylase catalyses the decarboxylation of pyruvate into acetaldehyde and CO_2 [144]; and alanine dehydrogenase allows the recycling of pyruvate into alanine (the amino donor), using ammonia and NADH as a cofactor [145].

If IPA is used as amino donor, acetone is produced as by product. Then, alcohol dehydrogenases (*e.g.* yeast alcohol dehydrogenase, YADH) can catalyse the reduction of acetone into isopropyl-alcohol, as proposed by Berglund *et al.* [146] (Figure 17).

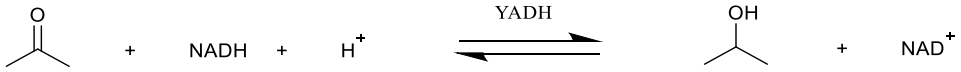

Figure 17. Reaction catalysed by yeast alcohol dehydrogenase. Yeast alcohol dehydrogenase (YADH) catalyses the reduction of acetone in the presence of NADH.

Many of those enzymes are using NADH as reducing agent, in stoichiometric amount. However, this reagent is highly expensive and thus, needs to be recycled. Two main enzymes allow the recycling of NADH (towards the implementation of parallel cascades): glucose dehydrogenase (GDH) and formate dehydrogenase (FDH). GDH catalyses the oxidation of D-glucose by NAD^+ (the oxidized form of NADH) into ∂-gluconolactone (releasing NADH; Figure 18). This method has been extensively studied [86,132,145,147]. Formate dehydrogenase catalyses the oxidation of formic acid in the presence of NAD^+, into CO_2 and allows the recycling of NADH [146,148].

Figure 18. Reaction catalysed by glucose dehydrogenase. Glucose dehydrogenase (GDH) catalyses the oxidation of glucose by NAD^+ to form ∂-gluconolactone and NADH.

4.2.3 Enhancing recoverability and reusability: the key role of immobilization

The great efficiency of enzymes is well established. Once the gene coding for the enzyme of interest is known, it is usually possible to produce the latter at large scale and to isolate it. It may be noted that technical difficulties can be encountered, related to the lack of stability for highly engineered enzymes, or with purification (e.g. filtration is not straightforward; ATA-117 monomer is 3 nm in size [74]). More significantly, for the subsequent use of the free enzymes in industrial processes, poor long-term stability and difficult recovery and recycling often represent the most important shortcomings [149–151].

Immobilizing the enzymes on solid carriers allows envisaging a facile recovery of the biocatalysts at the end of the reaction. Thanks to immobilization, it can be envisioned to reuse the enzymes, or to implement continuous processes, where the enzymes are maintained in the reactor while the reaction medium is flowed through (*vide infra*, Section 5) [151–153]. The facile

separation of the solid biocatalyst from the reaction medium also allows minimizing or avoiding protein contamination of the product [154,155]. Furthermore, some immobilized enzymes have shown remarkable enhancement of their properties as compared to the free enzyme: *e.g.* enhanced selectivity [156], improved stability towards storage and operational conditions [157,158]. While most enzymes are inactive or perform poorly in organic solvents, immobilized enzymes may exhibit a higher activity in organic [159].

Since one particular challenge is to make the enzymes recyclable while maintaining their activity, the enzyme leaching from the surface of the support during operation must be prevented. Avoiding enzyme leaching is of upmost importance regarding process sustainability and can be more challenging to achieve in continuous flow-mode as compared to batch. In most cases, a compromise has to be found between a good immobilization and a good retention of enzyme activity [160]. Indeed, the immobilization can strongly affect the enzyme structure or/and reduce the accessibility to active sites, and therefore, the enzymatic activity [157,161]. Therefore, the main challenges of immobilizing enzymes are: (i) getting an efficient attachment of the enzymes on the carrier to avoid the enzyme leaching, while concomitantly (ii) retaining the enzymatic activity.

It is generally admitted that enzyme immobilization has to be envisaged case-by-case, as a function of the enzyme properties (surface composition, charge, active site location), of the reaction of interest (operating conditions), of the solid carrier that is envisaged, and depending on the targeted improvements (stability, activity, substrate specificity, product selectivity, etc.). Immobilization methods are generally sorted in three categories: (i) Enzyme hooked at the surface of a support (either by adsorption, site-specific affinity attachment or covalent grafting), (ii) enzyme entrapment and encapsulation, (iii) enzyme cross-linking. Noteworthily, a combination of two immobilization strategies is often implemented in order to overcome the drawbacks presented by one immobilization strategy (*e.g.* cross-linking of entrapped enzymes to prevent their leaching from the carrier porosity) [154,162,163].

Many excellent reviews cover extensively enzyme immobilization methods [154,159,161,164–166]. Here, we provide the reader with a concise summary in Table 1 with the aim to highlight, for each immobilization strategy, the type of interactions that are involved, the spatial localisation of the enzyme, and the pros and cons.

Table 1. Summary of enzyme immobilization strategies and some of their main features.

		Entrapment	Adsorption (electrostatic or hydrophobic interactions)	Site-specific affinity attachment	Covalent grafting	Cross linked enzyme aggregates or crystals (CLEAs or CLECs)
Type of interactions involved		Reversible (Van der Waals, H-bonds)	Reversible (hydrophobic interactions)	Reversible (electrostatic interactions)	Reversible or irreversible	Reversible or irreversible
Enzymes localization		Carrier porosity	Carrier surface	Carrier surface	Carrier surface	Carrier-free
Features	**pros**	Mild enzyme distortions Enzyme protection by the carrier Direct assembly of the solid catalyst (carrier + immobilized enzyme in one pot)	Mild enzyme distortions Enzyme immobilization is tuneable (adapting carrier hydrophobicity or pH and pI during adsorption)	Mild enzyme distortions Possibly combined with enzyme purification Controlled enzyme orientation	Enzyme leaching prevention (strong interactions)	No need for enzyme carrier High catalyst productivity (kg product per kg catalyst) Enzyme leaching prevention (strong interactions)
	cons	Enzyme leaching (low stability) Possible diffusional limitations through carrier's pores	Enzyme leaching (low stability)	Enzyme leaching (low stability)	Possible rigidification of the enzyme structure	Possible diffusional limitations Possible rigidification of the enzyme structure

Typical immobilized enzymes formulations	Encapsulation into a polymer or a sol-gel matrix	Adsorption onto hydrophobized silica (with carbon moieties) Electrostatic interactions with polyelectrolytes (*e.g.* chitosan), pristine silica, etc.	His-tag binding onto metal-derivatized carriers	Covalent grafting onto epoxy-resins Covalent grafting onto glutaraldehyde functionalized carriers	Enzymes aggregates cross-linked with glutaraldehyde
Useful ref.	167,168	163,169–172	173,174	131,175	176–178

Focusing specifically on transaminases, Table 2 highlights examples of the strategies that have been reported to prepare efficient heterogeneous biocatalysts for transamination reactions. Most of the time, immobilization allowed improving the performance of the transaminase, either in terms of stability or activity.

Table 2. Non-exhaustive list of examples of transaminase immobilization reported in the literature.

Method of Immobilization	**Material**	**Enzyme and type of reaction catalysed**	**Ref.**
His-tag	Glass carrier	ω-TA (kinetic resolution)	179
Adsorption	Sepabeads® octadecyl-grafted resin	ATA-117-11Rd (asymmetric synthesis, excess of IPA and acetone removal)	180
Covalent grafting	Chitosan + glutaraldehyde	ω-TA (kinetic resolution)	181–183
Entrapment	Sol-gel matrix (+ celite)	ω-TA (kinetic resolution and deracemization)	167,184
CLEAs	Aggregation using glutaraldehyde	Glutamic transaminases	185

Lee *et al.* [181] have conducted the covalent immobilization of ATAs (from *Vibrio fluvialis* JS17) on chitosan beads, using glutaraldehyde as cross-linker agent. Residual activity of such heterogeneous catalyst reached 18 %. Similarly, Bornscheuer *et al.* [182,183] have covalently immobilized a series of ATAs (from *Giberella zeae*, *Neosartorya fischeri*, *Aspergillus fumigatus*, *Ruegeria pomeroyi* and *Rhodobacter sphaeroides*) on chitosan beads, using glutaraldehyde as crosslinking agent. In a model kinetic resolution reaction, an enhanced thermal stability was observed: when the enzymes were heated (to 60 °C for 4 hours) before reaction, the immobilized ones were more than twice more active than the free ones.

Encapsulation of ATAs (ATA-113, ATA-117 and *Vf*-ATA) was successfully performed by Kroutil *et al.* [167], using a sol-gel matrix (with celite inclusion as porous additive). Encapsulated enzymes exhibited activity even at pH 11 (whereas free enzymes were strongly deactivated in such extreme conditions), were stable over 5 cycles, and maintained their enantioselectivity (enantiomeric excess was over 99 %). Transamination reactions were performed both in the kinetic resolution mode, and in the deracemization (one-pot two steps) mode using lactate dehydrogenase or alanine dehydrogenase for driving equilibrium. This system was used to demonstrate the biocatalytic synthesis of pharmaceutically relevant chiral amines (S-Mexiletine and S-4-phenyl-2-butylamine). Kanerva *et al.* [184] recently performed the kinetic resolution of racemic amines, using ATA from *Arthrobacter* sp. (*As*-ATA) encapsulated in sol-gel matrix (with controlled hydrophobicity, using Methyltriethoxysilane, MTES, during the sol-gel synthesis). Catalysts were shown to be reusable after 5 cycles.

Recently, Cassimjee *et al.* [179] achieved the immobilization of *Cv*-ATA through His-tag, on a glass carrier, derivatized with cobalt ions (EziG™ support). The catalyst was active in methyl *tert*-butyl ether as solvent and at 50 °C. *rac*-MBA was used as amino donor in the kinetic resolution mode, for the amination of 1-phenoxypropan-2-one.

Hydrophobic interactions for immobilization enhancement was also exploited by Truppo *et al.* [180] for the immobilization of engineered ATA-117-11Rd transaminase on Sepabeads® resin EXE 120 (polystyrene resin grafted with octadecyl moieties). The solid biocatalyst was active in an organic medium (water saturated isopropyl acetate as solvent), at high temperature (up to 60 °C) for the asymmetric synthesis of Sitagliptin. To reach high product yield, they used a large excess of IPA as amino donor and shifting the equilibrium by further converting acetone as proposed by Savile *et al.*[17].

To our knowledge, a simple physical adsorption was never reported as a successful immobilization strategy for transaminase. Concerning the immobilization through CLEA and CLEC formation, Patramani *et al.* [185] have tried to form transaminases (glutamic-transaminases) aggregates using glutaraldehyde as cross-linking agent, for antibody isolation. However, the CLEA were not active anymore after reticulation.

5. Continuous flow mode transamination reactions: literature survey

In general, batch processes involve significant maintenance time after each synthesis (for reactor washing and reconditioning for the next synthesis) during which synthesis is in pause. Also, reaction parameters (i.e. product and reagent concentrations) evolve with time, which implies that the catalyst is not running at full speed during the whole duration of the synthesis. Flow processes generally allow decreasing drastically the maintenance time and accelerating biotransformations due to enhanced mass transfer, making large-scale production more economically viable [186,187]. Moreover, flow processes afford a better control on conversion, as it is a function of reactor length (space-time yield) and not of reaction time. As a result, flow processing generally features increased scalability [188,189], higher space-time yields [190] and thus, enhanced productivity levels with respect to batch processes [164,191–197]. Finally, the outflows can be analysed in real time, and subsequent unit operations such as in-line liquid–liquid extraction, crystallization, membrane separation (*e.g.* for by-product elimination) can be integrated to the biotransformation [164,186].

Thus, performing biocatalytic transamination reactions in continuous flow mode is primed to solve many issues chemist and industrial chemists have to face when trying to design an efficient and green production process [198,199]. Table 3 gathers the scholarly reports in which biocatalytic transamination reactions have been demonstrated in continuous flow mode. In the following sections, we discuss sequentially the cases where the enzyme is used in whole cells or as a stand-alone enzyme, in combination with other enzymes, and with co-immobilized cofactor. Figure 19 shows the pictograms used to represent each component that are included in the process schemes discussed in the following section.

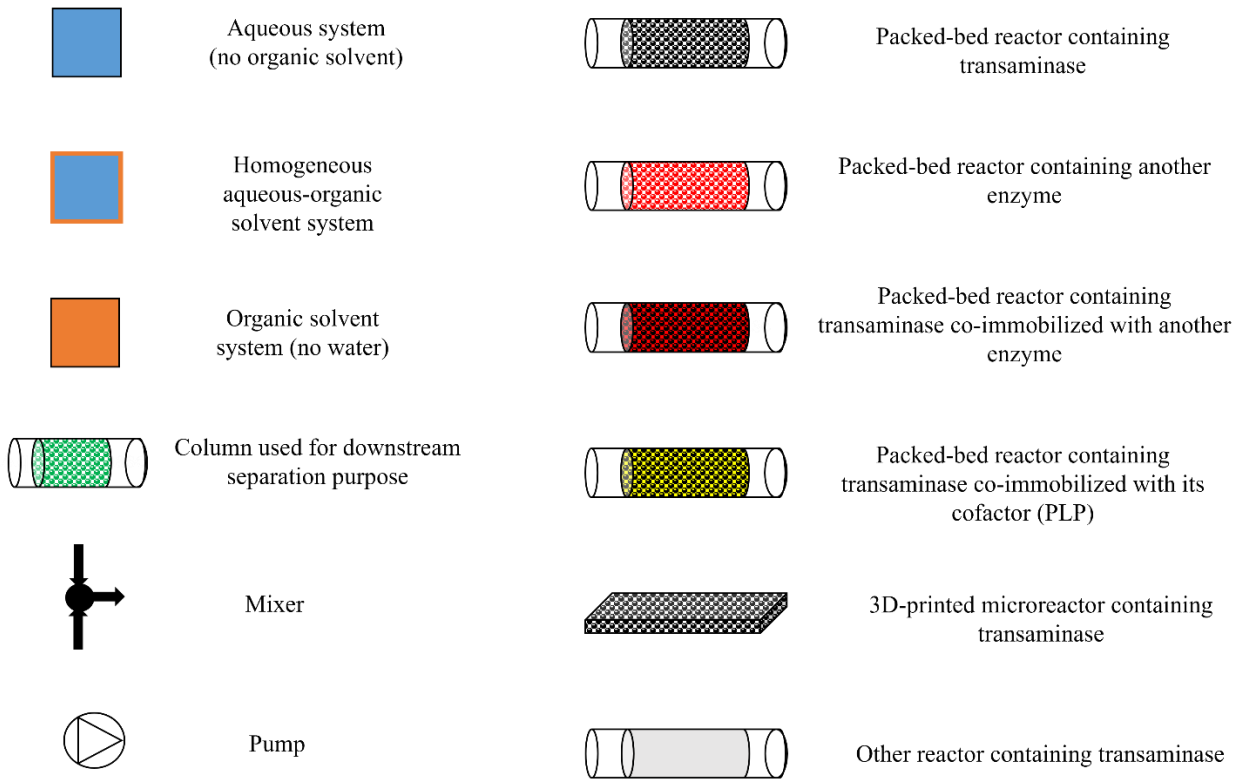

Figure 19. Representation of each components featured in the transaminase-catalysed continuous process schemes included in the following section.

Table 3 – Overview of the reported examples of transaminations in continuous flow.

Immobilization	Materials	TA	Reaction	Ref.
TA in immobilized whole cells				
Encapsulation	Ca-Alginate beads	Whole cells (*Vibrio fluvialis* JS17)	Kinetic resolution (continuous removal of ketone)	136
Encapsulation	Chitosan	Whole cells (*Escherischia coli*)	Asymmetric synthesis (continuous removal of product, using SLM)	200
Encapsulation	Hollow silica microspheres	Whole cells (*Escherischia coli*)	Kinetic resolution and asymmetric synthesis	201
Covalent grafting	Methacrylate beads	Whole cells (*Escherischia coli*)	Asymmetric synthesis (favourable thermo-dynamics)	202
Covalent grafting	Cycloolefin polymer microchannels + APTES[b] + Glutaraldehyde	Whole cells (*Escherischia coli*)	Deamination	203
Immobilized TAs				
His-tag immobilization	EziG™ supports + Fe^{3+} derivatization	ω-TAs	Kinetic resolution	204
His-tag immobilization	Derivatized EziG™ supports	*Aspergillus fumigatus* ω-TA mutant	Asymmetric synthesis (following a Suzuki–Miyaura reaction)	205
His-tag immobilization	EziG™ supports + Fe^{3+} derivatization	ω-TAs	Amination (in multi-enzymatic cascade reactions)	206

Covalent grafting (and His-tag driving)	Sepabeads® + Co^{2+} derivatization	*Halomonas elongata* ω-TA	Amination	131
Covalent grafting (and His-tag driving)	Sepabeads® + Co^{2+} derivatization	*Halomonas elongata* ω-TA	Asymmetric synthesis of cyclic chiral amines	207
Covalent grafting (and His-tag driving)	Sepabeads® + Co^{2+} derivatization	*Halomonas elongata* ω-TA	Asymmetric synthesis of 2-aminobutane	208
Covalent grafting (and His-tag driving)	Sepabeads® + Co^{2+} derivatization	*Halomonas elongata* ω-TA	Deamination	209
Covalent grafting (and His-tag driving)	Sepabeads® + Co^{2+} derivatization	*Halomonas elongata* ω-TA and Horse liver alcohol dehydrogenase	Deamination or kinetic resolution (followed by aldehyde reduction into alcohol)	210
Covalent grafting (and ionic driving)	Epoxy resin 107s (Xi'an Lan Xiao Technology Co. Ltd) + ethylenediamine derivatization	*Caulobacter sp.* ω-TA	Asymmetric synthesis of S-1-Boc-3-aminopiperidine	211
Covalent grafting	Aminoalkyl-functionalized resins (ReliZyme^{TM} EA) + bisepoxides	*Chromobacterium violaceum* ω-TA mutant	Kinetic resolution	212
Covalent grafting	Glyoxyl-agarose beads	*Vibrio fluvialis* ω-TA	Asymmetric synthesis of AZD1480 intermediate	213
Hydrophilic interactions	DIAION HP2MG resin (Mitsubishi)	ω-TA mutant	Asymmetric synthesis of R-sitagliptin (in wet isopropylacetate, acetone evaporation by N_2 sparging)	214

Covalent grafting	Amine-functionalized beads (ReliZyme™ HA 403) + glutaraldehyde	*Silicibacter pomeroyi* ω-TA	Amination of furan aldehydes	[215]
Covalent grafting	Cellulose (+ APTES[b] + glutaraldehyde) or (+ GLYMO)	*Vibrio fluvialis* ω-TA	Asymmetric synthesis (using LDH and GDH)	[216]
Electrostatic interactions	Derivatized lignin + PEI[a]	*Halomonas elongata* ω-TA	Amination (of cynnamaldehyde) and deamination (of S-MBA)	[217]
Covalent grafting	Silica monolith + APTES[b] + glutaraldehyde	ATA-117	Kinetic resolution	[175] and [218]
His-tag immobilization	Silica capillary + Ni^{2+} derivatization	Immobilized ω-TA and transketolase	Asymmetric synthesis (following formation of chiral ketone)	[219]
His-tag immobilization	Agarose beads + Ni^{2+} derivatization	Immobilized ω-TA and transketolase	Asymmetric synthesis (following formation of chiral ketone)	[220]
Covalent grafting	3D-printed Nylon matrix (Taulman) + Glutaraldehyde + PEI[a]	ω-TAs	Kinetic resolution	[221]
Encapsulation	Lentikats® (polyvinyl alcohol gel)	ω-TA	Deamination	[222]
Co-immobilized TAs and cofactor (PLP)				
Covalent grafting (and His-tag driving)	Epoxy-activated methacrylate beads + PEI[a]	Co-immobilized ω-TAs and PLP	Amination (of cynnamaldehyde) and deamination (of S-MBA)	[223]

Covalent grafting (and His-tag driving)	Epoxy-activated methacrylate beads + PEI[a]	Co-immobilized H*alomonas elongata* ω-TA and PLP	Deamination	224
Covalent grafting	Epoxy-resin (Xi'an Lan Xiao Technology Co. Ltd)	Co-immobilized ω-TA and PLP	Asymmetric synthesis of R-sitagliptin	225
Entrapment	Copolymer hydrogel of polyvinyl alcohol and sodium alginate	Co-immobilized ω-TA and PLP	Deamination	168
Combining TAs with other enzymes				
Covalent grafting	Silica capillary + APTES[b] + Glutaraldehyde	Co-immobilized glutamic-pyruvic transaminase, glutamate dehydrogenase	Asymmetric synthesis	148
Covalent grafting	Polymethacrylate-based porous beads Relisorb® EP400SS	Co-immobilized H*alomonas elongata* ω-TA with Horse liver alcohol dehydrogenase and NADH oxidase	Amination (following the oxidation of alcohol into aldehyde)	226
Covalent grafting	Polymethacrylate-based porous beads Relisorb® EP400SS	Co-immobilized H*alomonas elongata* ω-TA with Horse liver alcohol dehydrogenase and NADH oxidase	Amination (following the oxidation of alcohol into aldehyde)	227
Combining TAs with other enzymes in whole cells				
Encapsulation	Hollow silica microspheres	Co-immobilized Whole cells (*Escherischia coli*) and *Lodderomyceselongisporus* yeast with ketoreductase activity	Kinetic resolution (followed by ketone reduction into chiral alcohol and amines) - one-pot cascade	228

[a] PEI = polyethyleneimine

[b] APTES = (3-aminopropyl)triethoxysilane, respectively.

5.1 Flow mode transamination with ATAs in immobilized whole cells

Shin *et al.* [136] were the first to report a biocatalytic transamination reaction in flow mode. Whole cells of *Vibrio fluvialis* JS17 containing overexpressed transaminases were entrapped in calcium-alginate beads, and used to form a packed-bed reactor (PBR). As compared to the cell-free extract, a change in the pH optimum was observed (from 9 to 8) and the substrate and product inhibition was lower. They successfully perform the kinetic resolution of *rac*-MBA, using alanine as the amino donor. The ketone product (acetophenone) was continuously removed using a hydrophobic membrane contactor (Figure 20). Noteworthily, the authors also performed such continuous transamination process using an enzyme membrane reactor (EMR) in place of a PBR. In this case, the *Vibrio fluvialis* whole cells were entrapped in a hydrophilic ultrafiltration membrane [229].

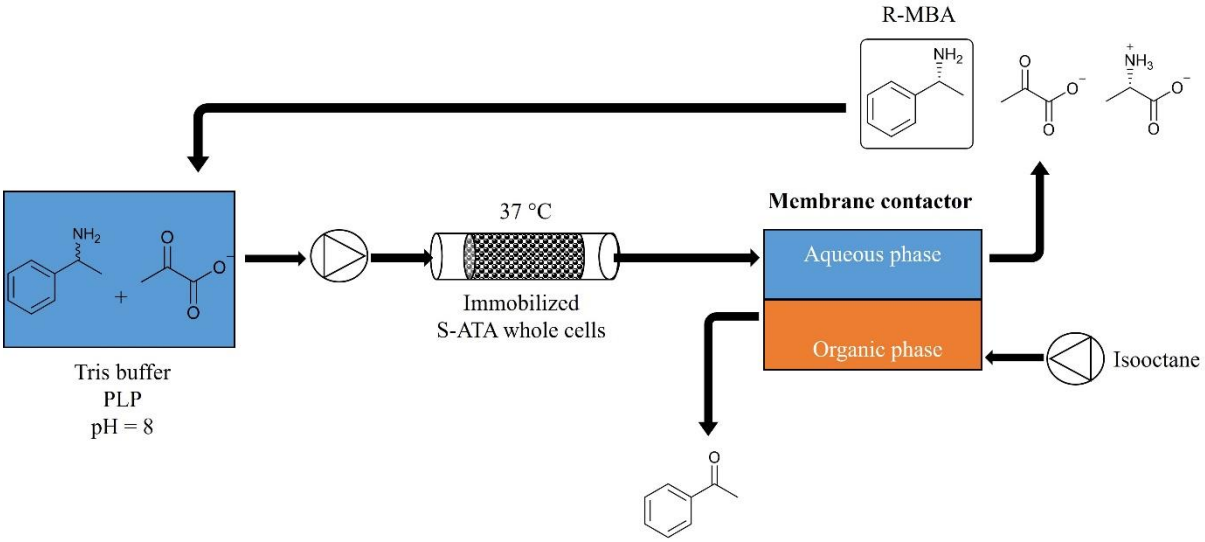

Figure 20. Schematic representation of the continuous transamination process described by Shin *et al.* [136].

Escherichia coli whole cells containing over-expressed ATA from *Arthrobacter citreus* were also entrapped in chitosan matrix and placed in a PBR by Rehn *et al.* [200] for the asymmetric synthesis of S-MBA (Figure 21). Large excess of amino donor (IPA) was employed, and the equilibrium was additionally shifted towards completion through a continuous and selective extraction of MBA using a SLM contactor (*i.e.* a porous membrane, with pores filled with undecane allowing the transfer of the amine). This system led to 98 % conversion in flow mode. Final product concentration was as high as 55 g/L (obtained by processing the flow setup for 80 h).

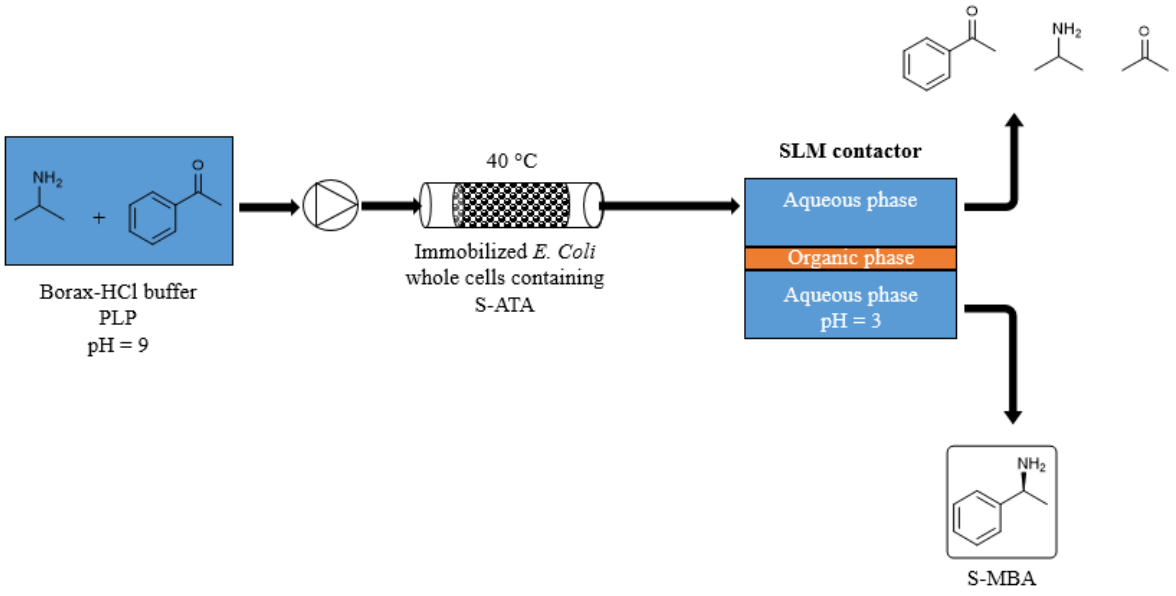

Figure 21. Schematic representation of the continuous transamination process described by Rehn *et al.* [200].

In 2019, the Poppe group [201] performed the immobilization of six different ATAs (three S-selective and three R-selective) overexpressed in *Escherichia coli* whole cells entrapped into hollow silica microspheres forming a sol-gel matrix. The resulting sol-gel system allowed quantitative immobilization (~100 % immobilization yield) even at high enzyme loading. Notably, ~9 g of dry heterogeneous TA biocatalyst could be produced from 10 g of wet cells. Moreover, despite the harsh immobilization conditions, ATAs-containing whole cells were able to efficiently catalyse the kinetic resolution of various amines in batch. Interestingly, they remained catalytically active even after many months of air-storage. Subsequently, the most efficient S and R-selective immobilized ATAs were selected to run the kinetic resolution in continuous flow mode, in a PBR. Both solid biocatalysts exhibited excellent yield and good enantiomeric excess under various flow rates and substrate concentrations. Eventually, the continuous production of the two pure enantiomers of the drug-like 1-(3,4-dimethoxyphenyl)ethan-1-amine (DMPEA) (Figure 22) was demonstrated, with space-time yields of 1.8 $g.L^{-1}.h^{-1}$ and 4.8 $g.L^{-1}.h^{-1}$ for S- and R-enantiomers, respectively, and showed remarkable operational stability.

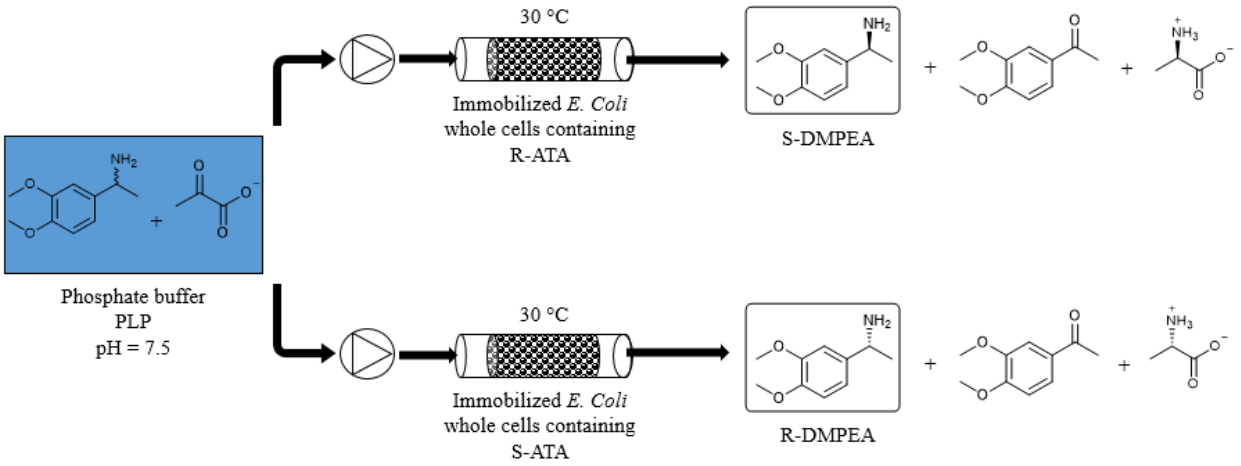

Figure 22. Schematic representation of the continuous kinetic resolution of *rac*-1-(3,4-dimethoxyphenyl)ethan-1-amine (DMPEA) described by Poppe *et al.* [201].

In another study, Jamison *et al.* [202] reported on the flow transamination for the thermodynamically favourable asymmetric synthesis of non-natural amines in organic solvent (methyl *tert*-butyl ether). *Escherichia coli* whole cells containing both over-expressed R-selective transaminases and entrapped PLP cofactor were grafted on methacrylate beads (*via* grafting of the peptidoglycan layer present in the cell wall). The API R-mexiletine was synthesized in 94 % yield using IPA as the amino donor (residence time was 60 min). PLP leaching was avoided thanks to the organic solvent (the cofactor stayed in the aqueous phase entrapped in the beads). The biocatalysts were stable up to 10 days. The continuous reaction was followed by a downstream purification step (*i.e.* a catch-and-release system), allowing the recovery of highly pure chiral amine products (Figure 23).

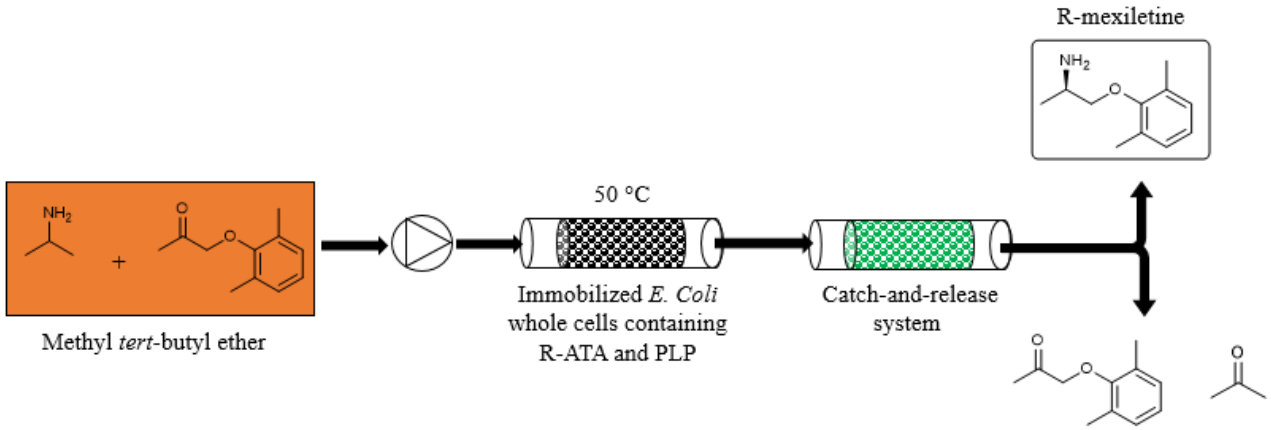

Figure 23. Schematic representation of the continuous process leading to the asymmetric synthesis of R-mexiletine in organic solvent, described by Jamison *et al.* [202].

Žnidaršič-Plazl *et al.* [203] developed three microscale reactors containing ATAs immobilized on the inner wall surface, using different immobilization strategies. On the one hand, *Escherichia coli* whole cells (overexpressing the ATA) were immobilized on the surfaces of cycloolefin polymeric microchannels (COP, Zeonor®) through surface silanization (with APTES) and glutaraldehyde coupling. On the other hand, a glass microchannel reactor was used for the immobilization of a genetically engineered ATA featuring a silica-binding module tag (SBM tag) at the N-terminus (N-SBM-ATA), leading to immobilization *via* electrostatic interactions. The catalytic performance of the resulting biocatalytic microreactors were evaluated towards the continuous deamination of S-MBA into acetophenone using pyruvate as the amine acceptor. Both whole cells (overexpressing ATA) and N-SBM-ATA were efficiently immobilized and displayed high productivities (space time yields were 11.53 $g.L^{-1}.h^{-1}$ and 14.42 $g.L^{-1}.h^{-1}$, respectively). However, whole cells showed negligible leaching and enhanced operational stability while N-SBM-ATA productivity dropped quickly, which was suggested to indicate rapid leaching from the reactor.

5.2 Flow mode transamination with immobilized ATAs

Among the different reported supports hosting immobilization of stand-alone ATAs used in flow applications, porous glass-based materials and functionalized polymeric resins are the ubiquitous supports. For example, EziG™ materials are based on controlled porosity glass (featuring additional polymer coating in some case) that easily chelate metal cations and therefore can also bind proteins equipped with affinity tags [179]. This allows combining enzyme purification and immobilization in a straightforward manner.

Mutti et al. [204] achieved the immobilization of two His-tagged ATAs (*As*-ATA and *Cv*-ATA) on different EziG™ supports, loaded with iron ions. Three types of EziG carrier material possessing distinct surface polarities were tested: EziG1 (Fe-Opal, hydrophilic derivatized silica surface), EziG2 (Fe-Coral, coated with hydrophobic polymer), and EziG3 (Fe-Amber, covered with semi-hydrophobic polymer). The impact of immobilization conditions (buffer composition, concentration, pH and PLP concentration) on immobilization efficiency was assessed. EziG3 provided the highest immobilization yield when performing immobilization in optimal conditions, and *As*-ATA showed highest specific activity in batch experiments. Thus, EziG3-*As*-ATA (with 20 wt % ATA) was selected to run the flow kinetic resolution of *rac*-

MBA (Figure 24). The resulting PBR was operated for 96 hours without any detectable loss of activity nor enantioselectivity, and high space-time yield (335 $g.L^{-1}.h^{-1}$) was achieved.

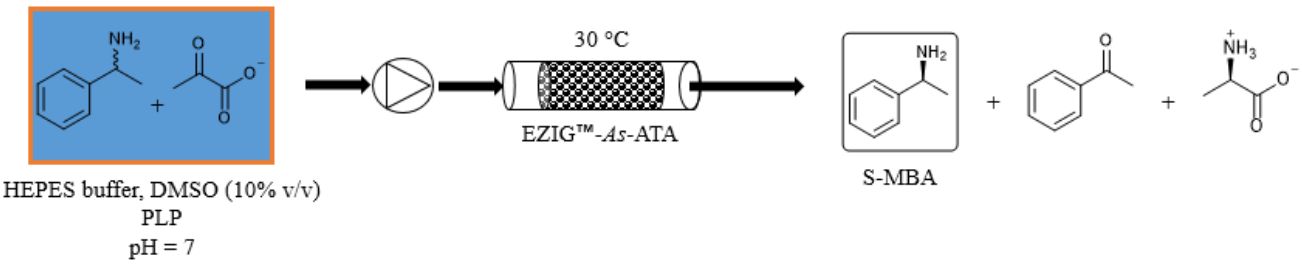

Figure 24. Schematic representation of the continuous kinetic resolution of *rac*-methylbenzylamine (MBA) described by Mutti *et al.* [204].

Bornscheuer *et al.* [205] also immobilized a variant ATA from *Aspergillus fumigatus* (*Af*-ATA) on an EziG™ support to perform a cascade combining chemo- and biocatalytic reactions in continuous flow mode. More precisely, the cascade featured a combination of the palladium-catalysed Suzuki–Miyaura coupling producing biphenyl ketones followed by transamination (*i.e.* asymmetric synthesis of high-value chiral biaryl amines). The soluble Pd species ($PdCl_2$, as a homogeneous coupling catalyst) was continuously fed but the enzyme was fixed in a single PBR. In other words, two reaction solutions (the crude Suzuki–Miyaura reaction mixture producing the ketone, and an IPA/PLP-containing solution) were pumped through the PBR (Figure 25). The cascade resulted in 43% overall conversion at a flow-rate of 0.1 $mL.h^{-1}$ (210 minutes residence time) when employing 30% (v/v) DMF for transamination reaction. Such an achievement highlights the excellent compatibility of chemo- and biocatalysis for such cross-coupling reaction in DMF/water mixtures as well as the robustness of the employed ATA variant in the presence of reagents required for the chemocatalytic reaction (*e.g.* $PdCl_2$).

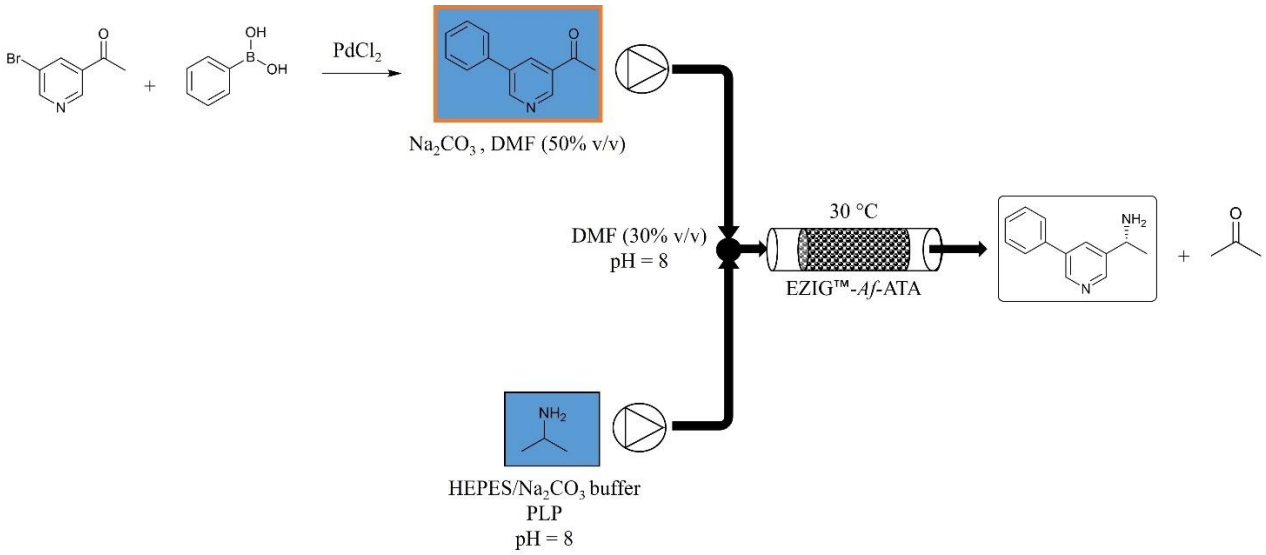

Figure 25. Schematic representation of the continuous process leading to the asymmetric synthesis of R-1-(5-phenylpyridin-3-yl)ethan-1-amine (framed compound), described by Bornscheuer *et al.* [205]**.** Suzuki–Miyaura reaction by-products were intentionally omitted for clarity purpose.

Flitsch *et al.* [206] exploited the combined use of alcohol oxidase, transaminase, and imine reductase (IR) to synthesize various primary and secondary amines. Such a three enzymes system is not viable in batch mode, due to incompatible substrates or enzyme combination (*e.g.* cross-reactivity and inhibition issues). Thus, as a proof-of-concept, they designed a sequential flow mode process. A first reaction involved an alcohol oxidase to form aldehyde intermediates from alcohols, using catalase-generated oxygen (from the decomposition of hydrogen peroxide). The reactive aldehyde were then passed through a series of packed-bed modules loaded with ATA or IR immobilized on EziG™ amber based-carriers. ATA, fed with alanine, was used to generate primary amines (Figure 26**a**) or intermediate amines that were subsequently non-catalytically carbonylated (into imines) and then reduced on the IR (using glucose as co-substrate and Nicotinamide Adenine Dinucleotide Phosphate ($NADP^+$) as the cofactor) into the targeted secondary amines (Figure 26**b**). This method proved to greatly improve the overall yields and the biocatalytic productivity with respect to the equivalent sequential batch reactions.

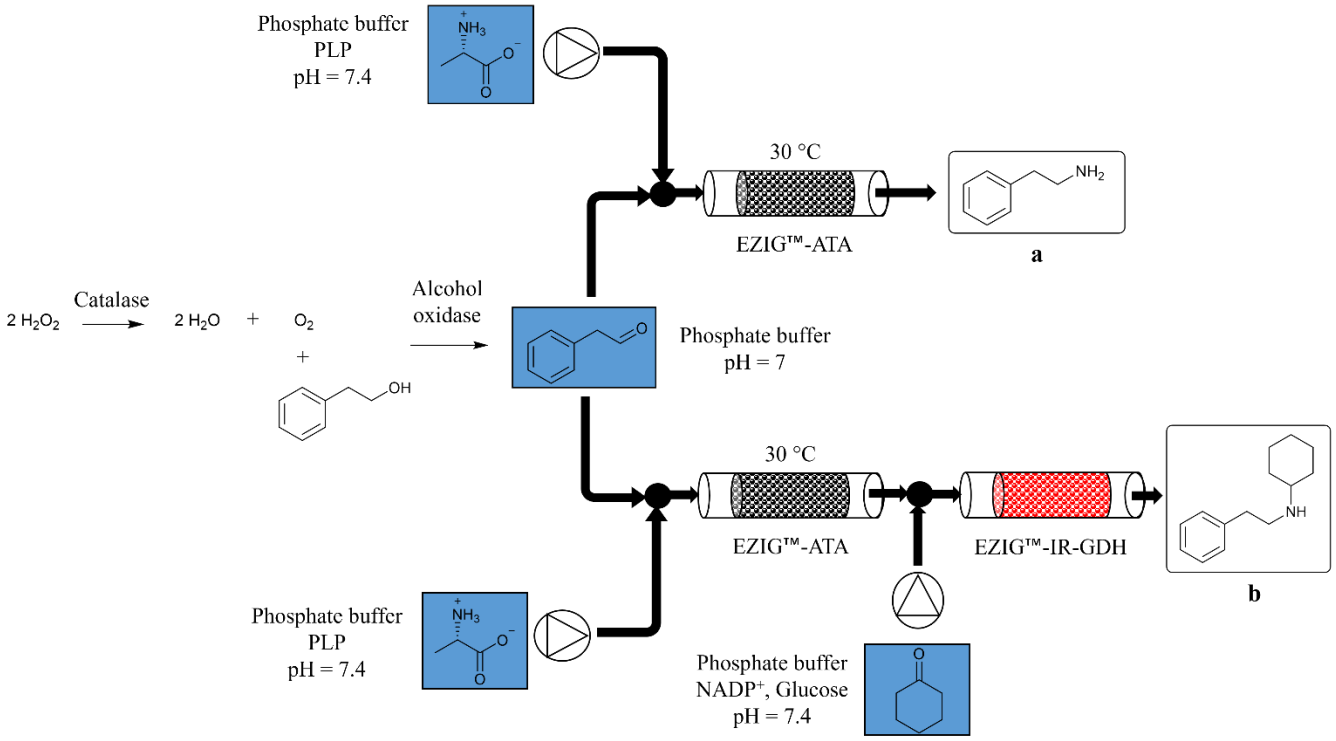

Figure 26. Schematic representation of the continuous transaminase-mediated process leading to primary (**a**) and secondary (**b**) amines, described by Flitsch *et al.* [206]**.** The first cascade reaction (involving soluble catalase and alcohol oxidase) was performed in a multipoint injection reactor. By-products of transamination (pyruvate) and glucose dehydrogenation (gluconolactone) were intentionally omitted for clarity purpose.

Commercial epoxy-activated (usually made of methacrylate or polyacrylic matrix) resins such as Sepabeads® are also widely employed as carrier for TA immobilization. Their surface epoxy-groups are especially useful as they afford the coupling with different nucleophilic species. As ready-to-use carriers they directly bind to the nucleophilic groups on the enzyme surface (i.e. Lys or Cys residues). However, due to the low reactivity of the epoxy groups, a second functional group (*e.g.* amines or metal chelates) is frequently added to the support to drive the enzyme toward the epoxy-carrier surface [211,217,230].

As matter of illustration, a metal-derivatized epoxy-resin (Sepabeads® EC-RP/S) was used by Paradisi *et al.* [131] for the continuous flow synthesis of a range of achiral amines, using immobilized *Halomonas elongata* ω-transaminases (HeWT). The beads were activated with iminodiacetic acid (IDA) and $CoCl_2$ solutions, resulting in cobalt chelates able to drive the covalent immobilization of HeWT (by His-Tag binding). The resulting immobilized enzyme retained 40% activity and displayed increased organic solvent tolerance (with respect to the free

form). The amination of *p*-NO_2-benzaldehyde into *p*-NO_2-benzylamine was successfully performed (> 99% yield in 2 minutes residence time) and coupled to on-line product purification device (*i.e.* basification of the reaction stream followed by extraction with ethyl acetate). Additionally, cinnamylamine (a valuable building block for the synthesis of biologically active material) was efficiently produced through amination (90% yield in 2 minutes residence time) using alanine as the amino donor (Figure 27).

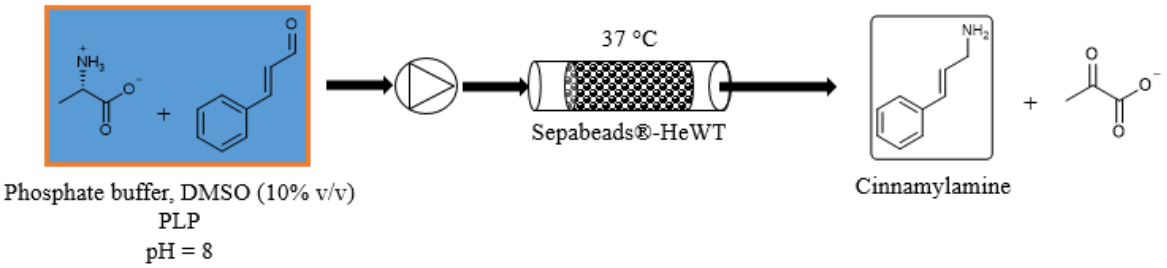

Figure 27. Schematic representation of the continuous transaminase-mediated production of cinnamylamine, described by Paradisi *et al.* [131].

Similarly, the Paradisi group relied on the same biocatalytic system for different applications. For example, they exploited this system to produce a range of small cyclic chiral amines in continuous flow. [207] Cyclic pro-chiral ketones were used as starting reagent, along with along with S-MBA, and no particular equilibrium shifting strategy was used for this synthesis. Remarkably, complete conversion of tetrahydrofuran-3-one and tetrahydrothiophene-3-one was achieved in 5- and 10-min residence times, respectively. However, the enantiomeric excess for these rapid transamination reactions did not exceed 30 % (while soluble HeWT reached 60 to 70 %). Molecular docking studies suggested that the rigidification imposed by the immobilization of HeWT could explain the relatively lower selectivity displayed by the heterogeneous biocatalyst for the conversion of such small cyclic ketones. Nevertheless, the efficient production of bulkier cyclic chiral amines such as S-1-methyl-piperidin-3-ylamine (MPPA; Figure 28) with enhanced enantioselectivity (90%) was achieved with longer contact times (30 to 45 minutes).

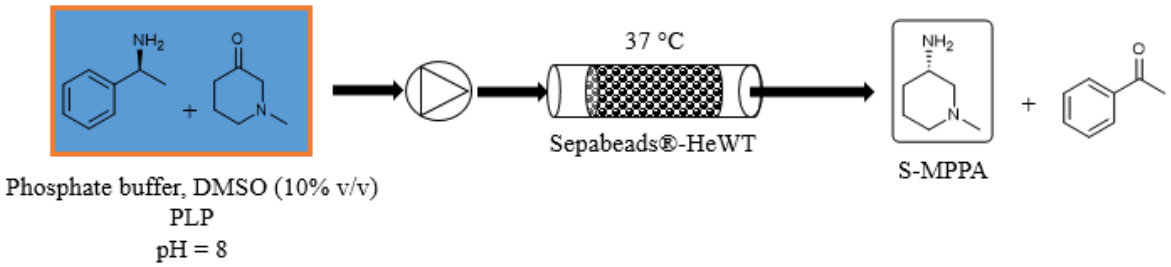

Figure 28. Schematic representation of the continuous asymmetric synthesis of S-1-methyl-piperidin-3-ylamine (MPPA) using immobilized transaminase, described by Hegarty and Paradisi [207].

The flow asymmetric synthesis of both enantiomers of 2-aminobutane from butanone was also reported,[208] using the same immobilized transaminases system as described above. Notably, R-2-aminobutane is a sub-unit of drug candidate XL888, which is currently used in clinical trials for cancer treatment [231]. After screening a panel of ATAs, two candidates were identified: the S-selective HeWT and a commercial R-selective ATA (*RTA-X43, from Johnson Matthey). Notably, a single strategic point mutation enhanced the enantioselectivity of HeWT from 45 to > 99.5% enantiomeric excess. Once immobilized, the resulting HeWT mutant (HeWT-F48W) and RTA-X43 enabled the multi-gram production of S- and R-2-aminobutane at high concentration (Figure 29), which were subsequently purified by three fractional distillations under atmospheric pressure. Both biocatalysts displayed excellent stability, especially the immobilized HeWT-F48W which did not show any activity loss over 7 days of operation. As a result, it achieved a space-time yield of 3.6 $g.L^{-1}.h^{-1}$. IPA (1.5 M) was employed as amino donor.

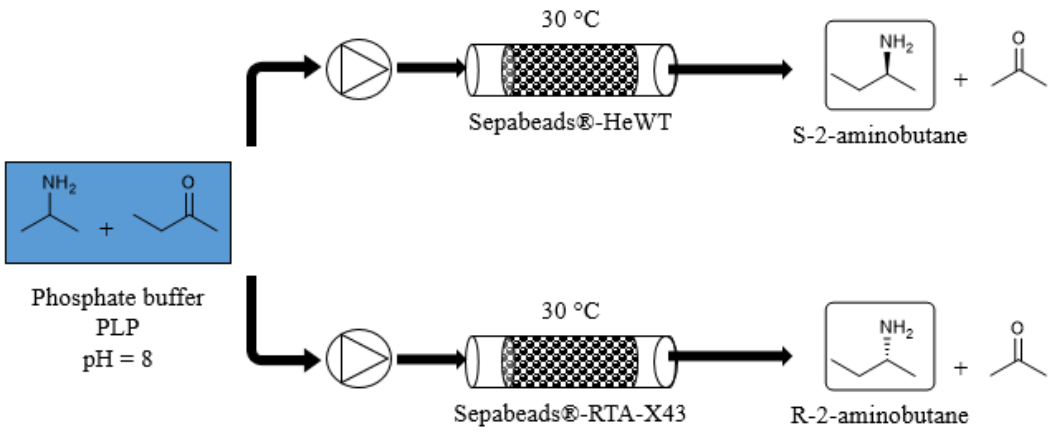

Figure 29. Schematic representation of the continuous asymmetric synthesis of R- and S-2-aminobutane using immobilized transaminase, described by Paradisi *et al.* [208].

HeWT immobilized on this metal-derivatized epoxy resin was also used for the flow production of aromatic primary and secondary alcohols starting from aromatic amines. [210] The flow-mode transamination reactions (*i.e.* deamination or kinetic resolution) were followed by the reduction of the aldehyde product into the targeted alcohol in a subsequent PBR, *via* immobilized Horse liver alcohol dehydrogenase (HLADH) or ketoreductase (KRED). For example, starting from dopamine (biologically available substrate) and using a biphasic stream (HEPES buffer/toluene 85:15), the authors successfully synthesized hydroxytyrosol (an antioxidant compound) in high yield (82 %). The flow setup was connected to an in-line purification device, allowing cofactor recycling and product isolation (Figure 30).

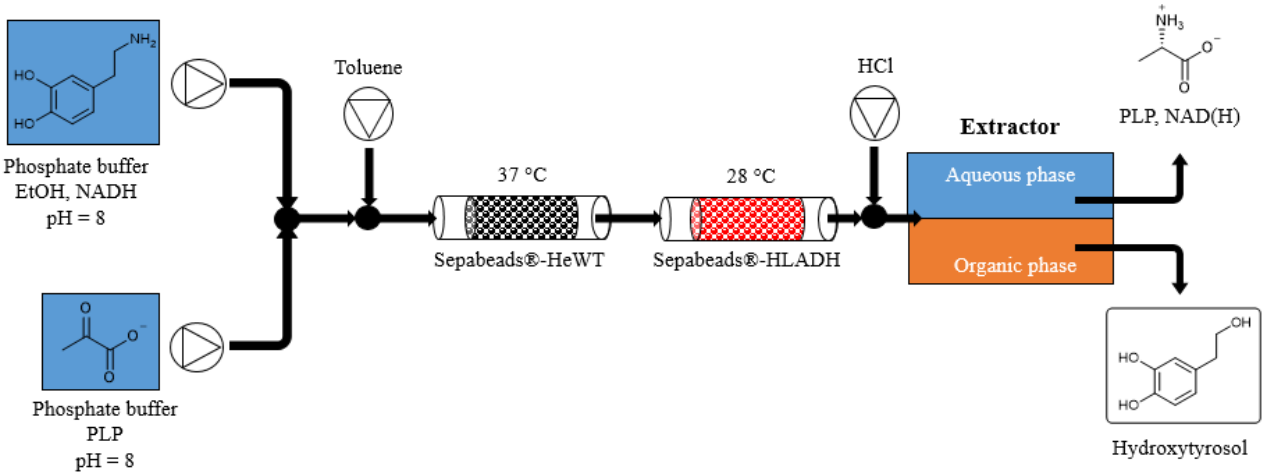

Figure 30. Schematic representation of the process leading to the continuous multienzymatic synthesis of hydroxytyrosol, described by Contente and Paradisi [210]. NADH cofactor was regenerated in-situ by ethanol (EtOH) dehydrogenation into acetaldehyde. By-products of alcohol dehydrogenations (acetaldehyde and 2-(3,4-dihydroxyphenyl)acetaldehyde) were intentionally omitted for clarity.

Employing such immobilized HeWT, Paradisi *et al.* [209] also performed the flow synthesis of a plethora of valuable aromatic aldehydes (featuring key applications as components of flavours and fragrances). Using very short residence times (3-15 min), the biocatalyst allowed obtaining at least 90% yield (with pyruvate as amino acceptor). An elegant in-line extraction step was implemented, which afforded the recovery of the targeted pure aldehydes in the organic stream.

Wang *et al.* [211] also managed to covalently immobilize an ATA from *Caulobacter* sp. (ATA-W12) on derivatized epoxy resins. Here, the resin was partially aminated with ethylenediamine (EDA) in order to drive the adsorption of ATA *via* electrostatic interactions, and thus to favor its subsequent covalent anchoring on the epoxide functions. Such derivatization enabled to

improve the heterogeneous biocatalyst residual specific activity and stability. Indeed, after 15 consecutive cycles in batch, the EDA-treated biocatalyst retained >90 % of specific activity, while the ATA immobilized on the pristine epoxy resin lost half of its specific activity. The resulting immobilized ATA was used to run the flow asymmetric synthesis of S-1-Boc-3-aminopiperidine (a key intermediate for the synthesis of CHK1 inhibitor), in a PBR (Figure 31). After 24 h of continuous operation at 0.4 mL.min^{-1}, the conversion rate was maintained at > 90 %, resulting in a space-time yield of 38.8 g·L^{-1}·h^{-1}.

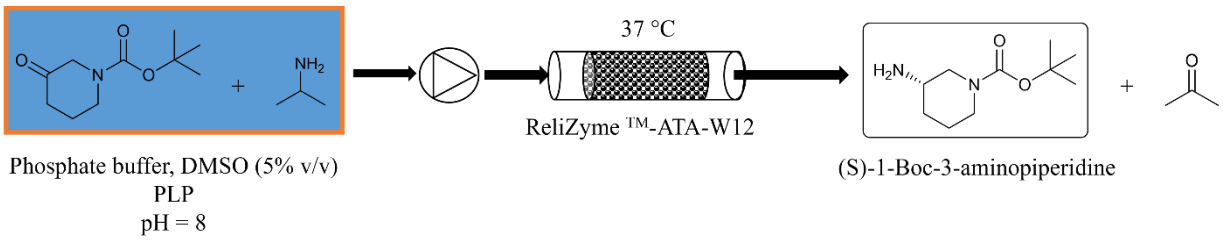

Figure 31. Schematic representation of the continuous synthesis of S-1-Boc-3-aminopiperidine using immobilized transaminase, described by Wang *et al.* [211]

Poppe *et al.* [212] successfully immobilized a *Cv*-ATA mutant through covalent attachment on bisepoxide-activated aminoalkyl resins (ReliZyme™ EA403/S) for the kinetic resolution of racemic amines in continuous flow mode. The impact of the hydrophilicity and length of the linker arm (i.e. bisepoxide coupling agents) on ATA specific activity was assessed. It was found that the specific activity is boosted when the enzyme is attached to the polymeric resin *via* short and hydrophilic linkers, such as glycerol diglycidyl ether. With this optimized biocatalyst in hand, the authors carried out a recycling study in batch mode and proved its high operational stability (98% retained activity over 19 consecutive cycles). Subsequently, a kinetic resolution was efficiently achieved in flow mode, resulting notably in pure R-4-phenylbutan-2-amine, a precursor of antihypertensive drug Dilevalol (Figure 32**a**). Space-time yield was 45.8 g.L^{-1}.h^{-1} (0.5 mL.min^{-1} contact time, without organic solvent). Additional flow experiments performed in water/DMSO systems (50% v/v) further allowed producing R-1-aminotetraline (a component used in the synthesis of Sertraline) with an enantiomeric excess > 95% at 0.1 mL.min^{-1} (Figure 32**b**). Such result highlights the enhanced solvent tolerance of such immobilized *Cv*-ATA mutant with respect to its free form, which could be attributed to a significant stabilization of its tertiary structure upon immobilization (due to multipoint covalent fixation).

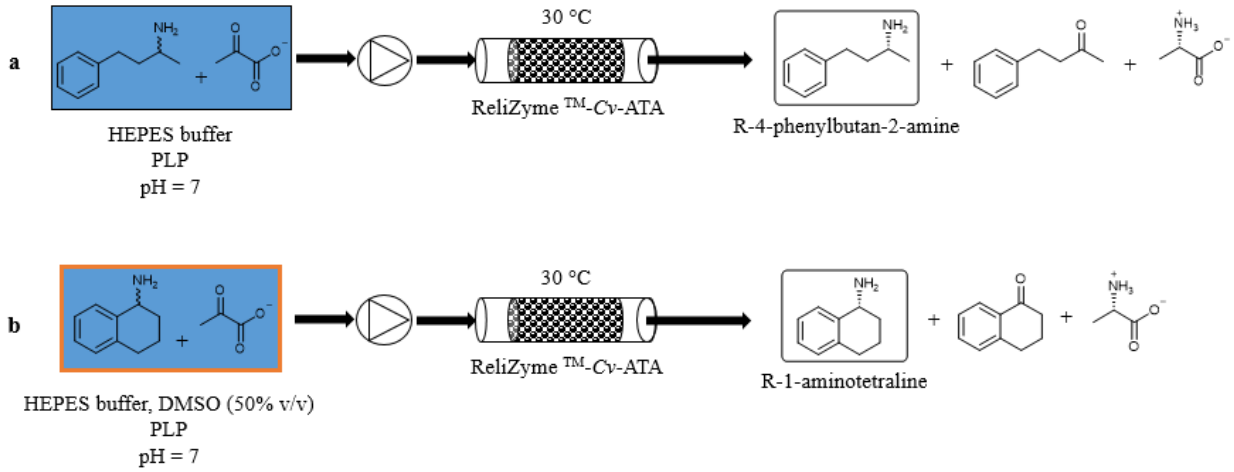

Figure 32. Schematic representation of the continuous kinetic resolution of *rac*-4-phenylbutan-2-amine (**a**) and *rac*-1-aminotetraline (**b**) using immobilized transaminase, described by Poppe *et al.* [212].

Ubiali *et al.* [213] reported on the covalent immobilization of *Vf*-ATA on glyoxyl-agarose beads, by exploiting the reactivity of the lysine residues of the enzyme towards the aldehyde groups of the carrier. The formed imine bond was further reduced to stabilize the anchoring and avoid leaching. Two reducing agents ($NaBH_4$, $NaBH_3CN$) were used in under different conditions, in attempts to minimize the negative impact of this reduction on the enzyme activity. The optimal immobilized biocatalyst (obtained using $NaBH_3CN$ at 4°C) retained c.a. 30% of activity and similar stability with respect to its free form. The immobilized biocatalyst was tested in batch and flow mode (in a PBR, using 10 minutes residence time) for the synthesis of S-1-(5-fluoropyrimidin-2-yl)-ethanamine, a key intermediate of AZD1480 kinase inhibitor. For a similar degree of conversion, the specific reaction rate of the flow reaction resulted to be about 22-fold higher than the batch reaction. Moreover, DMSO could be replaced by dimethyl carbonate (5% v/v) as a greener co-solvent, further enhancing the sustainability performance of the process. An in-line downstream purification was developed for product isolation using an ion-exchange resin. Using S-MBA as the amino donor, optically pure S-1-(5-fluoropyrimidin-2-yl)-ethanamine (enantiomeric excess > 99%) was isolated in 35% yield (Figure 33).

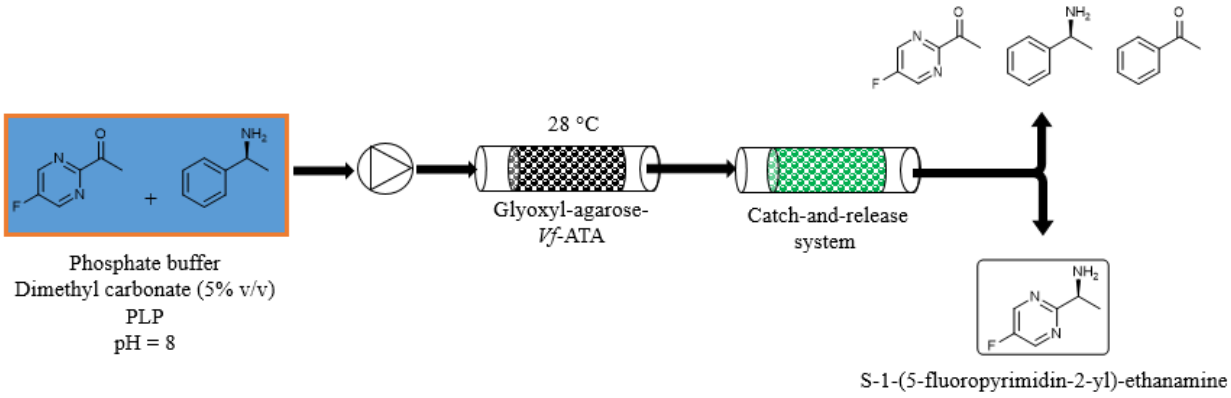

Figure 33. Schematic representation of the process leading to the continuous asymmetric synthesis of S-1-(5-fluoropyrimidin-2-yl)-ethanamine using immobilized transaminase, described by Ubiali *et al.* [213].

In a recent patent, Truppo and co-workers at Merck [214] demonstrated the use of immobilized recombinant transaminases to manufacture R-sitagliptin in batch and continuous flow mode. The employed immobilized ATA consisted in commercial methacrylate-based carrier (DIAION HP2MG resin (Mitsubishi)) linked to the recombinant ATA through hydrophilic interactions. Impressively, such biocatalyst remained highly active and stable in organic solvent systems (i.e. comprising at least 90% of organic solvent). Isopropylacetate (IPAc) was used as main solvent for the reaction and isopropylamine as the amino donor. Acetone evaporation (high temperature and N_2 sparging) enabled to displace the position of the transamination equilibrium towards the formation of products. In the continuous operation, the immobilized ATA was packed into a column (as a PBR). At 60 °C and with a flow rate of 63 µL.min^{-1} (corresponding to 1h of residence time), the conversion was 45%; it reached 85% when the residence time was set to 4h. Optically pure R-sitagliptin (enantiomeric excess > 99.5%) was successfully obtained (Figure 34).

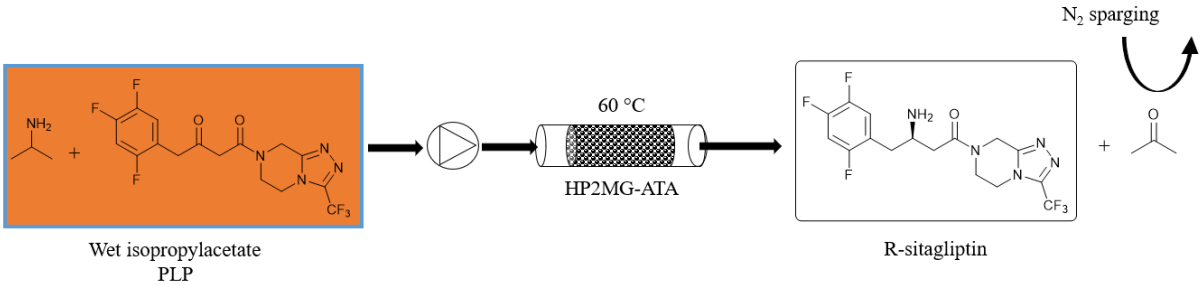

Figure 34. Schematic representation of the process leading to the continuous asymmetric synthesis of R-sitagliptin using immobilized transaminase, described by Truppo *et al.* [214].

In 2023, the Berglund and Bornscheuer groups [215] demonstrated the reductive aminations of biobased furan aldehydes, namely 5-(hydroxymethyl)furfural (HMF) and 2,5-diformylfuran (DFF), in batch and flow mode using immobilized ATAs. Different ATAs were immobilized on glutaraldehyde-functionalized amine beads (ReliZyme^{TM}, HA 403), and both alanine and isopropylamine were tested as amino-donors. Among the different heterogeneous biocatalysts developed, the ATA from *Silicibacter pomeroyi* (*Spo*-ATA) exhibited enhanced recyclability towards the different aminations in batch experiments. It was therefore selected to run the reductive amination of HMF into 5-(hydroxymethyl)furfurylamine (HFMA) in continuous flow-mode, with alanine (Figure 35**a**) or isopropylamine (Figure 35**b**) as co-substrate. After 12 days of continuous operation at a flow rate of 0.05 mL.min^{-1} (4 minutes residence time), the heterogenous biocatalyst lost c.a. half of its initial activity, but still showed high HMF conversions (i.e. 48% and 41%, with alanine and isopropylamine, respectively).

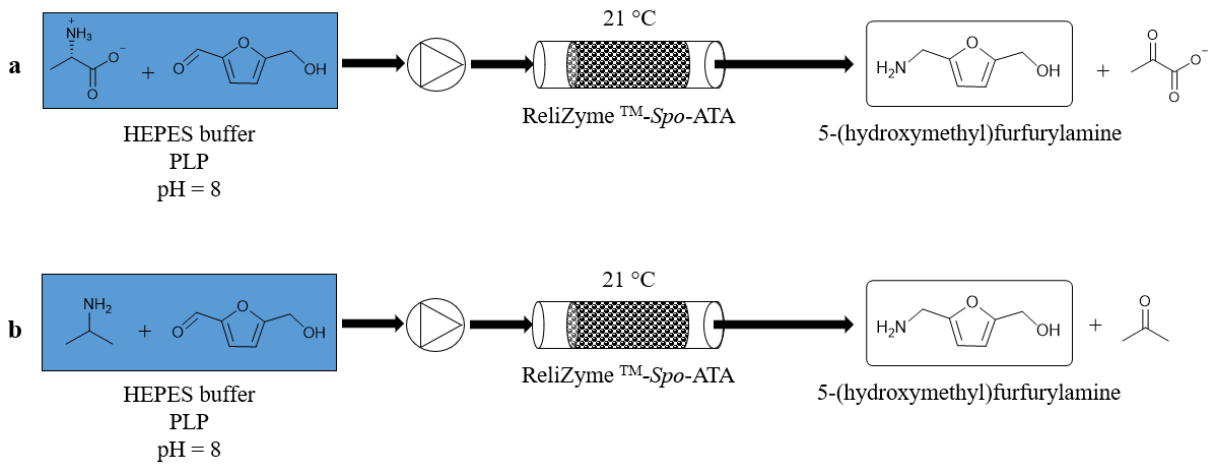

Figure 35. Schematic representation of the process leading to the continuous reductive amination of 5-(hydroxymethyl)furfural into 5-(hydroxymethyl)furfurylamine (HFMA) using immobilized transaminase, described by Berglund *et al*. **[215]**.

Other carriers were also employed as enzyme support to run transamination reactions in continuous flow-mode. For example, de Souza *et al.* [216] managed to covalently immobilize *Vf*-ATA onto two distinct functionalized cellulose. To provide the anchoring points for covalent grafting, the hydroxyl groups of cellulose were silanized either using APTES (followed by glutaraldehyde activation) or by (3-glycidyloxypropyl)trimethoxysilane (GLYMO), prior enzyme immobilization to ensure the covalent grafting. This epoxy-modified cellulose gave rise to high enzyme loading (40 mg.g$_{carrier}^{-1}$) and the resulting immobilized *Vf*-ATA demonstrated good catalytic activity and recyclability in batch (towards the kinetic resolution of *rac*-MBA). Subsequently, the biocatalyst was employed for the asymmetric synthesis of S-

MBA (using the multienzymatic LDH-GDH system to shift the equilibrium) in continuous flow-mode, in a PBR (Figure 36). LDH and GDH enzymes were continuously fed in the free form (in a buffered solution containing also alanine and acetophenone) to the PBR. The continuous operation resulted in enhanced productivity with respect to batch processes: the reaction time was reduced from 48 h to 90 min, while the conversion was increased from 30% to 80%.

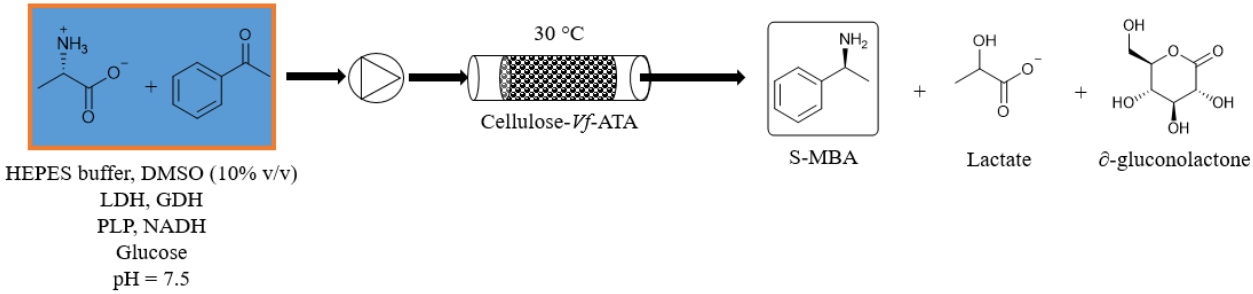

Figure 36. Schematic representation of the process leading to the continuous asymmetric synthesis of S-methylbenzylamine (S-MBA) using immobilized transaminase, described by de Souza *et al.* [216]. The LDH-GDH system was employed to shift the thermodynamic equilibrium (and for NADH cofactor regeneration).

Very recently, lignin derivatives were valorised as carrier for the immobilization of a battery of enzymes, including transaminases [217]. A number of lignin functionalization strategies were attempted to provide various anchoring points (namely aldehydes, epoxy, cobalt chelates and amines) for the subsequent ATAs immobilization. Among all the screened enzymes and activated supports, the HeWT transaminase reversibly immobilized on PEI-derivatized lignin showed the highest immobilization and catalytic performance (17% retained specific activity). Importantly, despite the weak ionic interactions between HeWT and the PEI-lignin, no enzyme leaching was detected after 8 catalytic cycles in batch. Owing to its enhanced efficiency and recyclability, such heterogeneous biocatalyst was integrated to a PBR to run the flow amination of cinnamaldehyde into of cinnamylamine (Figure 37). At a flow rate of 0.35 $mL.min^{-1}$ (2 minutes retention time), ≥80% conversion was achieved during the 100 minutes of continuous operation.

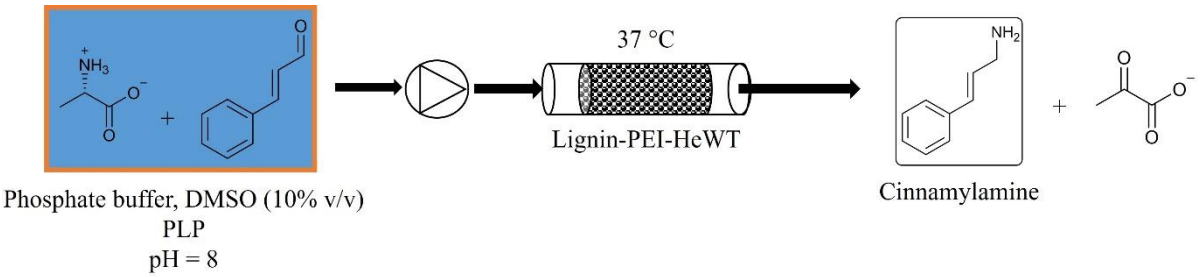

Figure 37. Schematic representation of flow synthesis of cinnamylamine using PEI-lignin-immobilized transaminase, described by Luterbacher *et al.* [217].

In 2017, Žnidaršič-Plazl *et al.* [222] successfully achieved the flow transamination of S-MBA (deamination) with pyruvate using ATAs encapsulated in a polyvinyl alcohol matrix (Lentikatz®) placed in a PBR. After 21 days of process (at flow rate of 0.5 µL.min^{-1}), the catalyst still exhibited up to 80 % initial activity.

Debecker *et al.* [175] recently reported on the use of ATA-117 transaminase, covalently immobilized on a macroporous silica monolith prepared by emulsion-based sol-gel method (denoted "Si(HIPE"), in flow. To this aim, the Si(HIPE) was first aminated through silanization using APTES and further modified by glutaraldehyde, which provided suitable anchoring points for the ATA. The resulting bioreactor was then to run the kinetic resolution of racemic bromo-α-methylbenzylamine (*rac*-BMBA) in continuous flow-mode (Figure 38). This texture of the Si(HIPE) ensured a plug-flow regime through the macroporous support. The most productive biocatalyst yielded 6.2 % of BAP with 10 minutes contact time (corresponding to 16 % residual activity with respect to free enzymes in batch reactor). Simply placing 8 monoliths in series (to increase the contact time) allowed pushing the reaction to completion (i.e. ~50% conversion). In a second work [218], the APTES silanization and enzyme grafting steps were improved by optimizing some technical parameters (humidity, temperature, concentrations) which resulted a significant specific activity boost. The optimized immobilized biocatalyst reached 30 % conversion with 10 minutes contact time.

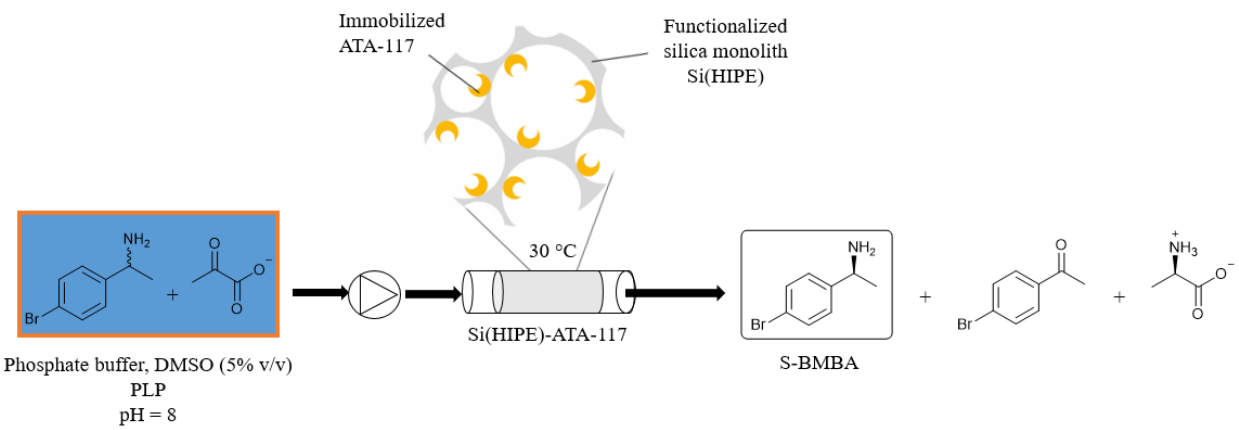

Figure 38. Schematic representation of the continuous kinetic resolution of *rac*-bromo-α-methylbenzylamine (*rac*-BMBA) using immobilized transaminase described, by Debecker *et al.* [175].

Very recently, Corma *et al.* [232] managed to immobilize an ATA on 2D ITQ-2 zeolites, for the obtention of valuable chiral amines from prochiral ketones derived from biomass through a chemo-enzymatic cascade in continuous flow-mode. The zeolite surface was functionalized with amino groups (using APTES, through silanization) in order to reversibly immobilize the ATA (*via* electrostatic interactions). The resulting heterogeneous biocatalyst showed enhanced stability in batch and flow model transamination experiments, and no enzyme leaching was detected. The solid was exploited to run the chemo-enzymatic production of S-4-(4-methoxyphenyl)-2-butananamine production from 4-(4-methoxyphenyl)-2-butanone and acetone. Two reactors were placed in series: the first step of the cascade, a chemo-catalytic aldol-reduction, was performed in a semi-continuous batch reactor (in presence of Pd/MgO catalyst and under pressurized hydrogen) while the subsequent transamination took place in a fixed-bed reactor, in flow mode (Figure 39). At a flow rate of 0.25 $mL.h^{-1}$, the S-4-(4-methoxyphenyl)-2-butanamine yield was maintained over 90% during the 160 hours of operation.

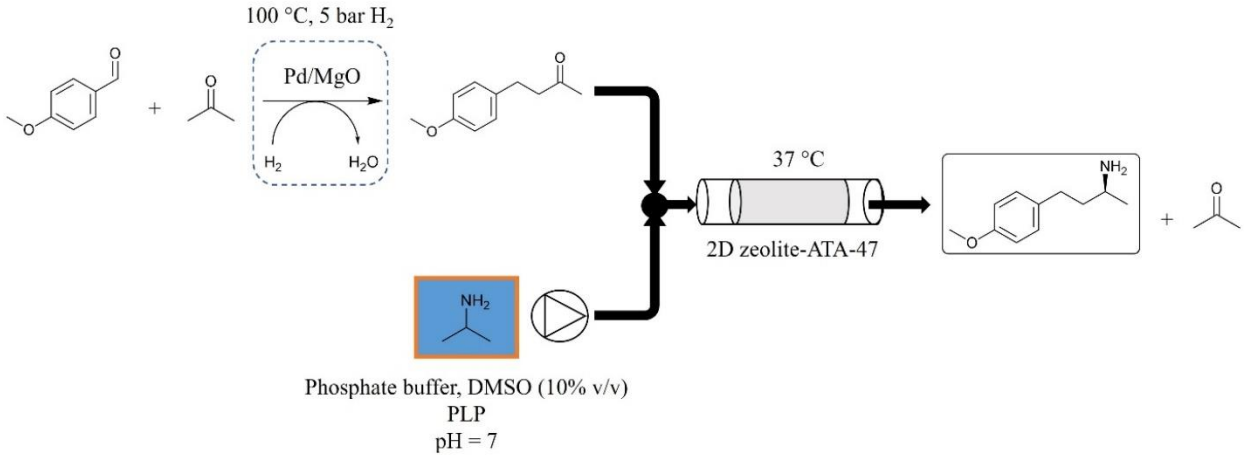

Figure 39. Schematic representation of the chemo-enzymatic process involving a flow asymmetric synthesis of S-4-(4-methoxyphenyl)-2-butanamine (framed compound), described by Corma *et al.* [232]. The dotted area represents the semi-continuous batch reactor hosting the chemocatalytic step of the cascade (aldol-reduction).

Silica-based micro-reactors also were handled by Baganz *et al.* [219] for the immobilization of transaminase and transketolase (TK) enzymes, and exploited for the flow cascade synthesis of a valuable chiral amino-alcohol: (2R,3S)-3-aminobutane-1,2,4-triol (a building block used in pharmaceutical industry). Nickel-derivatized silica (previously made more hydrophobic *via* MTES grafting) was employed for His-tag affinity immobilization. To perform the multi-enzymatic cascade, two separated micro-reactors containing the respective enzymes were placed in series. The first immobilized enzyme (TK) catalysed the model conversion of lithium-hydroxypyruvate and glycolaldehyde to L-erythrulose (ERY), while the second micro-reactor unit (loaded with immobilized ATA) converted ERY into aminobutanetriol. Transamination was conducted in the asymmetric synthesis mode, using S-MBA as amino donor. Similarly, authors from the same group [220] achieved such flow mode synthesis of chiral aminobutanetriol amino-alcohols, but with a different support for the immobilized ATA and TK enzymes (i.e. Ni-NTA derivatized agarose beads ; Figure 40).

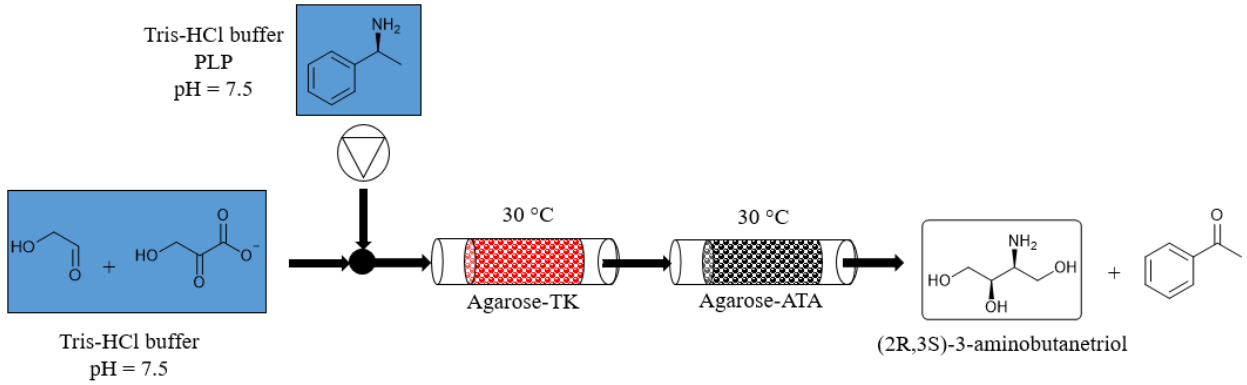

Figure 40. Schematic representation of the process leading to the continuous multienzymatic synthesis of (2R,3S)-3-aminobutanetriol, described by Baganz *et al.* [219]. By-product (CO_2) and intermediate compound (L-erythrulose) generated by transketolation were intentionally omitted for clarity purpose.

In 2017, Sans *et al.* [221] demonstrated the first example of modified 3D-printed devices for the immobilization and application of ATAs in continuous flow-mode. A commercially available Nylon (Taulman 645 and 618) was 3D-printed and chemically modified in order to ensure subsequent covalent grafting of ATAs. More precisely, Nylon was treated with HCl in order to generate superficial amine groups, which were then modified with alternated glutaraldehyde-polyethyleneimine (PEI) layers to provide covalent anchoring points for the enzymes. The authors first used the transamination of S- and R-MBA with pyruvate in batch mode, using both S- and R-selective commercial ATAs to showcase the technology. The immobilized R-selective ATA-117 was then selected for the continuous flow experiment (*i.e.* flow kinetic resolution of *rac*-MBA Figure 41). When working with a residence time of 50 min, almost full conversion and enantiomeric excess were observed. Moreover, the immobilized biocatalyst showed good operational stability as it displayed stable performance during ~100 hours of time on stream.

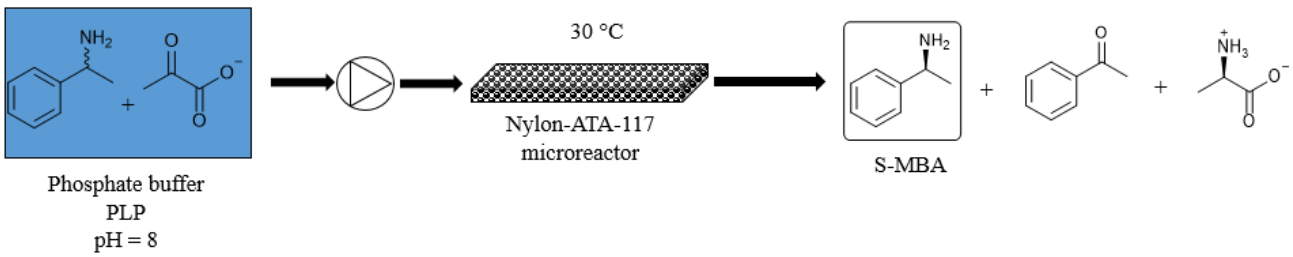

Figure 41. Schematic representation of the continuous kinetic resolution of *rac*-methylbenzylamine (*rac*-MBA) using immobilized transaminase, described by Sans *et al.* [221].

5.3 Flow mode transamination with ATA co-immobilized with its cofactor (PLP)

Sticking to the aim of developing more robust biocatalysts with enhanced operational life-span and enhanced cost efficiency, the López-Gallego and Paradisi groups have developed novel strategies to co-immobilize enzymes and their phosphorylated cofactors (e.g. PLP and NADH onto a plethora of porous beads) [233,234]. Such novel biocatalyst formulation should allow processing flow enzymatic reactions without additional (exogeneous) feed of the cofactor during operation. The authors managed to demonstrate such model of self-sufficient heterogeneous biocatalysts by co-immobilizing ATAs and PLP onto metal derivatized commercial epoxy-activated methacrylate beads (Lifetech Purolite® ECR and Sepabeads® EC-EP/S) [223]. The metal derivatization (leading to cobalt chelates) was first performed as described by Paradisi *et al* [131]. A fraction of the remaining epoxy-groups of the carriers were subsequently modified with amine groups (reaction with ethanolamine (eA), hydroxylamine (hA) or polyethyleneimine (PEI)). Modification with eA and hA provide electrostatic interaction points for PLP adsorption. Modification with PEI additionally allows establishing reversible covalent (imine) bonds between the carrier and PLP (Figure 42). ATA immobilization was promoted by His-tag affinity and consisted in a multi-covalent attachment on the residual epoxy groups present on the carriers.

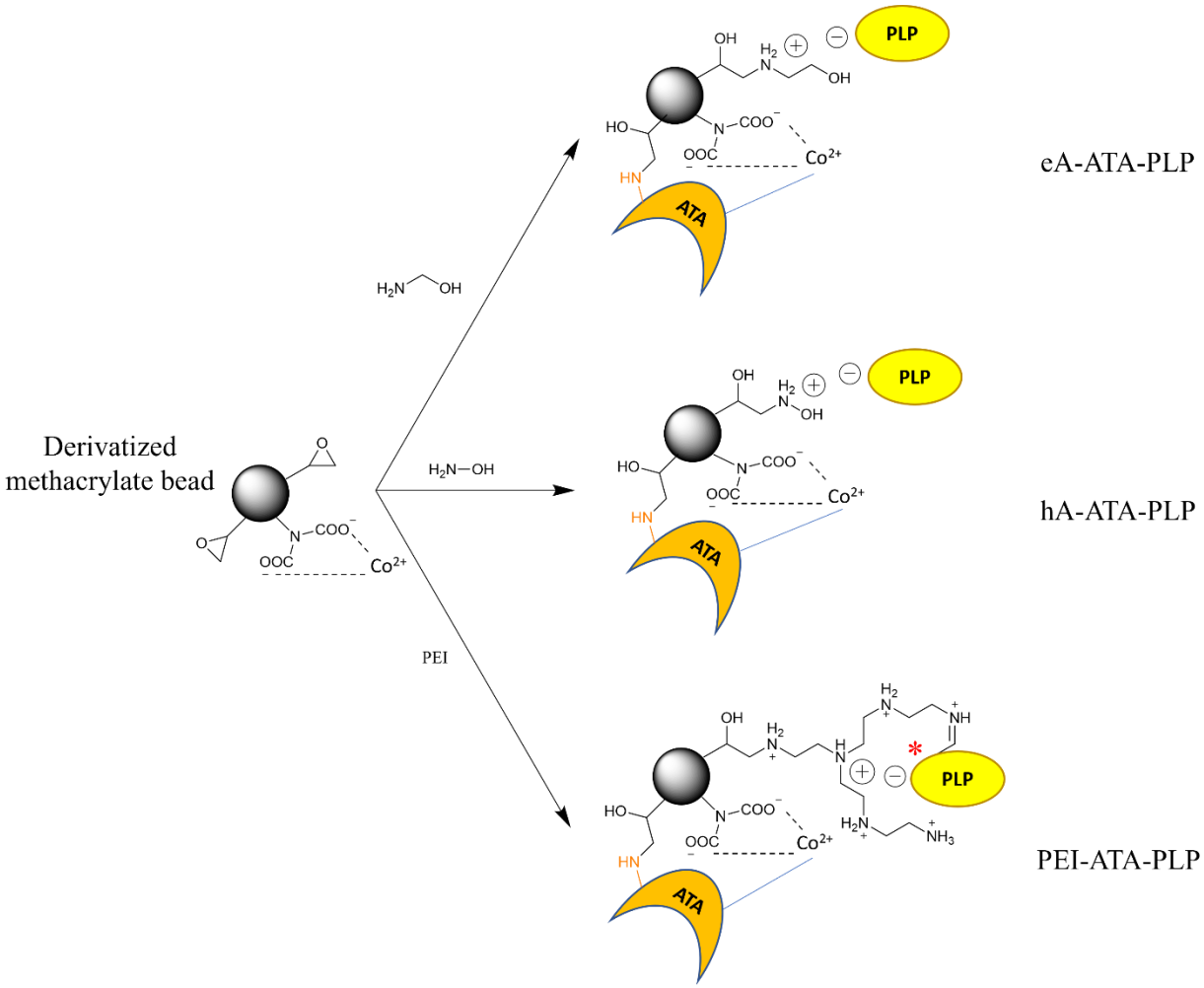

Figure 42. Preparation of self-sufficient biocatalysts. Methacrylate-based carriers activated with epoxy groups were first pre-functionalized (not shown) with cobalt chelates able to drive the His-tagged ATA immobilization. The resulting carrier was further activated with amine groups from ethanolamine (eA), hydroxylamine (hA) and polyethyleneimine (PEI) for the PLP co-immobilization. Red asterisk highlights the dual binding of PLP on the PEI layer. Note that the orange bonds represent the ATA lysine groups involved in the covalent attachment (with the residual epoxy groups of the carriers). Adapted from [223].

The catalytic performance of the resulting self-sufficient heterogeneous biocatalysts were evaluated towards the flow deamination of S-MBA into acetophenone (in a PBR), without exogenous addition of PLP. The beneficial impact of such dual PLP binding (enabled by the PEI) on catalytic performance was clearly highlighted by the greater operational stability displayed by the PEI-coated biocatalyst, EC/PEI-HeWT-PLP. Pleasingly, EC/PEI-HeWT-PLP even displayed higher stability than the corresponding biocatalytic system continuously supplied with exogenous PLP, for 100 minutes of time on stream (in the flow synthesis of cinnamylamine ; Figure 43). Finally, the authors expanded this concept of self-sufficient heterogeneous biocatalysts to other ATAs: *Cv*-ATA and the ATA from *Pseudomonas fluorescens*, *Pf*-ATA. Interestingly, clear differences in terms of operational stabilities were

observed between the ATAs when performing the deamination of S-MBA into acetophenone in flow. The obtained trend was as follow: HeWT > *Pf*-ATA > *Cv*-ATA. The cofactor loading was around 7.5 µmol.g^{-1} on all the EC/PEI-ATA-PLP catalysts.

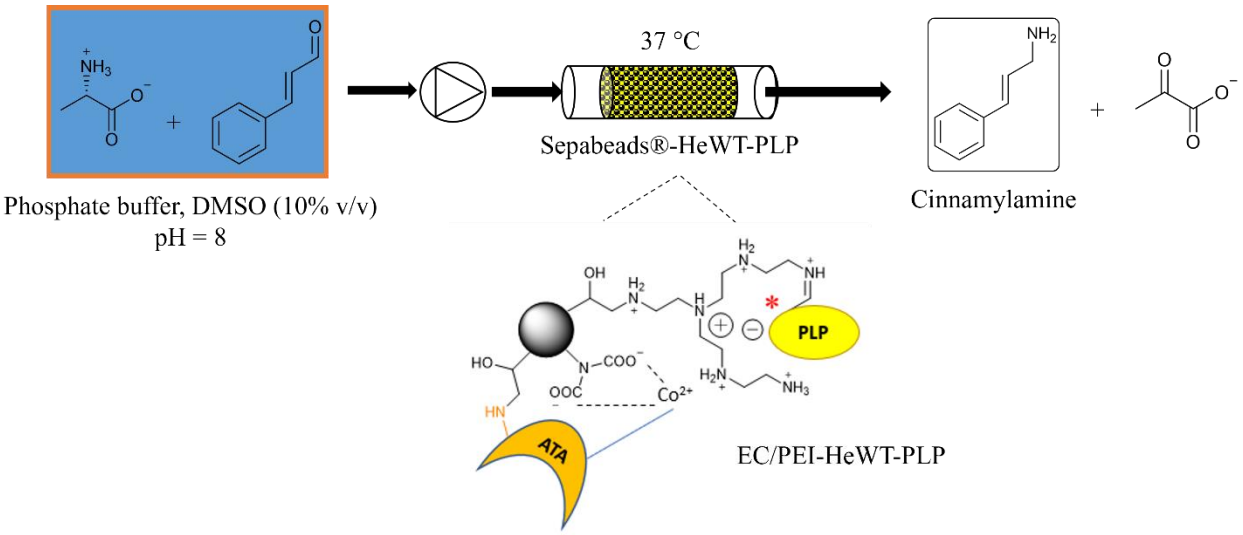

Figure 43. Schematic representation of the continuous production of cinnamylamine (employing self-sufficient immobilized transaminase, without exogeneous PLP addition), described by Lopez-Gallego *et al.* [223].

This self-sufficient co-immobilized biocatalyst system was also used for the synthesis of high value biogenic aldehydes in a PBR (using HeWT) [224]. The packed enzyme column was fed by a segmented biphasic flow stream (80:20 buffer/toluene) formed through toluene addition at the entrance of the reactor. Such biphasic system allowed an in-line separation of pure aldehydes (recovered in the toluene stream) from L-alanine and unreacted amines (that remained in the aqueous phase) without affecting the biocatalyst's activity.

Similarly, Liu and co-workers managed to covalently co-immobilize both an ATA and PLP on functional epoxy resins [225]. Thus, compared to the previously reported self-sufficient ATA catalysts (on which PLP is immobilized through reversible covalent interactions) [223], here, the epoxy groups of the resin formed irreversible covalent bonds with the phosphate group of the PLP. They also afforded the covalent immobilization of the ATA *via* grafting of its lysine residues. A linker, with appropriate length (12 carbons), ensured a high PLP-epoxy binding efficiency and did not alter PLP conformation. Similar cofactor loadings to those previously obtained on epoxy-activated methacrylate beads (c.a. 7 µmol.g^{-1}) were achieved through this protocol. This self-sufficient biocatalyst was employed in the flow asymmetric synthesis of R-sitagliptin in a PBR for > 500 hours of time of stream, without exogenous addition of PLP

(Figure 44). IPA (35 g/L) was used as amino donor. For each column volume (*i.e.* 45 min residence time), the yield and enantiomeric excess of R-sitagliptin reached at least 90% and 99%, respectively. An overall space-time yield of 40.0 $g.L^{-1}.h^{-1}$ was obtained.

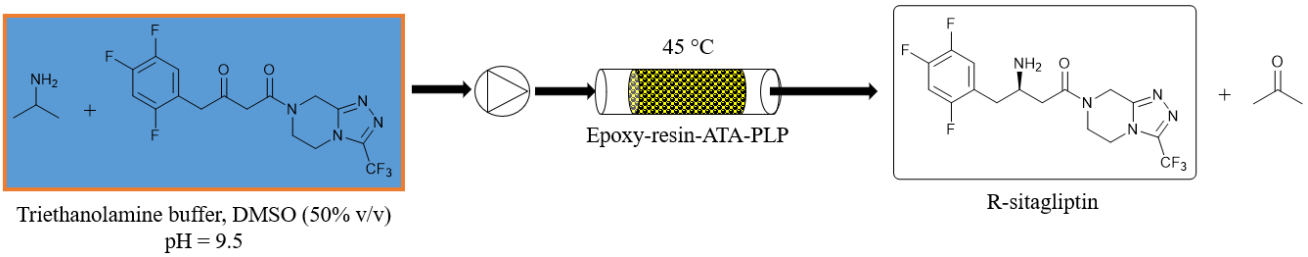

Figure 44. Schematic representation of the continuous asymmetric synthesis of R-sitagliptin (employing self-sufficient immobilized transaminase, without exogeneous PLP addition), described by Liu *et al.* [225].

Noteworthily, the PEI-derivatized lignin carrier discussed above [217] (see section 5.2) also enabled the co-immobilization of ATA and PLP. The cofactor was immobilized by dual reversible interactions on the PEI layer, which allow it to travel to the enzyme active site without diffusing through the lignin network. PLP loading yielded c.a. 7 $\mu mol.g^{-1}$, like on others self-sufficient biocatalysts [223,225]. Such biocatalyst was integrated in a PBR to perform the flow synthesis of cinnamalylamine. At a flow rate of 0.35 $mL.min^{-1}$, the self-sufficient biocatalyst showed stable performance and maintained > 50% conversion during the 100 minutes of operation.

Independently, Menegatti and Žnidaršič-Plazl [168] also demonstrated the possibility to obtain such self-sufficient heterogeneous biocatalyst *via* enzyme and cofactor entrapment into a microreactor containing a polyvinyl alcohol (PVA) and sodium alginate copolymer hydrogel. The microreactor was composed of two PMMA rectangular plates (200 µm thick, 25 mm wide, 50 mm long), filled with the hydrogel. The ATA and PLP were first immersed into the polymeric network, and a $CaCl_2$ post-treatment was eventually applied to reduce the pore size to <5 nm. The resulting biocatalytic microbioreactor was employed to run the model deamination of S-MBA and pyruvate into acetophenone and L-alanine in flow mode. 92% of the initial productivity was retained and no leaching of PLP or enzyme from the hydrogel was observed after 10 days of continuous operation. Similar performance was obtained with and without addition of exogenous PLP, suggesting an efficient cofactor immobilization. The space-time yield was 19.91 $g\ L^{-1}\ h^{-1}$.

5.4 Flow mode transamination with ATA co-immobilized with other enzymes

Enzymatic cascade reactions exploiting multi-enzyme systems appear a highly attractive solution for the design of greener synthesis processes. Here too, (co)-immobilization is considered as the key, allowing to envisage robust processes where (multi)-functional biocatalysts can be (i) recovered and reused in batch mode, or (ii) exploited in continuous flow mode. Materials featuring several co-immobilized enzymes are primed to simplify and intensify continuous processes, *e.g.* by using a single PBR, avoiding transitional separation and purification of intermediates, and displacing equilibria towards product formation [235,236]. Examples of multi-enzyme heterogeneous biocatalysts featuring immobilized ATA operating in continuous flow are discussed below.

In 2009, Yang *et al.* [148] reported on the combined use of transamination and dehydrogenation, for the flow mode glutamate quantification in rat plasma. Glutamic-pyruvic transaminase (GPT) and glutamate dehydrogenase were co-immobilized into a glass micro-capillary previously functionalized with APTES and glutaraldehyde. The transaminase was used for the recycling of α-keto-glutarate (previously produced by glutamate dehydrogenation) into glutamate, as shown in Figure 45. Glutamate concentration was indirectly monitored through NADH product quantification. As the transaminase catalyses the reaction between the natural amino acid and α-keto acid, the chemical equilibrium was highly favourable.

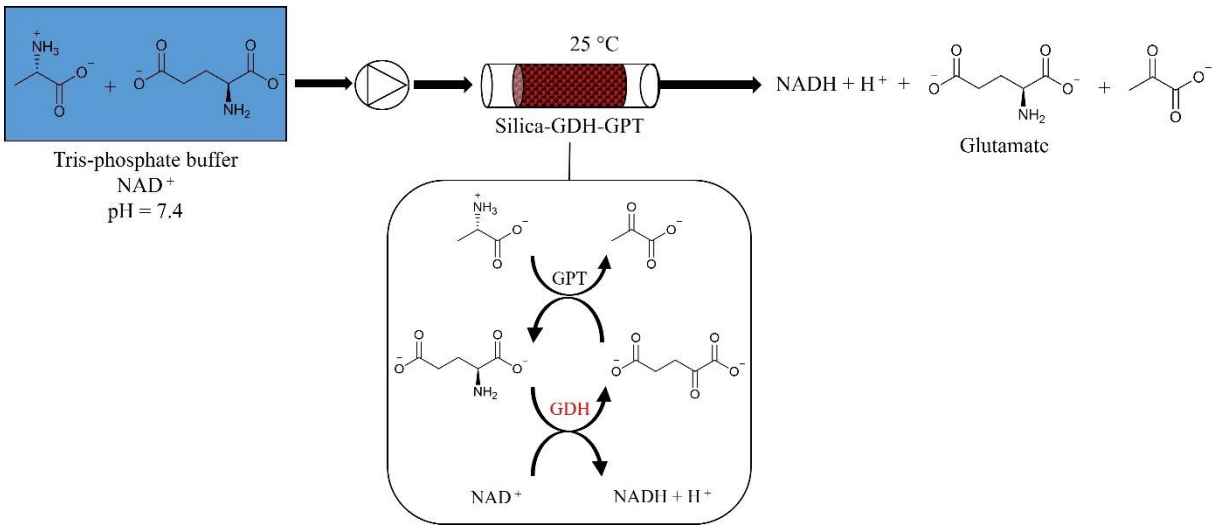

Figure 45. Schematic representation of the multienzymatic one-pot process described by Yang *et al.* [148] (including flow transamination, in combination with a flow glutamate

dehydrogenation) resulting in the continuous blood glutamate determination. The complete cascade reaction is highlighted in the frame. GPT and GDH stand for glutamic-pyruvic transaminase and glutamate dehydrogenase, respectively.

In 2021, Romero-Fernandez and Paradisi [226] synthesized the drug betazole by co-immobilizing alcohol dehydrogenase, HLADH (i.e. a NADH-dependent enzyme that oxidizes alcohols into aldehydes) and HeWT onto functionalized epoxy-activated methacrylate beads (Relisorb® EP400SS). In order to shift the equilibrium of the alcohol oxidation (and thus, of the entire cascade) and enable the *in-situ* continuous recycling of the NADH cofactor, a third enzyme was grafted on the carrier: the NADH oxidase (NOX). Since NOX uses O_2 as oxidant (generating H_2O as by-product), the multifunctional heterogeneous biocatalyst a constant supply of oxygen was fed through a segmented air-liquid flow. The resulting multifunctional biocatalyst allowed performing a flow-cascade in a PBR, starting from 2-(1H-pyrazol-3-yl)ethanol and yielding betazole in good yields (73 %) (Figure 46). A space-time yield up to 2.59 $g.L^{-1}.h^{-1}$ with 15 min residence time was achieved.

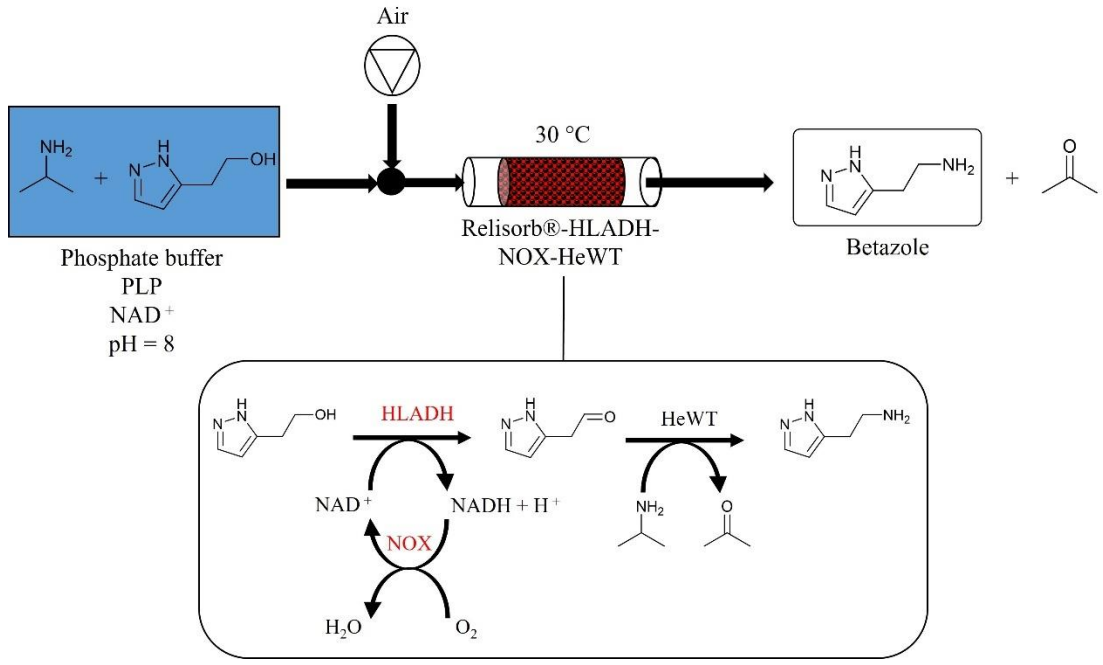

Figure 46. Schematic representation of the one-pot multienzymatic production of betazole drug described by Romero-Fernandez and Paradisi **[226]** (including flow transamination, in combination with flow alcohol dehydrogenation and NADH oxidation). The complete cascade reaction is highlighted in the frame. NOX cofactor (FAD) was intentionally omitted for clarity.

Paradisi et al. [227] employed this same co-immobilized HLADH-NOX-HeWT biocatalysts system to access the flow cascade synthesis of 6-aminocaproic acid (a Nylon 6 precursor) from ϵ-caprolactone. The enzymes were combined with commercially available *Candida antarctica*

lipase B (CalB, Novozym® 435), which performed the first step of the cascade (i.e. hydrolysis of ϵ-caprolactone into 6-hydroxycaproic acid). A substrate solution was flowed into the two sequential PBRs, respectively containing immobilized CalB (10 min residence time) and co-immobilized HLADH-HeWT-NOX (15 min residence time). A segmented air-liquid flow was also fed into the second PBR, in order to feed oxygen to the NOX enzyme for the *in-situ* continuous recycling of the NADH (Figure 47). A final conversion of 34 %, associated with a space-time yield of 3.31 $g.L^{-1}.h^{-1}$, was achieved. Remarkably, this study represents the first biocatalytic synthesis route of 6-aminocaproic acid from ϵ-caprolactone, which can be derived from lignocellulosic biomass. It is also the first synthesis of this platform chemical in continuous flow-mode.

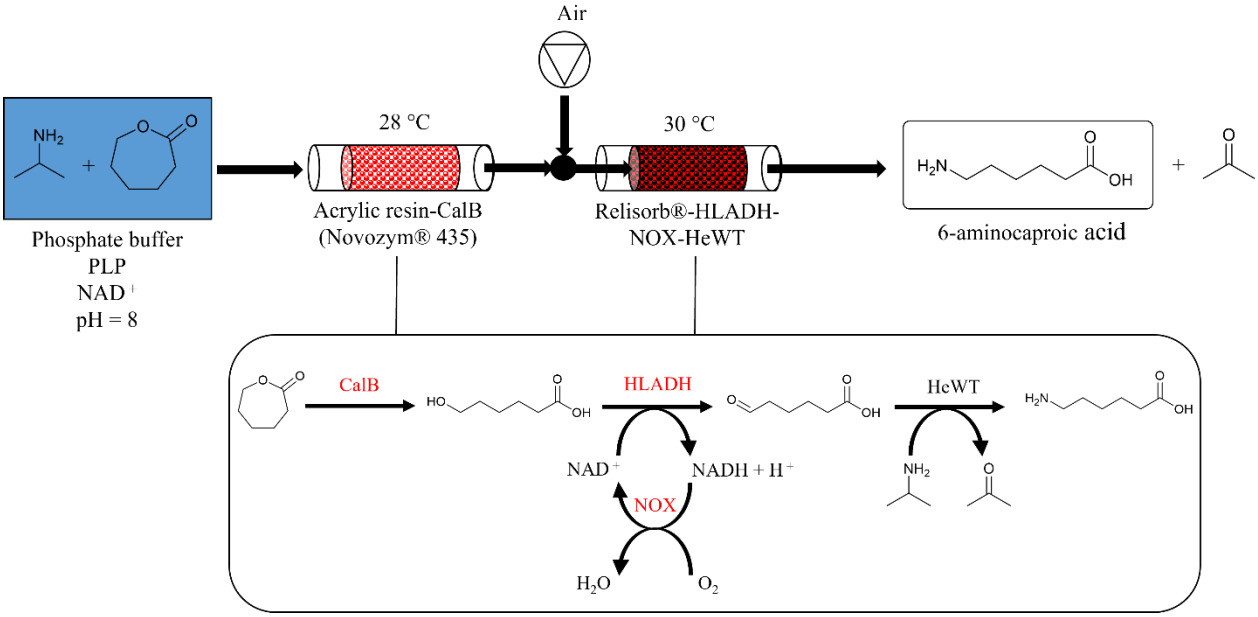

Figure 47. Schematic representation of the one-pot multienzymatic production of 6-aminocaproic acid (a Nylon 6 precursor), including flow transamination, in combination with flow alcohol dehydrogenation and NADH oxidation [227]. The complete cascade reaction is highlighted in the frame. NOX cofactor (FAD) was omitted for clarity.

It should be noted that the combination of several enzymes in one continuous flow process can also be applied with whole cells biocatalysts. A sol–gel process was exploited by Poppe *et al.* [228] to co-immobilize *Escherichia coli* whole cells with *Cv*-ATA activity and *Lodderomyceselongisporus* yeasts with ketoreductase activity (*Le*KRED) in hollow silica microspheres. The bifunctional biocatalyst allowed performing a cascade of reactions to convert racemic amines into a mixture of the corresponding enantiomerically pure R-amine and S-alcohol in continuous flow mode. In other words, the kinetic resolution catalysed by *Cv*-ATA let enantiopure R-amine unreacted as it enabled the bioconversion of the S-amine into the

corresponding ketone, which was subsequently reduced into the corresponding S-alcohol by *Le*KRED (Figure 48). Notably, the authors managed to obtain simultaneously two different APIs : R-4-phenylbutan-2-amine (a constituent of Dilevalol drug) and S-4-phenyl-2-butanol (a precursor to antiepileptic agents). Moreover, they demonstrated that the use of such bifunctional heterogeneous biocatalyst containing both co-immobilized whole cells (with overexpression of the enzyme) in a single reactor enhances the activity and the operational stability of the system compared to that of the cascade featuring single-cells immobilized in separated reactors (placed in series).

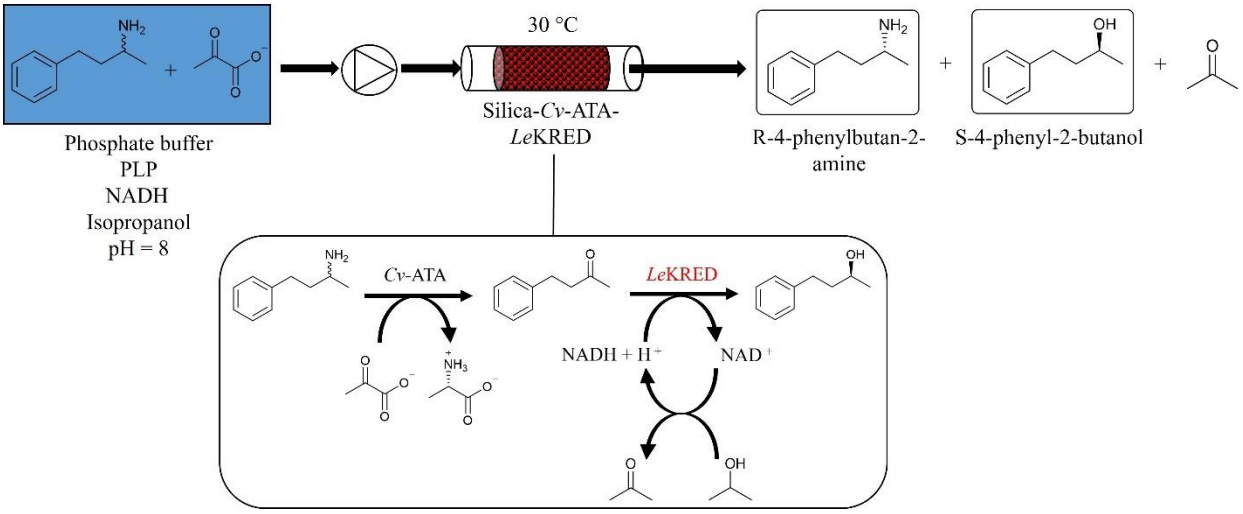

Figure 48. Schematic representation of the one-pot multienzymatic production of R-4-phenylbutan-2-amine and S-4-phenyl-2-butanol (including flow transamination, in combination with flow ketone reduction) described by Poppe *et al.* [228]. The complete cascade reaction is highlighted in the frame. *Le*KRED stands for *Lodderomyceselongisporus* yeast displaying ketoreductase activity.

6. Concluding remarks

Transaminases have gained immense interest lately as their potential to produce enantiopure amines at a lower environmental cost is now well-established. Considerable efforts have been deployed to mitigate the limitations that used to hinder their application at large-scale. In particular, implementing equilibrium displacement methods and leveraging effective enzyme immobilization strategies made the application of transaminases more realistic. Moving further, we argue that embracing a transfer from batch processes – where the enzyme is soluble in the liquid phase – to heterogeneous flow processes – where the enzyme is immobilized on a solid carrier, is a key step in the development of biocatalytic transamination for organic synthesis.

The present review extensively covers and discuss applications featuring immobilized transaminases in continuous flow-mode. As illustrated with a variety of successful examples, the opportunities offered by continuous flow mode processing for the biocatalytic production of chiral amines are multiple: in addition to enhance their productivity as well as scalability (due to improved mass transfer and biocatalyst reusability), it facilitates the combination with other reactions, it is amenable to multi-enzymatic cascade reactions and it allows envisaging useful in-line separations such as product purification (*e.g. via* catch-and-release systems, membrane separation, etc.). Integrated processes allowing to simultaneously perform flow transamination reactions and product separation (to drive the equilibrium), are of particular interest [103,237]. We argue that the implementation of novel hybrid reactors which simultaneously host the immobilized enzymes and perform product separation (*e.g.* in membrane reactors), will foster further advances in the field of greener chiral amine synthesis.

It appears undisputable that continuous flow mode biocatalytic processes pave the way for the development of more efficient, industrially relevant, greener, and intensified organic synthesis [238]. This report should provide useful guidelines to industrial chemists who envisage turning to flow biocatalysis for their drug production, but also academic researchers who will keep inventing greener routes to high-value molecules. The deployment of flow biocatalysis is a multidisciplinary challenge that requires various expertise. Arguably, the "cross-fertilization" – illustrated in this review – between the fields of biocatalysis and organic synthesis on the one hand, and process and materials engineering on the other hand, is crucial for both academic and industrial developments.

Acknowledgments

This research was funded by the Actions de Recherche Concertée ARC (grant number 20-25/108) and by the Fonds Spécial de recherche (UCLouvain). DPD thanks the Francqui Foundation for the Francqui Research Professor chair.

References

1 M. D. Truppo, *ACS Med. Chem. Lett.*, 2017, **8**, 476–480.

2 R. A. Sheldon and J. M. Woodley, *Chem. Rev.*, 2018, **118**, 801–838.

3 D. J. C. Constable, P. J. Dunn, J. D. Hayler, G. R. Humphrey, J. Johnnie L. Leazer, R. J. Linderman, K. Lorenz, J. Manley, B. A. Pearlman, A. Wells, A. Zaks and T. Y. Zhang, *Green Chem.*, 2007, **9**, 411–420.

4 T. C. Nugent, *Chiral Amine Synthesis. Methods, Developments and Applications. Edited by Thomas C. Nugent.*, 2010, vol. 49.

5 L. J. Diorazio, P. Richardson, H. F. Sneddon, A. Moores, C. Briddell and I. Martinez, *ACS Sustain. Chem. Eng.*, 2021, **9**, 16862–16864.

6 M. D. Patil, G. Grogan, A. Bommarius and H. Yun, *Catalysts*, 2018, **8**, 254.

7 D. Ghislieri and N. J. Turner, *Top. Catal.*, 2014, **57**, 284–300.

8 Iwao Ojima, *Catalytic Asymmetric Synthesis*, John Wiley & Sons, Hoboken, 2010.

9 J. Ward and R. Wohlgemuth, *Curr. Org. Chem.*, 2010, **14**, 1914–1927.

10 T. C. Nugent and M. El-Shazly, *Adv. Synth. Catal.*, 2011, **353**, 804–804.

11 P. Kelefiotis-Stratidakis, T. Tyrikos-Ergas and I. V. Pavlidis, *Org. Biomol. Chem.*, 2019, **17**, 1634–1642.

12 P. T. Anastas and J. C. Warner, *Green Chemistry: Theory and Practice*, Oxford University Press, New York, 1998, vol. 2.

13 D. P. Debecker, K. Kuok (Mimi) Hii, A. Moores, L. M. Rossi, B. Sels, D. T. Allen and B. Subramaniam, *ACS Sustain. Chem. Eng.*, 2021, **9**, 4936–4940.

14 C. Jimenez-Gonzalez, C. S. Ponder, Q. B. Broxterman and J. B. Manley, *Org. Process Res. Dev.*, 2011, **15**, 912–917.

15 P. J. Dunn, A. S. Wells and M. T. Williams, *Green Chemistry in the Pharmaceutical Industry*, Wiley-VCH, Mörlenbach, 2010.

16 F. Hollmann, D. J. Opperman and C. E. Paul, *Angew. Chem. Int. Ed.*, 2021, **60**, 5644–5665.

17 C. K. Savile, J. M. Janey, E. C. Mundorff, J. C. Moore, S. Tam, W. R. Jarvis, J. C. Colbeck, A. Krebber, F. J. Fleitz, J. Brands, P. N. Devine, G. W. Huisman and G. J. Hughes, *Science*, 2010, **329**, 305–309.

18 I. Slabu, J. L. Galman, R. C. Lloyd and N. J. Turner, *ACS Catal.*, 2017, **7**, 8263–8284.

19 T. Sehl, H. C. Hailes, J. M. Ward, R. Wardenga, E. Von Lieres, H. Offermann, R. Westphal, M. Pohl and D. Rother, *Angew. Chem. - Int. Ed.*, 2013, **52**, 6772–6775.

20 F. Guo and P. Berglund, *Green Chem.*, 2017, **19**, 333–360.

21 S. G. Koenig, D. K. Leahy and A. S. Wells, *Org. Process Res. Dev.*, 2018, **22**, 1344–1359.

22 L. A. Nguyen, H. He and C. Pham-Huy, *Int. J. Biomed. Sci.*, 2006, **2**, 85–100.

23 I. Slabu, J. L. Galman, C. Iglesias, N. J. Weise, R. C. Lloyd and N. J. Turner, *Catal. Today*, 2018, **306**, 96–101.

24 D. L. Nelson and M. M. Cox, *Lehninger Principles of Biochemistry*, Macmillan Learning, New-York, 2013, vol. 1.

25 Roger Crossley, 1992, **48**, 8155–8178.

26 J. S. Lee, W. K. Yang, E. Y. Han, S. Y. Lee, Y. H. Park, M. A. Lim, H. S. Chung and J. H. Park, *Forensic Sci. Int.*, 2007, **173**, 68–72.

27 W. F. Kean, H. E. Howard-Lock and C. J. L. Lock, *The Lancet*, 1991, **338**, 1565–1568.

28 W. H. De Camp, *J. Pharm. Biomed. Anal.*, 1993, **11**, 1167–1172.

29 U.S. Food and Drug Administration, *Chirality*, 1992, **4**, 338–340.

30 B. Yuan, D. P. Debecker, X. Wu, J. Xiao, Q. Fei and N. J. Turner, *ChemCatChem*, 2020, **12**, 6191–6195.

31 Sanofi-Aventis, sanofi, http://en.sanofi.com/Images/13723_20100326_Clopidogrel_en.pdf, (accessed 30 August 2015).

32 J. M. Grohol, psychcentral, http://psychcentral.com/lib/top-25-psychiatric-medication-prescriptions-for-2011, (accessed 30 August 2015).

33 A. Petri, V. Colonna and O. Piccolo, *Beilstein J. Org. Chem.*, 2019, **15**, 60–66.

34 H. U. Blaser, F. Spindler and M. Studer, *Appl. Catal. Gen.*, 2001, **221**, 119–143.

35 H. U. Blaser, A. Indolese and A. Schnyder, *Curr. Sci.*, 2000, **78**, 1336–1344.

36 D. J. Cole-Hamilton, *Science*, 2003, **299**, 1702–1706.

37 D. Ager, *Handbook of Chiral Chemicals*, Taylor & Francis, Boca Raton, 2005.

38 L. Yin, W. Shan, X. Jia, X. Li and A. S. C. Chan, *J. Organomet. Chem.*, 2009, **694**, 2092–2095.

39 World Intellectual Property Organization, WO2009080469A1, 2009.

40 K. B. Hansen, Y. Hsiao, F. Xu, N. Rivera, A. Clausen, M. Kubryk, S. Krska, T. Rosner, B. Simmons, J. Balsells, N. Ikemoto, Y. Sun, F. Spindler, C. Malan, E. J. J. Grabowski and J. D. Armstrong, *J. Am. Chem. Soc.*, 2009, **131**, 8798–8804.

41 D. J. Ager, *Platin. Met. Rev.*, 2009, **53**, 203–208.

42 P.-C. Yan, G.-L. Zhu, J.-H. Xie, X.-D. Zhang, Q.-L. Zhou, Y.-Q. Li, W.-H. Shen and D.-Q. Che, *Org. Process Res. Dev.*, 2013, **17**, 307–312.

43 M. Breuer, K. Ditrich, T. Habicher, B. Hauer, M. Keßeler, R. Stürmer and T. Zelinski, *Angew. Chem. - Int. Ed.*, 2004, **43**, 788–824.

44 R. W. Stringham and Y. K. Ye, *J. Chromatogr. A*, 2006, **1101**, 86–93.

45 Q. He, S. Rohani, J. Zhuh and A. Gomaa, *Chirality*, 2012, **24**, 119–128.

46 K. Vukics, T. Fodor, J. Fischer, I. Fellegvari and S. Levai, *Org. Process Res. Dev.*, 2002, **6**, 82–85.

47 World Intellectual Property Organization, WO2006027658A2, 2006.

48 K. E. Jaeger, *Curr. Opin. Biotechnol.*, 2004, **15**, 269–271.

49 F. H. Arnold, *Angew. Chem. Int. Ed.*, 2019, **58**, 14420–14426.

50 R. C. Simon, N. Richter, E. Busto and W. Kroutil, *ACS Catal.*, 2014, **4**, 129–143.

51 F. Rudroff, M. D. Mihovilovic, H. Gröger, R. Snajdrova, H. Iding and U. T. Bornscheuer, *Nat. Catal.*, 2018, **1**, 12–22.

52 A. Schmid, F. Hollmann, J. B. Park and B. Bühler, *Curr. Opin. Biotechnol.*, 2002, **13**, 359–366.

53 S. C. Cosgrove, A. Brzezniak, S. P. France, J. I. Ramsden, J. Mangas-Sanchez, S. L. Montgomery, R. S. Heath and N. J. Turner, in *Methods in Enzymology*, ed. N. Scrutton, Academic Press, 2018, vol. 608, pp. 131–149.

54 A. Schmid, J. S. Dordick, B. Hauer, A. Kiener, M. Wubbolt and B. Witholt, *Nature*, 2001, **409**, 258–268.

55 N. J. Weise, F. Parmeggiani, S. T. Ahmed and N. J. Turner, *J. Am. Chem. Soc.*, 2015, **137**, 12977–12983.

56 T. Knaus, W. Böhmer and F. G. Mutti, *Green Chem.*, 2017, **19**, 453–463.

57 A. K. Gilio, T. W. Thorpe, N. Turner and G. Grogan, *Chem. Sci.*, 2022, **13**, 4697–4713.

58 G. A. Aleku, S. P. France, H. Man, J. Mangas-Sanchez, S. L. Montgomery, M. Sharma, F. Leipold, S. Hussain, G. Grogan and N. J. Turner, *Nat. Chem.*, 2017, **9**, 961–969.

59 R. Kumar, M. J. Karmilowicz, D. Burke, M. P. Burns, L. A. Clark, C. G. Connor, E. Cordi, N. M. Do, K. M. Doyle, S. Hoagland, C. A. Lewis, D. Mangan, C. A. Martinez, E. L. McInturff, K. Meldrum, R. Pearson, J. Steflik, A. Rane and J. Weaver, *Nat. Catal.*, 2021, **4**, 775–782.

60 J. A. McIntosh, P. S. Coelho, C. C. Farwell, Z. J. Wang, J. C. Lewis, T. R. Brown and F. H. Arnold, *Angew. Chem. - Int. Ed.*, 2013, **52**, 9309–9312.

61 E. O'Reilly and N. J. Turner, *Perspect. Sci.*, 2015, **4**, 55–61.

62 I. Rowles, K. J. Malone, L. L. Etchells, S. C. Willies and N. J. Turner, *ChemCatChem*, 2012, **4**, 1259–1261.

63 F. Hollmann, I. W. C. E. Arends and D. Holtmann, *Green Chem.*, 2011, **13**, 2285–2314.

64 L. J. Hepworth, S. P. France, S. Hussain, P. Both, N. J. Turner and S. L. Flitsch, *ACS Catal.*, 2017, **7**, 2920–2925.

65 S. A. Kelly, S. Pohle, S. Wharry, S. Mix, C. C. R. Allen, T. S. Moody and B. F. Gilmore, *Chem. Rev.*, 2018, **118**, 349–367.

66 A. Gomm and E. O'Reilly, *Curr. Opin. Chem. Biol.*, 2018, **43**, 106–112.

67 R. A. John, *Biochim. Biophys. Acta*, 1995, **1248**, 81–96.

68 T. Lütke-Eversloh and G. Stephanopoulos, *Metab. Eng.*, 2008, **10**, 69–77.

69 W. D. Fessner, *New Biotechnol.*, 2015, **32**, 658–664.

70 P. K. Mehta, T. I. Hale and P. Christen, *Eur. J. Biochem.*, 1993, **561**, 549–561.

71 S. Mathew and H. Yun, *ACS Catal.*, 2012, **2**, 993–1001.

72 A. Iwasaki, Y. Yamada, N. Kizaki, Y. Ikenaka and J. Hasegawa, *Appl. Microbiol. Biotechnol.*, 2006, **69**, 499–505.

73 A. Iwasaki, K. Matsumoto, J. Hasegawa and Y. Yasohara, *Appl. Microbiol. Biotechnol.*, 2012, **93**, 1563–1573.

74 L.-J. Guan, J. Ohtsuka, M. Okai, T. Miyakawa, T. Mase, Y. Zhi, F. Hou, N. Ito, A. Iwasaki, Y. Yasohara and M. Tanokura, *Sci. Rep.*, 2015, **5**, 10753.

75 M. Girardin, S. G. Ouellet, D. Gauvreau, J. C. Moore, G. Hughes, P. N. Devine, P. D. O'Shea and L. C. Campeau, *Org. Process Res. Dev.*, 2013, **17**, 61–68.

76 C. Molinaro, P. G. Bulger, E. E. Lee, B. Kosjek, S. Lau, D. Gauvreau, M. E. Howard, D. J. Wallace and P. D. O'Shea, *J. Org. Chem.*, 2012, **77**, 2299–2309.

77 Sebastian Schätzle, Ernst-Moritz-Arndt-Universität Greifswald, 2011.

78 A. Mozzarelli and S. Bettati, *Chem. Rec.*, 2006, **6**, 275–287.

79 L. Rios-Solis, N. Bayir, M. Halim, C. Du, J. M. Ward, F. Baganz and G. J. Lye, *Biochem. Eng. J.*, 2013, **73**, 38–48.

80 D. Koszelewski, K. Tauber, K. Faber and W. Kroutil, *Trends Biotechnol.*, 2010, **28**, 324–332.

81 K. E. Cassimjee, B. Manta and F. Himo, *Org Biomol Chem*, 2015, **13**, 8453–8464.

82 K. E. Cassimjee, M. S. Humble, V. Miceli, C. G. Colomina and P. Berglund, *ACS Catal.*, 2011, **1**, 1051–1055.

83 J. S. Shin and B. G. Kim, *Biotechnol. Bioeng.*, 1999, **65**, 206–11.

84 M. D. Truppo, J. D. Rozzell and N. J. Turner, *Org. Process Res. Dev.*, 2010, **14**, 234–237.

85 M. M. Musa, F. Hollmann and F. G. Mutti, *Catal. Sci. Technol.*, 2019, **9**, 5487–5503.

86 D. Koszelewski, D. Clay, D. Rozzell and W. Kroutil, *Eur. J. Org. Chem.*, 2009, 2289–2292.

87 M. Fuchs, J. E. Farnberger and W. Kroutil, *Eur. J. Org. Chem.*, 2015, **2015**, 6965–6982.

88 O. US EPA, Presidential Green Chemistry Challenge, https://www.epa.gov/greenchemistry/presidential-green-chemistry-challenge-2010-greener-reaction-conditions-award, (accessed 17 May 2022).

89 A. A. Desai, *Angew. Chem. Int. Ed.*, 2011, **50**, 1974–1976.

90 I. K. Mangion, B. D. Sherry, J. Yin and F. J. Fleitz, *Org. Lett.*, 2012, **14**, 3458–3461.

91 D. J. Wallace, I. Mangion and P. Coleman, in *Comprehensive Accounts of Pharmaceutical Research and Development: From Discovery to Late-Stage Process Development Volume 1*, American Chemical Society, 2016, vol. 1239, pp. 1–36.

92 J. Y. L. Chung, Y.-L. Zhong, K. M. Maloney, R. A. Reamer, J. C. Moore, H. Strotman, A. Kalinin, R. Feng, N. A. Strotman, B. Xiang and N. Yasuda, *Org. Lett.*, 2014, **16**, 5890–5893.

93 J. Y. L. Chung, B. Marcune, H. R. Strotman, R. I. Petrova, J. C. Moore and P. G. Dormer, *Org. Process Res. Dev.*, 2015, **19**, 1418–1423.

94 L. Frodsham, M. Golden, S. Hard, M. N. Kenworthy, D. J. Klauber, K. Leslie, C. Macleod, R. E. Meadows, K. R. Mulholland, J. Reilly, C. Squire, S. Tomasi, D. Watt and A. S. Wells, *Org. Process Res. Dev.*, 2013, **17**, 1123–1130.

95 E. E. Ferrandi and D. Monti, *World J. Microbiol. Biotechnol.*, 2017, **34**, 13.

96 J.-S. Shin and B.-G. Kim, *Biotechnol. Bioeng.*, 1997, **55**, 348–358.

97 M. Burns, C. A. Martinez, B. Vanderplas, R. Wisdom, S. Yu and R. A. Singer, *Org. Process Res. Dev.*, 2017, **21**, 871–877.

98 S. J. Novick, N. Dellas, R. Garcia, C. Ching, A. Bautista, D. Homan, O. Alvizo, D. Entwistle, F. Kleinbeck, T. Schlama and T. Ruch, *ACS Catal.*, 2021, **11**, 3762–3770.

99 C. K. Chung, P. G. Bulger, B. Kosjek, K. M. Belyk, N. Rivera, M. E. Scott, G. R. Humphrey, J. Limanto, D. C. Bachert and K. M. Emerson, *Org. Process Res. Dev.*, 2014, **18**, 215–227.

100 K. S. Midelfort, R. Kumar, S. Han, M. J. Karmilowicz, K. McConnell, D. K. Gehlhaar, A. Mistry, J. S. Chang, M. Anderson, A. Villalobos, J. Minshull, S. Govindarajan and J. W. Wong, *Protein Eng. Des. Sel. PEDS*, 2013, **26**, 25–33.

101 S. Pedragosa-Moreau, A. Le Flohic, V. Thienpondt, F. Lefoulon, A. M. Petit, N. Rïos-Lombarda, F. Moras and J. Gonzalez-Saban, *Adv. Synth. Catal.*, 2017, **359**, 485–493.

102 E. Busto, R. C. Simon, B. Grischek, V. Gotor-Fernández and W. Kroutil, *Adv. Synth. Catal.*, 2014, **356**, 1937–1942.

103 J. Neuburger, F. Helmholz, S. Tiedemann, P. Lehmann, P. Süss, U. Menyes and J. von Langermann, *Chem. Eng. Process. - Process Intensif.*, 2021, **168**, 108578.

104 J. T. Kohrt, P. H. Dorff, M. Burns, C. Lee, S. V. O'Neil, R. J. Maguire, R. Kumar, M. Wagenaar, L. Price and M. S. Lall, *Org. Process Res. Dev.*

105 P. Grunwald, in *Biocatalysis: Biochemical Fundamentals and Applications*, Imperial College Press, Hamburg, Germany, 2009, pp. 727–729.

106 P. Tufvesson, J. Lima-Ramos, J. S. Jensen, N. Al-Haque, W. Neto and J. M. Woodley, *Biotechnol. Bioeng.*, 2011, **108**, 1479–1493.

107 U. T. Bornscheuer, G. W. Huisman, R. J. Kazlauskas, S. Lutz, J. C. Moore and K. Robins, *Nature*, 2012, **485**, 185–194.

108 S. Gargiulo and P. Soumillion, *Curr. Opin. Chem. Biol.*, 2021, **61**, 107–113.

109 H. Yun, B. Y. Hwang, J. H. Lee and B. G. Kim, *Appl. Environ. Microbiol.*, 2005, **71**, 4220–4224.

110 N. J. Turner and R. Kumar, *Curr. Opin. Chem. Biol.*, 2018, **43**, A1–A3.

111 S. A. Kelly, D. J. Magill, J. Megaw, T. Skvortsov, T. Allers, J. W. McGrath, C. C. R. Allen, T. S. Moody and B. F. Gilmore, *Appl. Microbiol. Biotechnol.*, 2019, **103**, 5727–5737.

112 J. A. Littlechild, *Front. Bioeng. Biotechnol.*

113 T. Börner, S. Rämisch, E. Reddem, S. Bartsch, A. Vogel, A.-M. Thunnissen, P. Adlercreutz and C. Grey, *ACS Catal.*, , DOI:10.1021/acscatal.6b02100.

114 G. Antranikian, C. E. Vorgias and C. Bertoldo, *Adv. Biochem. Eng. Biotechnol.*, 2005, **96**, 219–262.

115 J. A. Littlechild, J. Guy, S. Connelly, L. Mallett, S. Waddell, C. A. Rye, K. Line and M. Isupov, *Biochem. Soc. Trans.*, 2007, **35**, 1558–1563.

116 S. DasSarma and P. DasSarma, *Curr. Opin. Microbiol.*, 2015, **25**, 120–126.

117 T. Fukushima, T. Mizuki, A. Echigo, A. Inoue and R. Usami, *Extrem. Life Extreme Cond.*, 2005, **9**, 85–89.

118 D. Alsafadi and F. Paradisi, *Extrem. Life Extreme Cond.*, 2013, **17**, 115–122.

119 G. A. Sellek and J. B. Chaudhuri, *Enzyme Microb. Technol.*, 1999, **25**, 471–482.

120 T. N. Stekhanova, A. L. Rakitin, A. V. Mardanov, E. Y. Bezsudnova and V. O. Popov, *Enzyme Microb. Technol.*, 2017, **96**, 127–134.

121 K. M. Boyko, T. N. Stekhanova, A. Yu. Nikolaeva, A. V. Mardanov, A. L. Rakitin, N. V. Ravin, E. Yu. Bezsudnova and V. O. Popov, *Extremophiles*, 2016, **20**, 215–225.

122 L. Cerioli, M. Planchestainer, J. Cassidy, D. Tessaro and F. Paradisi, *J. Mol. Catal. B Enzym.*, 2015, **120**, 141–150.

123 S. A. Kelly, S. Mix, T. S. Moody and B. F. Gilmore, *Appl. Microbiol. Biotechnol.*, 2020, **104**, 4781–4794.

124 S. L. Márquez, J. Atalah and J. M. Blamey, *Enzyme Microb. Technol.*, 2019, **131**, 109423.

125 E. E. Ferrandi, A. Previdi, I. Bassanini, S. Riva, X. Peng and D. Monti, *Appl. Microbiol. Biotechnol.*, 2017, **101**, 4963–4979.

126 Y. Chen, D. Yi, S. Jiang and D. Wei, *Appl. Microbiol. Biotechnol.*, 2016, **100**, 3101–3111.

127 S. Mathew, K. Deepankumar, G. Shin, E. Y. Hong, B.-G. Kim, T. Chung and H. Yun, *RSC Adv.*, 2016, **6**, 69257–69260.

128 B. Guidi, M. Planchestainer, M. L. Contente, T. Laurenzi, I. Eberini, L. J. Gourlay, D. Romano, F. Paradisi and F. Molinari, *Sci. Rep.*, 2018, **8**, 16441.

129 C. M. Heckmann, L. J. Gourlay, B. Dominguez and F. Paradisi, *Front. Bioeng. Biotechnol.*

130 D. Koszelewski, M. Göritzer, D. Clay, B. Seisser and W. Kroutil, *ChemCatChem*, 2010, **2**, 73–77.

131 M. Planchestainer, M. L. Contente, J. Cassidy, F. Molinari, L. Tamborini and F. Paradisi, *Green Chem.*, 2017, **19**, 372–375.

132 M. D. Truppo, J. D. Rozzell, J. C. Moore and N. J. Turner, *Org Biomol Chem*, 2009, **7**, 395–398.

133 L. Rios-Solis, P. Morris, C. Grant, A. O. O. Odeleye, H. C. Hailes, J. M. Ward, P. A. Dalby, F. Baganz and G. J. Lye, *Chem. Eng. Sci.*, 2015, **122**, 360–372.

134 E. S. Park, J. Y. Dong and J. S. Shin, *Org. Biomol. Chem.*, 2013, **11**, 6929–6933.

135 R. E. Meadows, K. R. Mulholland, M. Schürmann, M. Golden, H. Kierkels, E. Meulenbroeks, D. Mink, O. May, C. Squire, H. Straatman and A. S. Wells, *Org. Process Res. Dev.*, 2013, **17**, 1117–1122.

136 J.-S. Shin, B.-G. Kim and D.-H. Shin, *Enzyme Microb. Technol.*, 2001, **29**, 232–239.

137 J. S. Shin and B. G. Kim, *Biotechnol. Bioeng.*, 2002, **77**, 832–837.

138 B. K. Cho, H. J. Cho, H. Yun and B. G. Kim, *J. Mol. Catal. B Enzym.*, 2003, **26**, 273–285.

139 D. Hülsewede, M. Tänzler, P. Süss, A. Mildner, U. Menyes and J. von Langermann, *Eur. J. Org. Chem.*, 2018, **2018**, 2130–2133.

140 A. P. Green, N. J. Turner and E. O'Reilly, *Angew. Chem. - Int. Ed.*, 2014, **53**, 10714–10717.

141 H. H. Lo, S. K. Hsu, W. De Lin, N. L. Chan and W. H. Hsu, *Biotechnol. Prog.*, 2005, **21**, 411–415.

142 D. Koszelewski, I. Lavandera, D. Clay, D. Rozzell and W. Kroutil, *Adv. Synth. Catal.*, 2008, **350**, 2761–2766.

143 F. G. Mutti, C. S. Fuchs, D. Pressnitz, J. H. Sattler and W. Kroutil, *Adv. Synth. Catal.*, 2011, **353**, 3227–3233.

144 M. Höhne, S. Kühl, K. Robins and U. T. Bornscheuer, *ChemBioChem*, 2008, **9**, 363–365.

145 D. Koszelewski, I. Lavandera, D. Clay, G. M. Guebitz, D. Rozzell and W. Kroutil, *Angew. Chem. - Int. Ed.*, 2008, **47**, 9337–9340.

146 K. E. Cassimjee, C. Branneby, V. Abedi, A. Wells and P. Berglund, *Chem. Commun.*, 2010, **46**, 5569.

147 S. Schätzle, F. Steffen-Munsberg, A. Thontowi, M. Höhne, K. Robins and U. T. Bornscheuer, *Adv. Synth. Catal.*, 2011, **353**, 2439–2445.

148 Y. Li, S. Jing, C. Cuijie, W. Shaoming, Z. Liande, X. Wenlin and G. Liping, *Electrophoresis*, 2009, **30**, 3527–3533.

149 R. Ye, J. Zhao, B. B. Wickemeyer, F. D. Toste and G. A. Somorjai, *Nat. Catal.*, 2018, **1**, 318–325.

150 D. P. Debecker, V. Smeets, M. Van der Verren, H. Meersseman Arango, M. Kinnaer and F. Devred, *Curr. Opin. Green Sustain. Chem.*, 2021, **28**, 100437.

151 U. T. Bornscheuer, *Angew. Chem. Int. Ed.*, 2003, **42**, 3336–3337.

152 J. M. Bolivar and F. López-Gallego, *Curr. Opin. Green Sustain. Chem.*, 2020, **25**, 100349.

153 D. Grajales, J. C. Mateos, D. Padro, P. Ramos-Cabrer and F. López-Gallego, *New Biotechnol.*, 2018, **47**, 25–30.

154 R. A. Sheldon and S. van Pelt, *Chem Soc Rev*, 2013, **42**, 6223–6235.

155 A. Basso and S. Serban, *Mol. Catal.*, 2019, **479**, 110607.

156 N. Khalaf, C. P. Govardhan, J. J. Lalonde, R. A. Persichetti, Y. F. Wang and A. L. Margolin, *J. Am. Chem. Soc.*, 1996, **118**, 5494–5495.

157 C. Mateo, J. M. Palomo, G. Fernandez-Lorente, J. M. Guisan and R. Fernandez-Lafuente, *Enzyme Microb. Technol.*, 2007, **40**, 1451–1463.

158 L. Cao, F. van Rantwijk and R. A. Sheldon, *Org. Lett.*, 2000, **2**, 1361–1364.

159 R. A. Sheldon, *Adv. Synth. Catal.*, 2007, **349**, 1289–1307.

160 U. Hanefeld, L. Gardossi and E. Magner, *Chem. Soc. Rev.*, 2009, **38**, 453–468.

161 D. N. Tran and K. J. Balkus, *ACS Catal.*, 2011, **1**, 956–968.

162 V. Smeets, W. Baaziz, O. Ersen, E. M. Gaigneaux, C. Boissière, C. Sanchez and D. P. Debecker, *Chem. Sci.*, 2020, **11**, 954–961.

163 M. Van der Verren, V. Smeets, A. vander Straeten, C. Dupont-Gillain and D. P. Debecker, *Nanoscale Adv.*, 2021, **3**, 1646–1655.

164 A. I. Benítez-Mateos, M. L. Contente, D. R. Padrosa and F. Paradisi, *React. Chem. Eng.*, 2021, **6**, 599–611.

165 R. A. Sheldon, R. Schoevaart and L. M. Van Langen, *Biocatal. Biotransformation*, 2005, **23**, 141–147.

166 J. Zdarta, A. Meyer, T. Jesionowski and M. Pinelo, *Catalysts*, 2018, **8**, 92.

167 D. Koszelewski, N. Müller, J. H. Schrittwieser, K. Faber and W. Kroutil, *J. Mol. Catal. B Enzym.*, 2010, **63**, 39–44.

168 T. Menegatti and P. Žnidaršič-Plazl, *Front. Bioeng. Biotechnol.*, 2021, **9**, 752064.

169 S. Zhang, P. Xin, S. Demoustier-Champagne and A. M. Jonas, *Colloids Surf. Physicochem. Eng. Asp.*, 2021, **631**, 127698.

170 C. Bernal, A. Illanes and L. Wilson, *Langmuir*, 2014, **30**, 3557–3566.

171 A. Vander Straeten, D. Lefèvre, S. Demoustier-Champagne and C. Dupont-Gillain, *Adv. Colloid Interface Sci.*, 2020, **280**, 102161.

172 C. Vranckx, L. Lambricht, V. Préat, O. Cornu, C. Dupont-Gillain and A. vander Straeten, *Langmuir*, 2022, **38**, 5579–5589.

173 K. E. Cassimjee, R. Kourist, D. Lindberg, M. Wittrup Larsen, N. H. Thanh, M. Widersten, U. T. Bornscheuer and P. Berglund, *Biotechnol. J.*, 2011, **6**, 463–469.

174 K. E. Cassimjee, M. Trummer, C. Branneby and P. Berglund, *Biotechnol. Bioeng.*, 2008, **99**, 712–716.

175 L. van den Biggelaar, P. Soumillion and D. P. Debecker, *Catalysts*, 2017, **7**, 54.

176 F. López-Gallego, L. Betancor, A. Hidalgo, N. Alonso, R. Fernández-Lafuente and J. M. Guisán, *Biomacromolecules*, 2005, **6**, 1839–1842.

177 F. López-Gallego, L. Betancor, C. Mateo, A. Hidalgo, N. Alonso-Morales, G. Dellamora-Ortiz, J. M. Guisán and R. Fernández-Lafuente, *J. Biotechnol.*, 2005, **119**, 70–75.

178 S. Velasco-Lozano, F. López-Gallego, J. C. Mateos-Díaz and E. Favela-Torres, *Biocatalysis*, 2016, **1**, 166–177.

179 K. E. Cassimjee, M. Kadow, Y. Wikmark, M. S. Humble, M. L. Rothstein, D. M. Rothstein and J.-E. Bäckvall, *Chem. Commun.*, 2014, **50**, 9134–9137.

180 M. D. Truppo, H. Strotman and G. Hughes, *ChemCatChem*, 2012, **4**, 1071–1074.

181 S. S. Yi, C. won Lee, J. Kim, D. Kyung, B. G. Kim and Y. S. Lee, *Process Biochem.*, 2007, **42**, 895–898.

182 H. Mallin, U. Menyes, T. Vorhaben, M. Höhne and U. T. Bornscheuer, *ChemCatChem*, 2013, **5**, 588–593.

183 H. Mallin, M. Höhne and U. T. Bornscheuer, *J. Biotechnol.*, 2014, **191**, 32–37.

184 M. Päiviö and L. T. Kanerva, *Process Biochem.*, 2013, **48**, 1488–1494.

185 I. Patramani, *Eur. J. Biochem.*, 1969, **11**, 28–36.

186 L. Tamborini, P. Fernandes, F. Paradisi and F. Molinari, *Trends Biotechnol.*, 2018, **36**, 73–88.

187 S. Mascia, P. L. Heider, H. Zhang, R. Lakerveld, B. Benyahia, P. I. Barton, R. D. Braatz, C. L. Cooney, J. M. B. Evans, T. F. Jamison, K. F. Jensen, A. S. Myerson and B. L. Trout, *Angew. Chem.*, 2013, **125**, 12585–12589.

188 S. G. Newman and K. F. Jensen, *Green Chem.*, 2013, **15**, 1456–1472.

189 D. Andrés-Sanz, E. Diamanti, D. Di Silvo, J. Gurauskis and F. López-Gallego, *ACS Appl. Mater. Interfaces*, 2022, **14**, 4285–4296.

190 R. Gérardy, D. P. Debecker, J. Estager, P. Luis and J.-C. M. Monbaliu, *Chem. Rev.*, 2020, **120**, 7219–7347.

191 G. Jas and A. Kirschning, *Chem. - Eur. J.*, 2003, **9**, 5708–5723.

192 A. Kirschning, W. Solodenko and K. Mennecke, *Chem. - Eur. J.*, 2006, **12**, 5972–5990.

193 M. P. Thompson, I. Peñafiel, S. C. Cosgrove and N. J. Turner, *Org. Process Res. Dev.*, 2019, **23**, 9–18.

194 P. D. Santis, L.-E. Meyer and S. Kara, *React. Chem. Eng.*, 2020, **5**, 2155–2184.

195 J. Britton, S. Majumdar and G. A. Weiss, *Chem. Soc. Rev.*, 2018, **47**, 5891–5918.

196 M. Santi, L. Sancineto, V. Nascimento, J. Braun Azeredo, E. V. M. Orozco, L. H. Andrade, H. Gröger and C. Santi, *Int. J. Mol. Sci.*, 2021, **22**, 990.

197 R. Gérardy, R. Morodo, J. Estager, P. Luis, D. P. Debecker and J.-C. M. Monbaliu, in *Accounts on Sustainable Flow Chemistry*, eds. T. Noël and R. Luque, Springer International Publishing, Cham, 2020, pp. 111–145.

198 W. Khanam and N. C. Dubey, *Mater. Today Chem.*, 2022, **24**, 100922.

199 L. Rogers and K. F. Jensen, *Green Chem.*, 2019, **21**, 3481–3498.

200 G. Rehn, P. Adlercreutz and C. Grey, *J. Biotechnol.*, 2014, **179**, 50–55.

201 Z. Molnár, E. Farkas, Á. Lakó, B. Erdélyi, W. Kroutil, B. G. Vértessy, C. Paizs and L. Poppe, *Catalysts*, 2019, **9**, 438.

202 L. H. Andrade, W. Kroutil and T. F. Jamison, *Org. Lett.*, 2014, **16**, 6092–6095.

203 N. Miložič, G. Stojkovič, A. Vogel, D. Bouwes and P. Žnidaršič-Plazl, *New Biotechnol.*, 2018, **47**, 18–24.

204 W. Böhmer, T. Knaus, A. Volkov, T. K. Slot, N. R. Shiju, K. Engelmark Cassimjee and F. G. Mutti, *J. Biotechnol.*, 2019, **291**, 52–60.

205 A. W. H. Dawood, J. Bassut, R. O. M. A. de Souza and U. T. Bornscheuer, *Chem. – Eur. J.*, 2018, **24**, 16009–16013.

206 A. P. Mattey, G. J. Ford, J. Citoler, C. Baldwin, J. R. Marshall, R. B. Palmer, M. Thompson, N. J. Turner, S. C. Cosgrove and S. L. Flitsch, *Angew. Chem. Int. Ed.*, 2021, **60**, 18660–18665.

207 E. Hegarty and F. Paradisi, *Chimia*, 2020, **74**, 890–894.

208 C. M. Heckmann, B. Dominguez and F. Paradisi, *ACS Sustain. Chem. Eng.*, 2021, **9**, 4122–4129.

209 M. L. Contente, F. Dall'Oglio, L. Tamborini, F. Molinari and F. Paradisi, *ChemCatChem*, 2017, **9**, 3843–3848.

210 M. L. Contente and F. Paradisi, *Nat. Catal.*, 2018, **1**, 452–459.

211 X. Wang, Y. Xie, Z. Wang, K. Zhang, H. Wang and D. Wei, *Org. Process Res. Dev.*, 2022, **26**, 1351–1359.

212 E. Abaházi, P. Sátorhelyi, B. Erdélyi, B. G. Vértessy, H. Land, C. Paizs, P. Berglund and L. Poppe, *Biochem. Eng. J.*, 2018, **132**, 270–278.

213 R. Semproli, G. Vaccaro, E. E. Ferrandi, M. Vanoni, T. Bavaro, G. Marrubini, F. Annunziata, P. Conti, G. Speranza, D. Monti, L. Tamborini and D. Ubiali, *ChemCatChem*, 2020, **12**, 1359–1367.

214 World Intellectual Property Organization, WO2014133928A1, 2014.

215 T. Heinks, L. M. Merz, J. Liedtke, M. Höhne, L. M. van Langen, U. T. Bornscheuer, G. Fischer von Mollard and P. Berglund, *Catalysts*, 2023, **13**, 875.

216 S. P. de Souza, I. I. Junior, G. M. A. Silva, L. S. M. Miranda, M. F. Santiago, F. L.-Y. Lam, A. Dawood, U. T. Bornscheuer and R. O. M. A. de Souza, *RSC Adv.*, 2016, **6**, 6665–6671.

217 A. I. Benítez-Mateos, S. Bertella, J. Behaghel de Bueren, J. S. Luterbacher and F. Paradisi, *ChemSusChem*, 2021, **14**, 3198–3207.

218 L. van den Biggelaar, P. Soumillion and D. P. Debecker, *RSC Adv.*, 2019, **9**, 18538–18546.

219 S. Matosevic, G. J. Lye and F. Baganz, *J. Biotechnol.*, 2011, **155**, 320–329.

220 A. Abdul Halim, N. Szita and F. Baganz, *J. Biotechnol.*, 2013, **168**, 567–575.

221 E. Peris, O. Okafor, E. Kulcinskaja, R. Goodridge, S. V. Luis, E. Garcia-Verdugo, E. O'Reilly and V. Sans, *Green Chem.*, 2017, **19**, 5345–5349.

222 M. Bajić, I. Plazl, R. Stloukal and P. Žnidaršič-Plazl, *Process Biochem.*, 2017, **52**, 63–72.

223 A. I. Benítez-Mateos, M. L. Contente, S. Velasco-Lozano, F. Paradisi and F. López-Gallego, *ACS Sustain. Chem. Eng.*, 2018, **6**, 13151–13159.

224 M. L. Contente and F. Paradisi, *ChemBioChem*, 2019, **20**, 2830–2833.

225 X.-J. Zhang, H.-H. Fan, N. Liu, X.-X. Wang, F. Cheng, Z.-Q. Liu and Y.-G. Zheng, *Enzyme Microb. Technol.*, 2019, **130**, 109362.

226 M. Romero-Fernandez and F. Paradisi, *Green Chem.*, 2021, **23**, 4594–4603.

227 M. Romero-Fernandez, C. M. Heckmann and F. Paradisi, *ChemSusChem*, 2022, **15**, e202200811.

228 L. Nagy-Győr, E. Abaházi, V. Bódai, P. Sátorhelyi, B. Erdélyi, D. Balogh-Weiser, C. Paizs, G. Hornyánszky and L. Poppe, *ChemBioChem*, 2018, **19**, 1845–1848.

229 J. S. Shin, B. G. Kim, A. Liese and C. Wandrey, *Biotechnol. Bioeng.*, 2001, **73**, 179–187.

230 C. Mateo, V. Grazú, B. C. C. Pessela, T. Montes, J. M. Palomo, R. Torres, F. López-Gallego, R. Fernández-Lafuente and J. M. Guisán, *Biochem. Soc. Trans.*, 2007, **35**, 1593–1601.

231 A. Azimi, S. Caramuta, B. Seashore-Ludlow, J. Boström, J. L. Robinson, F. Edfors, R. Tuominen, K. Kemper, O. Krijgsman, D. S. Peeper, J. Nielsen, J. Hansson, S. Egyhazi Brage, M. Altun, M. Uhlen and G. Maddalo, *Mol. Syst. Biol.*, 2018, **14**, e7858.

232 J. M. Carceller, K. S. Arias, M. J. Climent, S. Iborra and A. Corma, *Natl. Sci. Rev.*, 2022, **9**, nwac135.

233 S. Velasco-Lozano, A. I. Benítez-Mateos and F. López-Gallego, *Angew. Chem. Int. Ed.*, 2017, **56**, 771–775.

234 M. Romero-Fernández and F. Paradisi, *Curr. Opin. Chem. Biol.*, 2020, **55**, 1–8.

235 R. A. Sheldon, *ACS Sustain. Chem. Eng.*, 2018, **6**, 4464–4480.

236 J. H. Schrittwieser, S. Velikogne, M. Hall and W. Kroutil, *Chem. Rev.*, 2018, **118**, 270–348.

237 D. Hülsewede, E. Temmel, P. Kumm and J. von Langermann, *Crystals*, 2020, **10**, 345.

238 A. Adamo, R. L. Beingessner, M. Behnam, J. Chen, T. F. Jamison, K. F. Jensen, J.-C. M. Monbaliu, A. S. Myerson, E. M. Revalor, D. R. Snead, T. Stelzer, N. Weeranoppanant, S. Y. Wong and P. Zhang, *Science*, 2016, **352**, 61–67.